Las limitaciones de agua de riego para los cultivos asociadas a la escasez de los recursos hídricos, han propiciado el desarrollo de sistemas de ingeniería de riego y de manejo de las plantaciones encaminados a hacer un uso más eficiente del agua. La implantación de sistemas de riego por goteo o la programación de riego basado en déficits suponen algunos ejemplos destacados. Sin embargo, el aprovechamiento eficaz de las herramientas disponibles para alcanzar el objetivo de un aumento en la eficiencia en el uso del agua, dependen de una visión clara de las relaciones entre los elementos que componen el sistema suelo-agua-planta. En este sentido los modelos de simulación son una excelente herramienta tanto para sintetizar el conocimiento de cada uno de los elementos de manera concisa como para explorar las interacciones entre los mismos. El objetivo general de esta tesis comprende el desarrollo de un modelo de simulación capaz de capturar el comportamiento de los componentes relacionados con el balance de agua de cultivos arbóreos bajo riego sometidos a distintos niveles de estrés hídrico. Para lograrlo se han desarrollado ecuaciones que simulan la extracción de agua por las raíces y su relación con la conductancia estomática y la transpiración. El marco teórico se ha validado con experimentos tanto a escala de maceta como a escala de finca en olivos y almendros con notables resultados. Por último se han propuesto algunas recomendaciones derivadas del estudio de casos usando el modelo.

Modelización de la Transpiración del **Olivo y Almendro** en condiciones de Déficit Hídrico.

Modelización de la Transpiración del **Olivo** y **Almendro** en condiciones de Déficit Hídrico.

CSIC Consejo Superior de Investigaciones Científicas | Instituto de Agricultura Sostenible IAS

UNIVERSIDAD DE CÓRDOBA

Jul 2016

Tesis Doctoral Omar García Tejera

CSIC Consejo Superior de Investigaciones Científicas | Instituto de Agricultura Sostenible IAS

TITULO: *Modelización de la transpiración del olivo y el almendro en condiciones de déficit hídrico*

AUTOR: *Omar García Tejera*

Campus de Rabanales
Ctra. Nacional IV, Km. 396 A
14071 Córdoba

www.uco.es/publicaciones
publicaciones@uco.es

UNIVERSIDAD DE CÓRDOBA

DEPARTAMENTO DE AGRONOMÍA

Programa de doctorado

Biociencias y ciencias agroalimentarias

TESIS DOCTORAL

Modelización de la traspiración del olivo y el almendro en condiciones de déficit hídrico

Modelling transpiration of olive and almond trees under water deficit conditions

Autor

Omar García Tejera

Dirigido por

Dr. Luca Testi

Prof. Francisco J. Villalobos Martín

Tesis Financiada por el proyecto AGL-2010-20766 del Ministerio de Economía y Comtetitividad y por el séptimo programa marco de la Comunidad Europea (KBBE.2013.1.4-09) bajo el No. 613817 (MODEXTREME, modextreme.org)

Instituto de Agricultura Sostenible – CSIC

Junio 2016

TÍTULO DE LA TESIS: Modelización de la Transpiración del Olivo y el Almendro en condiciones de déficit hídrico.

DOCTORANDO/A: Omar García Tejera

INFORME RAZONADO DEL/DE LOS DIRECTOR/ES DE LA TESIS

(se hará mención a la evolución y desarrollo de la tesis, así como a trabajos y publicaciones derivados de la misma).

El Dr. **Luca Testi**, investigador del Instituto de Agricultura Sostenible (IAS) perteneciente al CSIC, y el Prof. **Francisco J. Villalobos Martín**, Catedrático de la Universidad de Córdoba y adscrito al IAS, como directores de la tesis doctoral con título: Modelización de la transpiración del olivo y el almendro en condiciones de déficit hídrico realizada por **Omar García Tejera**; informan que:

- Dicha tesis ha sido realizada bajo nuestra dirección
- Su principal objetivo el desarrollo de un modelo de simulación para estimar los componentes del balance de agua en olivo y almendros en condiciones de estrés hídrico y la

realización de experimentos tanto a escala de maceta como a escala de campo para testar la bondad de dicho modelo.

- Tanto las aproximaciones experimentales como los resultados y conclusiones obtenidas son de relevancia para un manejo sostenible y eficiente del riego.

- En su etapa pre-doctoral, Omar García Tejera ha realizado una estancia de 90 días, desde Septiembre a Diciembre de 2013, en el "Department of Plant Sciences" perteneciente a la universidad de Davis, California (UC Davis) bajo la tutela del profesor Theodor de Jong, cuyo objetivo fue la familiarización con el modelo de simulación L-Peach; ha co-dirigido una tesis de máster con título: "Papel del estrés hídrico sobre la resistencia al daño por heladas en plantas jóvenes de olivo y su relación con la aclimatación por frío" escrita por Facundo Vita Serman y ha colaborado en numerosas líneas de investigación y asistido a diversos congresos internacionales de los que se derivan las publicaciones siguientes:

Revistas incluidas en el Science Citation Index

- Villalobos FJ, Testi L, Orgaz F, **Garcia-Tejera O**, Lopez-Bernal A, Victoria Gonzalez-Dugo M, Ballester-Lurbe C, RamonCastel J, Alarcon-Cabanero J,Nicolas-Nicolas E, Girona J,Marsal J, Fereres E. 2013. Modelling canopy conductance and transpiration of fruit trees in Mediterranean areas: a simplified approach. Agric For Meteorol. 171:93-103

- López-Bernal A, **García-Tejera O**, Testi L, Orgaz F, Villalobos FJ. 2015. López-Bernal A, **García-Tejera O**, Testi L, Orgaz F, Villalobos FJ. 2015. Low winter temperature induce a disturbance of water relations in field olive trees. Trees. 29:1247-1257.

- López-Bernal A, **García-Tejera O**, Vega V, Hidalgo JC, Testi L, Orgaz F, Villalobos FJ. 2015. Using sap flow measurements to estimate the effects of water stress on net assimilation in fruit orchards. IrriSci.33:357-366

- **García-Tejera O**, López-Bernal A, Orgaz F, Testi L, Villalobos FJ. Effect of soil temperature on root resistance: implications for different fruit trees under Mediterranean conditions.2016. Tree Phys.36: 469-478

- **García-Tejera O,** López-Bernal A, Testi L and Villalobos FJ. A soil-plant-atmosphere continuum (SPAC) model for simulating tree transpiration with a soil multi-compartment solution. (Under review).

- **García-Tejera O,** López-Bernal A, Orgaz F, Testi L and Villalobos FJ. Field validation of the multi-compartment SPAC model for olive trees and analysis of the effect of wetted area on tree transpiration . (In preparation).

<u>Aportaciones a congresos internacionales</u>

- **García-Tejera O**, Villalobos FJ, Velasco L, Fernández-Martínez JM. 2012. Phenological characterization of sunflower cultivars for winter planting. *XII Congress of*

the European Society of Agronomy. Helsinky, Finland. 20-24 August.

- **García- Tejera O,** López-Bernal A, Orgaz F, Villalobos FJ, Testi L. 2014. Root distribution under different irrigation regimes. *XIII Congress of the European Society of Agronomy*. Debrecen, Hungary 20-24 August.

- López-Bernal A, **García- Tejera O**, Orgaz F, Testi L, Villalobos FJ. 2014. Olive bud dormancy is induced by low temepratures. *XIII Congress of the European Society of Agronomy*. Debrecen, Hungary 20-24 August.

- **García- Tejera O,** López-Bernal A, Orgaz F, Testi L, Villalobos FJ.2015. Root length density distribution according to two different irrigation strategies in a hedgerow olive plantation. *X International Symposium Modelling in Fruit Research and Orchard Management*. Montpellier, France 2-5 June

- Lopez-Bernal A, **García-Tejera O**, Orgaz F, Testi L, Villalobos FJ. Do olive vegetative buds undergo a real dormant state in winter? 2015.*X International Symposium Modelling in Fruit Research and Orchard Management*. Montpellier, France 2-5 June.

- **García- Tejera O,** López-Bernal A, Orgaz F, Testi L, Villalobos FJ.2015. Stomatal oscillations on potted olive trees. *VIII International Symposium on Irrigation of Horticultural Crops*, Lleida, Spain,8-11 June.

- Lopez-Bernal A, **Garcia-Tejera O**, Orgaz F, Testi L, Villalobos FJ.2015. Characterizing the spatial variability of sap flow in almond trees and its practical implications. *VIII International Symposium on Irrigation of Horticultural Crops*, Lleida, Spain, 8-11 June.

Por todo ello, se autoriza la presentación de la tesis doctoral.

Córdoba, 16 de Junio de 2016

Firma del/de los director/es

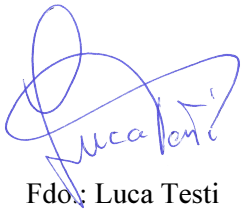

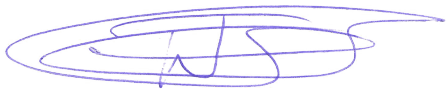

Fdo.: Luca Testi Fdo.: Francisco J. Villalobos Martín

“All models are wrong, but some are useful”

George E.P. Box

“La fuerza no proviene de la capacidad fisica sino de la voluntad indomable”

Gandhi

Agradecimientos

Es difícil condensar en unas pocas frases los años de estancia en esta tierra que se ha convertido en mi segundo hogar. En primer lugar me gustaría agradecer a mis directores Luca Testi y Francisco Villalobos por confiar en mí y darme la oportunidad de encontrar mi vocación dentro del mundo de la ciencia. También merece estar entre los dos primeros, aunque no figure como director, Francisco Orgaz. Los tres juntos, han sido para mí verdaderos maestros, en el amplio sentido de la palabra. Por las charlas durante el desayuno que comenzaban hablando de cosas irrelevantes y acababan convirtiéndose en clases magistrales sobre eficiencia en la transpiración o fotosíntesis, por la facilidad para dar soluciones a problemas que a mi parecer resultaban irresolubles y por encima de todo, por la capacidad de estar cuando más se les necesitaba. Por todo ello muchísimas gracias.

También me gustaría agradecer a Álvaro López mi compañero de batallas durante este proceso. Gracias prestarme tu ayuda sin ni siquiera pedírtela, por hacer que los ratos en los que mediamos en la Harina durante el verano fueran más agradables y sobre todo por aguantar mis locas teorías sobre el funcionamiento de las plantas.

A los técnicos Manolo Gonzalez, Jose Luis Vazquez, Ignacio Calatrava y Rafael del Río. Siempre dispuestos a ayudar y aportando magníficas soluciones técnicas. Sin ellos esta tesis no habría sido posible. Merecen también una mención especial Rafa Luque, Marcos Orgaz y Rafaela Gutiérrez, por estar dispuest@s a ayudar cuando el trabajo me desbordaba.

A Inian y Adam por las noches que se hacían mañanas, por iniciarme en la escalada y por las experiencias que vivimos juntos en Horno de Porras. A Carmen "*la paraguaya*" y a "*los mejicanitos*" Carlos y Liz por los postres riquísimos que alegraban el día más triste y por las risas constantes.

A Lola, por tu apoyo incondicional, tus abrazos y por bajarme los pies a la tierra cuando construía castillos en el aire.

A Mari Luz por regalarme una sonrisa nada más conocerme, a Rocío y Marimon por las fiestas y por un pack de calcetines que cambió mi vida, a Facundo por los asados y las agradables conversaciones sobre política, a Inma por regalarme siempre una sonrisa, a Manolo Gómez por esa sencillez y por llevar siempre la guitarra encima, a David Moldero por los ratos en el jardín, a Marga por su sencillez y dulzura y a Carmen Ruz por ser una súper organizadora y a Manolo por su disposición y a Elías Fereres me gustaría agradecerle sus consejos.

A Joaquín, Ana, Pedro y toda la gente de la pimentera que siempre me guardaban un hueco en la mesa.

Me gustaría agradecer también a la gente del otro lado del "charco", a mis amigos del team; como dijo uno una vez: "*Chicos sois los mejores*". A mi familia por todo el apoyo durante estos años fuera y por recordarme que, sin importar donde la vida me lleve, siempre tendré un hogar y un abrazo en ese pedazo de tierra en medio del Atlántico al que llamo *"mi isla"*.

Y a toda la gente sin la que esta estancia no hubiera sido tan magnifica

A todos, gracias.

Table of contents

List of figures

Fig 4.4. Measured and modelled daily transpiration *Ep* for treatments C (dots) and RDI (crosses) for years 2012 and 2013. The dash line represents the fitted 1:1 line. The adjusted R^2 from the linear regression was 0.81. The efficiency factor (EF) was 0.78 and the root mean square error (RMSE) 0.29 mm.

Fig 4.5. Midday measured (black dots) and simulated (white dots) leaf water potential for the control and the regulated deficit irrigation (RDI) treatments on years 2012 and 2013. The measured values correspond to the averages of the recorded values in four sun exposed leaves and the bars represent the standard error.

Fig 4.6. Variation of the relative E_p defined as ratio of actual E_p and E_{pmax} on a clear summer day, when the wet compartment is varied from 5 to 40% of total root space. Triangles: simulations assuming L_v profile for the wet compartment measured in the present experiment; circles: simulations with the maximum values reported for olive trees. Filled symbols: results for a clear day of August in Cordoba, Spain (VPD_{mean} = 3kPa) empty symbols: result from a clear day of August in a sub-tropical environment with lower VPD_{mean} (Güimar, Spain. VPD_{mean} = 1.7 kPa)

Fig 4.7. Effect on accumulated E_p during the irrigation campaign in 2013 (DOY 175 to DOY 294) on control (C, solid line) and the regulated deficit irrigation (RDI, dashed line) when the same amount of water devoted to each treatment is applied to different wetted surfaces expressed as percentages of total plant area.

Fig A1. Variation of measured and modelled fluxes for almond one and two at different irrigation phases. Black and red line are the measured fluxes from sides one and two while blue and purple lines correspond to modelled fluxes from sides one and two.

Fig A2. Measured (black) and modelled (green) E_p for the four trees used in the experiment.

Fig A3. Modelled (circles) and measured (triangles) soil water content at 1 hour (straight lines) and 8 hours (dotted lines) after irrigation.

Fig A4. Almond roots impacting the transparent sheet of the lysimeter before (left image) and after (right image) a drying cycle. Roots with a noticeable change in color after the dried phase have been highlighted with the red arrows. The black circle indicate a group of clumped roots.

List of tables

Table 4.1. Values for the parameters used in the photosynthesis and stomatal conductance models. Parameters for photosynthesis obtained from (Diaz-Espejo *et al.*, 2006) for olive trees are: the degree of curvature of the response to PAR of the electron transport rate (θ), the quantum efficiency (α) and values of activation energy (ΔH_a) and the scaling constants (c) for: Michaelis constant for CO_2 (K_c) and O_2 (K_o), CO_2 compensation point (Γ), maximum catalytic activity of Rubisco in the presence of saturating amounts of ribulose biphosphate and CO2 (V_{cmax}), maximum ratio of electron transport (J_{max}), and the rate of CO_2 evolution in the light resulting from process other than photorespiration (R_d). Parameters of the stomatal conductance for null net photosynthesis (g_0) and the parameters for the empirical model of Tuzet, namely, reference water potential (Ψ_f) and a sensitivity factor (s_f), have been obtained from the recorded sap flow values through a calibration procedure. The proportionality factor between photosynthesis and stomatal conductance (m) was acquired from (Moriana *et al.*, 2002).

Table 4.2. Initial parameters used in the simulations for both irrigation treatments in 2012 and 2013. $Root_{wet}$ and $Root_{dry}$ represents the total length of roots per square meter of soil in the wet and the dry compartment, a_{root} is the root radius, LAI is the leaf area index and GC is the percentage of ground cover. The root distribution measured in both compartments in 2013 was applied to the simulations in 2012.

Table 4.3. Monthly averages of tree transpiration (E_p) and resistances of the wet (R_{wet}) and the dry compartment (R_{dry}), together with the surface relations of roots and leaves ($Ar:Al$) and of roots in the dry and the wet compartment ($Ar_{wet}:Ar_{dry}$).

List of symbols

A'	Gross photosynthesis
A'_{sun}	Gross photosynthesis sunlit leaves
A'_{shade}	Gross photosynthesis shaded leaves
a_{root}	Root radius
$A_r{:}A_l$	Surface relation of roots and leaves
$A_{rwet}{:}A_{rdry}$	Surface relation of roots in the wet and the dry compartment
b	Shape factor
c	Dimensionless constant for the response to temperature
C_a	External concentration of CO_2
C_i	Internal concentration of CO_2
C_{isun}	Internal concentration of CO_2 for sunlit leaves
C_{ishade}	Internal concentration of CO_2 for shaded leaves
d	Soil layer depth
E_p	Transpiration
E_{ps}	Tree transpiration as a function of intercepted radiation
E_s	Evaporation from soil
$f_{(sun\ or\ shade)}$	Fraction of Leaf area index shaded or illuminated
$f(l)$	Frequency distribution of the path length
$f(\Psi_l)$	Empirical function relating stomatal conductance with leaf water potential
f_D	Fraction of diffuse radiation
$G(\theta_z)$	Projection function in the θ_z direction

g_{co2}	Stomatal conductance for CO_2
g_{co2sun}	Stomatal conductance for CO_2 of sunlit leaves
$g_{co2shade}$	Stomatal conductance for CO_2 of shaded leaves
g_{co2max}	Maximum stomatal conductance for CO_2 under no limiting leaf water potential
g_o	Night time stomatal conductance for CO_2 at null gross photosynthesis
i	Soil layer number
I_{diff}	Intercepted diffuse radiation
I_{dir}	Intercepted direct radiation
I_n	Irradiance in the direction normal to θ_z
j	Soil compartment number
J_{cmax}	Maximum ratio of electron transport
k	Unsaturated conductivity
K_c	Michaelis constant for CO_2
K_o	Michaelis constant for O_2
k_s	Saturated conductivity
L	Path length
Lv	Root length density
Lv'	Effective root length density
$LA:Lv$	Relation between leaf area and root length density
l_x	The maximum path length
m	Proportionality factor between photosynthesis and stomatal conductance
P	Atmospheric pressure

$PAR_{df,D}$	Daily diffuse Photosynthetically active radiation
$PAR_{G,D}$	Daily Photosynthetically active radiation reaching the ground
$PEA(\theta_z)$	Projected envelope area in the θ_z direction
Q	Fraction of photosynthetically active radiation intercepted by de canopy
r	Horizontal canopy radius
r'	Vertical canopy radius
R_d	Rate of CO_2 evolution in the light resulting from process other than photorespiration
R_{dry}	Resistance of the dry compartment
R_p	Radial root hydraulic specific resistance per square meter of root
R_{plant}	Resistance from root xylem to leaves (MPa s m^{-2} kg^{-1})
r_r	Root specific hydraulic resistance per meter of root
Rr	Total root system resistance
RR	Resistance of the total root system per square meter of soil in the radial direction
R_s	Radial root hydraulic specific resistance from the soil to the root surface
R_{soil}	Resistance from the soil to the root xylem
rt	Xylem specific hydraulic resistance
R_x	Total xylem resistance
R_{wet}	Resistance of the wet compartment
$S'_{df,D}$	Corrected daily diffuse solar radiation for Mie scattering
S_0	Extra-terrestrial solar radiation

$S_{0,D}$	Daily extra-terrestrial solar radiation
$S_{df,D}$	Daily diffuse solar radiation
s_f	Shape factor
S_G	Daily solar radiation
$S_{G,D}$	Daily solar radiation reaching the ground
S_k	Solar constant
SWA	Area of sapwood per unit ground area
$t(\theta_z)$	Canopy transmissivity
t_{sr}	Time of sun rise
t_{ss}	Time of sun set
V	Canopy volume
V_{cmax}	Maximum catalytic activity of Rubisco in the presence of saturating amounts ribulose biphosphate and CO_2
Z_{root}	Mean root depth
Z_{shoot}	Shoot height
α	Quantum efficiency
α'	r_r value at which $\theta_{soil}/\ \theta_{sat} = \delta'$
β'	Rate at which r_r approaches to infinity
β_s	Elevation angle of the sun
$\bar{\beta}$	Average solar elevation angle
Γ	CO2 compensation point
δ'	Critical value of $\theta_{soil}/\ \theta_{sat}$ at which r_r becomes limiting
ΔH_a	Activation energy
δ_s	Declination angle

θ	Degree of curvature of the response to PAR of the electron transport rate
θ_{ll}	Soil water content at permanent wilting point
θ_{sat}	Soil water content at saturation
θ_{soil}	Soil water content
θ_{ul}	Soil water content at field capacity
θ_z	Solar Zenith angle
λ_s	Latitude
μ	Leaf area density
τ_D	Transmission coefficient of the atmosphere
Ψ_c	Collar water potential
Ψ_e	Air entry water potential
Ψ_f	Reference water potential
Ψ_l	Leaf water potential
Ψ_{lsun}	Leaf water potential of sunlit leaves
Ψ_{lshade}	Leaf water potential of shaded leaves
Ψ_{mid}	Midday water potential
Ψ_s	Soil water potential

List of abbreviations

ABA	Abscisic acid
C	Control treatment
D	Dry one half
DI	Deficit irrigation
DL	Day length
DOY	Day of year
EF	Efficiency factor
ET0	Reference evapotranspiration
F	Full irrigation
F_{wet}	Wetted fraction of soil
GC	Ground cover
GMT	Greenwich meridian time
LA	Leaf area
LAD	Leaf area density
LAI	Leaf area Index
LAI_{shade}	Leaf area Index of shaded leaves
LAI_{sun}	Leaf area Index of sunlit leaves
RDI	Regulated deficit irrigation treatment
RMSE	Root mean square error
SD	Standard deviation
SPAC	Soil-plant-atmosphere continuum

SRL	Specific root length
T	Temperature
TDR	Time domain reflectometry
T_{soil}	Soil temperature
UTC	Coordinated universal time
V	Canopy volume
VPD	Vapour pressure deficit
VPD_{mean}	Mean daily vapour pressure deficit
Xmeas	Measured value
Xmod	Modelled value

Summary

The limitations of water for irrigation, has promoted the development of irrigation systems and crop management practices devoted to improve the efficient use of water. However, the best use of these tools requires a clear understanding of the components of the soil-water-plant system. In that sense, simulations models provide an excellent tool not only to synthesise the knowledge of each of the elements composing the system in a concise manner but to explore the interactions among them. The general objective of the present thesis is to develop a simulation model able to mimic the behaviour of each of the elements related to the water balance of tree crops under localised irrigation and submitted to any level of water stress.

One of the main constrains when modelling the water balance of a tree relates to the parametrization of the water uptake capacity of the roots. The water uptake capacity of a single root is not a fixed value but it varies with soil water content or the soil temperature. Although the effect of temperature on radial root hydraulic specific resistance (R_p) (a measure of the uptake capacity of a root) is a known phenomenon, the impact of R_p variations expected from soil temperature changes over the tree root system is not. The first experiments developed studied the change in R_p in olive (*Olea europaea L.*) 'Picual' and a widely used hybrid rootstock for stone fruits, GF677, at five different temperatures, showing that a variation of 3 and 4.5 folds exists for olive 'Picual' and GF677 respectively in the range from 10 to 20 ºC. The functions obtained were scaled up to show the theoretical changes of total radial root system resistance in a common tree orchard in a Mediterranean climate at a daily and seasonal scale, using recorded

soil temperature values. A difference between summer and winter of: 3.5 for olive 'Picual' and 9 folds for GF677 were observed. According to the results obtained it would therefore be advisable to assess them explicitly into soil-plant-atmosphere continuum (SPAC) models.

SPAC models have been widely used to simulate water balance on trees. In these types of models the plant is regarded as an electric circuit composed of resistances in series or in parallel. As part of the present thesis a SPAC model for simulating tree transpiration (E_p) and water potential with variable water stress and water distribution in the soil have been formulated. As a special feature of this model, the soil is not only divided into several layers but also into different compartments, thus capturing the heterogeneity in root length and soil water content present in trees, especially those in which drip or any type of localised irrigation is used. The multi-compartment function for the soil and roots is coupled to a simplified representation of the canopy using a sun/shade approach, thus building up a complete supply-demand framework.

The model was tested at two different scales. At a pot scale using a special lysimeter designed to accommodate split root young olive and almond (*Prunnus dulcis Mill.*) trees, and at a field scale on a hedgerow commercial olive orchard. In both experiment the model was able to successfully (lowest $R^2 = 0.81$) simulate transpiration and leaf water potential when different levels of stress were imposed. The study of tree water balance during water stress conditions performed with the model revealed that at high root length densities it is the uptake capacity of the root what governs the water withdrawal by the root system and that root clumping might play a major role reducing the

effective absorbing surface of the root system. Besides, at orchard level it was observed that the use of drip irrigation systems always limits the maximum attainable transpiration (E_{pmax}) for a given environment, and that the degree of limitation would depends on the ratio of areas of roots and leaves and the vapour pressure deficit. Finally, a case study exercise with the model showed that two different irrigation strategies could be followed depending on the available water. If sufficient water is available to meet tree transpiration demand, one should wet a soil volume high enough to ensure that E_p is as close as possible to E_{pmax}. Conversely, if a deficit is imposed, the strategy should be to reduce the wetted area in order to maximize the water routed to E_p

The model proved to be a tool robust enough to capture the trend in E_p and in leaf water potential for trees submitted to different irrigation regimes and allows the study of the interactions among irrigation, tree E_p and the environment.

Resumen

Las limitaciones de agua de riego para los cultivos ha propiciado el desarrollo de sistemas de ingeniería de riego y de manejo de las plantaciones encaminados a hacer un uso más eficiente del agua. Sin embargo, el aprovechamiento eficaz de las herramientas disponibles para alcanzar el objetivo de un aumento en la eficiencia en el uso del agua, dependen de una visión clara de las relaciones entre los elementos que componen el sistema suelo-agua-planta. En este sentido los modelos de simulación son una excelente herramienta tanto para sintetizar el conocimiento de cada uno de los elementos de manera concisa como para explorar las interacciones entre los mismos. El objetivo general de esta tesis comprende el desarrollo de un modelo de simulación capaz de capturar el comportamiento de los componentes relacionados con el balance de agua de cultivos arbóreos bajo riego localizado sometidos a distintos niveles de estrés hídrico.

Una de las principales limitaciones a la hora de modelizar el balance de agua en un árbol reside en la parametrización de la capacidad de extracción de agua por las raíces. La capacidad de extracción de una raíz no es un valor constante sino que varía con el contenido de agua y la temperatura del suelo. Aunque el efecto de la temperatura del suelo sobre la resistencia hidráulica radial específica (R_p) (una medida de la capacidad de extracción de agua por la raíz) es un fenómeno conocido, el impacto que las variaciones esperadas de R_p debidas a cambios en la temperatura del suelo tienen sobre el sistema radical no lo son. Los primeros experimentos desarrollados, estudiaron los cambios de R_p en olivos (*Olea europaea L.*) 'Picual' y en un patrón ampliamente usado en frutales de hueso, el GF677, a 5 temperaturas distintas, mostrando

que existía una variación de 3 y 4.5 veces para el olivo 'Picual' y el GF677 repsectivamente, en el rango de temperaturas que iban de 10 a 20 ºC. Las funciones obtenidas se escalaron para mostrar los cambios teóricos en la resistencia radial total del sistema radical a escala diaria y estacional para un cultivo tipo sembrado en clima mediterráneo usando registros de temperatura del suelo. Se encontró una diferencia entre el verano y el invierno de 3.5 veces para el olivo 'Picual y de 9 veces para el GF677. De acuerdo a los resultados obtenidos sería conveniente incluir explícitamente dichas variaciones en los modelos del continuo suelo-agua-planta (SPAC).

Los modelos SPAC han sido ampliamente usados para simular el balance de agua en árboles. En este tipo de modelos la planta es vista como un circuito eléctrico compuesto por resistencias en serie y en paralelo. Como parte de la presente tesis se ha desarrollado un modelo SPAC para simular la transpiración del árbol (E_p) y el potencial hídrico para condiciones de estrés y contenido de agua en el suelo variables. Una característica especial de éste modelo, es que el suelo no solo se divide en distintas capas sino también en diferentes compartimentos capturando así la heterogeneidad presente en el contenido de agua y longitud radical de los árboles, especialmente en aquellos en los que se usa riego localizado. La función de multi-compartimento para el suelo y las raíces se ha acoplado con una aproximación tipo hoja de luz/hoja de sombra para simular el dosel vegetal permitiendo así construir una función completa de oferta y demanda.

El modelo se testó a dos escalas distintas. A escala de maceta, usando un lisímitero diseñado para acomodar plantas jóvenes de olivo y

almendro (*Prunnus dulcis Mill.*) con la raíz dividida, y a escala de campo en un olivar comercial en seto. En ambos experimentos modelo fue capaz de simular con éxito (valor más bajo de R^2 = 0.81) la transpiración y el potencial hídrico bajo distintos niveles de estrés. El estudio del balance de agua del árbol durante condiciones de estrés hídrico reveló que para altas densidades de longitud radical, es la capacidad de extracción de agua por parte de las raíces lo que gobierna el flujo de agua hacia el sistema radical y que el agrupamiento de raíces podría jugar un papel importante en la reducción de la superficie de absorción efectiva por parte del sistema radical. Además, a nivel de parcela, se observó que el uso de sistemas de riego por goteo siempre limita la transpiración máxima esperable (E_{pmax}) para un ambiente determinado y que el grado de dicha limitación dependerá del cociente de las áreas de raíces y hojas así como del déficit de presión de vapor. Finalmente un estudio de casos usando el modelo, mostró que se podrían seguir dos estrategias de riego distintas dependiendo del agua disponible. Si se dispone de suficiente agua para cubrir las demandas de transpiración del árbol, se deberá regar intentando mojar un volumen de suelo lo suficientemente grande como para asegurar que E_p está lo más cerca posible de E_{pmax}. Por el contrario, si se impone un déficit, la estrategia debería ser la de reducir el área mojada para maximizar el agua disponible para E_p.

Chapter 1

General Introduction

1. General Introduction

1.1. Water use and crop production

Significant attention has been paid to rises in atmospheric CO_2 and its effect on climate change during the last decades. However, as Wallace (2000) stated, this special interest on CO_2 and warming has reduced the focus on another global change that is more certain and probably more important, the raise in global population. The forecasts for the next 50 years predict a median increase of 65% in human population (Wallace, 2000) raising the question of how to grow enough food when water resources are limited and already highly exploited, and an abrupt increase in future water needs to meet the demands for urban, industrial and environmental sectors is expected (Fereres & Soriano, 2007).

Globally, the water devoted to agriculture comprises around 75 % of total water withdrawal (FAO, 2016). Then again, more than 40% of food production comes from irrigated crops and uses only 17% of agricultural land area (Fereres & Connor, 2004). Those numbers generate two contradictories perceptions of the relation between water and agriculture. On the one hand, irrigation is viewed as a water wasting practice growing 'water-guzzling crops' while on the other, it is emphasised that irrigated crops are essential to meet future food demands (Fereres & Soriano, 2007). As an example, those two visions opened a social debate during the severe droughts suffered in California from 2011 to 2015 and raised the question of how state

water resources should be managed and if agriculture was a water wasting industry.

Almond (*Prunnus dulcis* Mill) and olive (*Olea europaea* L.) trees in Spain provide another good example of the competition for water resources. Olive trees are the main irrigated crop in Spain with nearly 731,025 ha with almost 98% under drip irrigation (MAGRAMA, 2012). For almond trees the numbers are much lower, from the 527,058 ha only 8% of the surface is irrigated; nevertheless, the rising prices of almond are inducing an increase of the irrigated area (MAGRAMA, 2012). The maintenance of the irrigated area for olive and the expansions of new almond trees plantations will depend on the availability of water resources, which are likely to be more limited for two reasons: first, a substantial increase in the demand of water is expected for other sectors with higher water productivity (ratio return/water used). Second, the projection of climate change for Spain, indicates a reduction of fresh water reservoirs in the future (IPCC, 2013).

This expected competition and reduced availability is now forcing a change towards an increase of water productivity in agriculture. Over the last decades significant advances have been taking place on irrigated agriculture, including new agronomical strategies, the modernization of irrigation schemes and the implementation of precise irrigation methods, like drip systems, which have played a major role in reducing water use for irrigation. Irrigation has been traditionally scheduled to meet crop evapotranspiration (ET) demands. Nevertheless, it is evident that this approach requires larges amount of water and is extremely challenging in regions where water is scarce.

As a consequence, on recent years, a strategic change is taking place reducing the amounts of water for irrigated agriculture and leaving the remainders for other sectors with higher priorities (Fereres & Soriano, 2007). When irrigation is applied below the ET requirements it is termed deficit irrigation (DI). Reducing ET is accompanied in general by a reduction in biomass production because a tight relation exists between transpiration and assimilation (De Wit, 1958); however, the impacts on yield can be damped by increasing the partitioning of carbohydrates to yield This is the basic idea behind all DI strategies.

1.2. Deficit irrigation on tree crops

DI strategies have been applied on tree crops and vines with prominent results given that farmer's profits are associated to fruit quality or size rather than production, partially decoupling yield from returns (Fereres *et al.*, 2004). Besides, imposing moderate water stress at certain phenological phases can result in low or even negligible yield reductions while controlling the vegetative growth or even improving fruit quality (Chalmers *et al.*, 1981, Goldhamer *et al.*, 2006, Iniesta *et al.*, 2009).

With DI, part of the water transpired by the crop comes from soil water storage, which may compensate, at least partly, the impact of reducing irrigation volume on crop ET (Fereres & Soriano, 2007). If ET is maintained and the water extracted from the soil is replenished by rainfalls, the DI is sustainable and will produce water savings, yet, if ET is reduced, the effect on yield will depend on the level of stress imposed and the time when it occurs.

Chalmers *et al.* (1981) working on peach trees, used DI in order to control tree vegetative growth and observed that when the restrictions where applied at a certain fruit developmental stage the reduction in ET was not accompanied by significant yield decreases. This approach was named regulated deficit irrigation (RDI). The operating mechanism behind RDI is related to the higher sensitivity of expansive growth to water stress as compared to that of photosynthesis, affecting the partitioning of carbon assimilates in a phenological stage (usually pit hardening) when fruit growth is not affected by mild water deficit (Girona *et al.*, 1993). As an example, Iniesta *et al.* (2009), working on olive trees under RDI, observed a reduction on canopy size while the oil production per unit of intercepted PAR remained almost the same.

In the implementation of a DI strategy as a way to optimise the use of available water, there is a high uncertainty in the expected results because the associated reductions in ET depend on the interaction of multiple factors like the cultivar, the soil type, the evaporative demand or the irrigation system. By way of illustration, the first attempts to recreate in California and Spain the RDI experiments performed in New Zealand in the early 70's failed to reproduce the results (Fereres *et al.*, 2004), which exemplifies the specificity of any DI management practice.

There are different ways to face the problem of specificity. In the traditional, empirical approach, tree water requirements are quantified for each site using energy or water balance measurements. Although valid to provide useful knowledge of the behaviour of the cultivar in the place under study, this approach is site specific and it would take

decades to study each particular case (Testi *et al.*, 2006). The other option involves the use of a simulation model to study a representative number of scenarios providing management rules to the farmers based on scientific knowledge.

1.3. The role of a model

The research activity can be divided into three different processes. The first one is the acquisition of knowledge related to the research problem, the second relates to the ordering of the acquired knowledge and the start of an understanding of the problem we are facing, and the third one is the application of the knowledge or the understanding to solve the problem. It is important to be aware that knowledge and understanding are not exchangeable terms. Knowledge relates to the awareness of a fact or facts, like a child that first discover the rain, while understanding deals with the explanation of a phenomenon based on the previously acquired knowledge (Charles-Edwards *et al.*, 1986). Models cover the last two aspects of the research activity. Imagine that one has measured tree transpiration (E_p) and the soil water content (θ_{soil}). A model can help in understanding how those two variables are related and what are the mechanisms behind such relations, and if it successfully describes the mechanisms, it can be used to explore what can be the best strategy to maximize the transpiration for a given soil water content.

In modelling the plant growth and function the system can be divided into different hierarchical levels each one composed of an organised

arrangement of the elements from the lower level. According to Passioura (1979) and Thornley and Johnson (2000) those are:

- Crop
- Plant
- Organ (leaf, stem, root)
- Tissue (epidermis, mesophyll)
- Cell
- Organelle (chloroplast, mothocondria)
- Molecule

Thornley and Johnson (2000) made important points when one is researching at any particular level in the hierarchy. The first one is that each level has it owns language. For instance, the terms crop yields or dry mass have little meaning at cell level. The second states that the relationships between two successive levels are not symmetric, in other words, the functioning of a hierarchal level requires that the lower level works effectively but the contrary is not true. The example relating tree E_p and θ_{soi}l, can be used to clarify this. Tree E_p for a variety of θ_{soil} can be described through our understanding of the water uptake by the roots, the changes in the stomata conductance and the relation between them through the water potential, but the level of understanding of the processes of water withdrawal by the roots or the stomata movements due to environmental changes, in no way depends upon our ability to describe tree E_p.

For the last point, Thornley and Johnson (2000) make the important indication that events happening at one hierarchical level may be linked to the next higher level in a mechanistic way. Going back to the example of tree E_p and θ_{soi}l, this imply that it is possible to describe

tree E_p as a functions of the known properties of the individual parts involved (Thornley & Johnson, 2000).

The hierarchical description of the plant system is the base of a reductionist approach and represents the philosophy of the mechanistic models. Building a model using a reductionist approach is equal to constructing a tower by putting bricks together. That is, trying to understand the system at a certain level using the knowledge behaviour of the part at the level just below (Chalmers *et al.*, 1981). The main strength of a mechanistic model is that they provide a systematic way to articulate separate ideas and offers a tool to interpret and explain the research results. During its development and testing the knowledge gaps at a certain level can be detected aiding into the address of new research questions. Finally, it also allows researchers to ask, what-if questions. An example of a mechanistic model is the one developed by Testi *et al.* (2006) to simulate the water requirements of olive orchards for well-watered conditions. After the successful validation of the model with measured values of ET, the authors quantified the impact of rainfall on crop coefficients due to the variation in soil evaporation.

On the other hand, empirical models can be used to summarize past data and may be used to interpolate within the measured range (Boote *et al.*, 1996). The idea is to use an equation or set of equations that best fit the data giving a way to re-represent them (Thornley & Johnson, 2000). The main limitations of empirical models are that they neither give any explanatory interpretation of the observed data nor can be extrapolated outside the range of values for which it was fitted.

The distinction between into empirical and mechanistic models should be taken as an indicative classification, as a model is never completely mechanistic and some empiricism is usually necessary at a certain hierarchical level (Boote *et al.*, 1996).

1.4. Why develop a crop model?

Boote *et al.* (1996) answered to this question giving three reasons: to synthetize the research knowledge, to provide a crop system management decision tool and for policy analysis. The role of the models as a research tool has been defined in the previous section highlighting its strength as an instrument to connect ideas and as a way to integrate knowledge. As a crop system management tool, models have been used to assist in the evaluation of risks considering yield response to different planting density, crop varieties, planting date and so on when applying long-term weather data (Boote *et al.*, 1996). For instance, working with the OILCROP-SUN model (Villalobos *et al.*, 1996), a model specifically developed for sunflower, García-Tejera (2011) re-analysed the experiments of Gimeno *et al.* (1989), who showed that early sunflower planting increased yields in a Mediterranean climate, characterized by a low evaporative demand and rains during autumn and winter. The result of the simulations indicated that yields could be increased if sowings were displaced to an earlier date than that reported by Gimeno *et al.* (1989) as long as the cultivars had a strong photoperiodic response that prevented the occurrence of flower initiation during the period of higher frost probability (García-Tejera, 2011).

As a policy analysis tool, crop models have been widely used to study the impacts on the environment of different agronomic practises like the application of different fertilizer amounts or the effect on soil erosion of a specific crop management practise (Boote *et al.*, 1996). Another use that is becoming very popular is the analysis of future climate scenarios to predict possible effects on crop performance. Morales *et al.* (2016) used a simulation model of olives to compare actual and future yields at two different planting densities, super-intensive (~1667 trees ha^{-1}) and intensive (~400 trees ha^{-1}) and concluded that yield remained almost the same for the two orchards types, but the higher future temperature expected led to some sterile years due to a lack of chilling.

The steeply increase of the computational power in the last decades has favoured the implementation of more complex models. Consequently, a significant amount of crop models can be found in the literature. However, each model is framed to the assumptions made to develop the equations that describe a specific process. As Campbell and Norman (1998) stated, models are a simplified representation of a more complex reality, and is the way that those simplifications are arranged what sets the applicability limits of the model.

Let's assume that we want to compute the photosynthesis at a canopy scale. One could use two formulations already available in the literature, a big-leaf or a radiation penetration approach. In big-leaf models the canopy is treated as a single leaf that averages canopy properties while the radiation penetration models divide the canopy into several layers with different leaf angle distributions (dePury & Farquhar, 1997). The problem with the big-leaf approach is that it

obviates the inherent heterogeneity present in the canopy resulting in deviations of the simulated values. The radiation penetration approach can be extremely complex and difficult to parametrize. As a solution dePury and Farquhar (1997) developed a sun/shade approach to account for the heterogeneity at a canopy scale, while keeping the equations required to compute photosynthesis simple. Following Albert Einstein words: "everything should be made as simple as possible, but not simpler".

1.5. Models of tree transpiration

Traditionally, E_p has been viewed as a process modulated either by the canopy or the roots, depending on the area of research. Micrometeorologists, for example, view the regulation of E_p of a plant or a stand of plants as being mediated by the available energy reaching the leaves and the atmospheric demand (Jarvis & McNaughton, 1986); whilst, for soil scientists, it is the rate of water withdrawn by the roots that controls transpiration (Javaux *et al.*, 2013)

Several examples can be provided of these two visions. Villalobos *et al.* (2013), for instance, developed a model to compute daily transpiration of fruit trees, including olive and almond, a function of the radiation intercepted by the canopy. The model successfully computes E_p when the tree is well-watered but should not be used under water stress conditions. Root models for trees are also available in the literature. Feddes *et al.* (1978), formulated a model of root water uptake with an empirical reduction function to consider the decrease of water withdrawal associated to lowsoil water potential.

However, in modelling the plant-water relations one should be aware of the interaction and the scales at which the different elements of the system work. Transpiration and photosynthesis occur in the leaves and are influenced by the local microclimate conditions, but the demand of water from the leaves must be matched by the uptake from the roots which in turns depends on their spatial distribution and on the soil water content (Clothier & Green, 1994, Williams *et al.*, 1996).

The integration of the root-soil system (supply function) together with the canopy (demand function) to model the soil-plant-atmosphere continuum (SPAC), has been traditionally formulated using the catenary hypothesis first proposed by van den Honert (1948), in which the plant is regarded as an electric circuit composed of resistances in series or in parallel. Several examples of SPAC models for trees using the catenary hypothesis are available in the literature (Williams *et al.*, 1996, Sperry *et al.*, 1998, Deckmyn *et al.*, 2008). The problem is that, in those models there is an unbalanced description of the demand and the supply functions. Whilst the canopy is treated in detail to account for the inherent heterogeneous distribution of leaves and branches, the soil-root part is modelled assuming that only differences in depth are present.

The soil environment is even more heterogeneous in nature than the canopy, especially when anthropic effects like irrigation or other agronomic practices are present. While simple one-dimensional models may be suitable when the soil is uniformly wetted and the roots are evenly distributed, in many field conditions, and particularly for row crops, and/or trees watered with localised irrigation systems, they are not, as very large variations in θ_{soil} throughout the root zone

are present. Big differences in θ_{soil} are usually accompanied by a significant variability in root density as roots tend to grow faster in portions of the soil whose conditions are favourable to their function (Klepper, 1991). In this case, the use of one-dimensional models to compute root water extraction would fail to account for preferential water uptake from the wetted areas or the differences in root activity (Clothier & Green, 1997).

1.6. Objectives and outline of the thesis

The general aim of this thesis is to develop a model able to calculate tree transpiration and water potential of olives and almonds when some degree of water stress is present, considering the heterogeneity in soil water content and root length density and integrating the functioning of the roots and the canopy together with their interactions with the soil and the aerial environment. The specific objectives are:

i) To determine the absorption capacity of roots of olive trees and the GF677 rootstock, the widest used rootstock for almond trees, and the changes of this uptake capacity with temperature.

ii) To formulate a soil-plant-atmosphere continuum model for almond and olive trees to compute root water uptake and tree transpiration and test it using split root plants.

iii) To validate the model in a commercial olive orchard and to provide management irrigation rules based on the analysis performed with the model.

The thesis is presented in chapters, which have the structure used by peer-reviewed publications. The first chapter has been already published and the second has been reviewed and will be resubmitted after the necessary corrections. Each chapter deals with one of the specific objectives listed above.

In Chapter 2 the water uptake capacity of the two species of interest is studied and empirical functions to calculate root radial resistance as a function of soil temperature are determined. The implications of such functions are then studied using two consecutive years of soil temperature measurements.

In Chapter 3 a soil-plant-atmosphere model based on a multi-compartment solution to account for root and soil water heterogeneity is formulated. Then the model is tested, using sap flow, time domain reflectrometry and weight changes in split root trees placed on specially designed lysimeters. The errors of the model are discussed and possible explanations are provided.

Finally, in Chapter 4 model predictions of tree transpiration and water potential are compared with measurements in a hedgerow commercial olive orchard monitored with sap flow sensors in which periodic measurements of leaf water potential were performed. Simulation experiments are then used to study the effect of soil wetted area on tree transpiration, which has important practical consequences.

References

Boote K.J., Jones J.W. & Pickering N.B. (1996) Potential Uses and Limitations of Crop Models. *Agronomy Journal*, **88**, 704-716.

Campbell G.S. & Norman J.M. (1998) *Introduction to environmental biophysics*. (2nd ed.). Springer, New York.

Clothier B.E. & Green S.R. (1994) Rootzone processes and the efficient use of irrigation water. *Agricultural Water Management*, **25**, 1-12.

Clothier B.E. & Green S.R. (1997) Roots: The big movers or water and chemical in soil. *Soil Science*, **162**, 534-543.

Chalmers D.J., Mitchell P.D. & Vanheek L. (1981) Control of peach-tree growth and productivity by regulated water-supply, tree density, and summer pruning. *Journal of the American Society for Horticultural Science*, **106**, 307-312.

Charles-Edwards D.A., Doley D. & Rimmington G.M. (1986) *Modelling plant growth and development*. Academic Press.

De Wit C.T. (1958) *Transpiration and Crop Yields*. Institute of Biological and Chemical Research on Field Crops and Herbage.

Deckmyn G., Verbeeck H., Op de Beeck M., Vansteenkiste D., Steppe K. & Ceulemans R. (2008) ANAFORE: A stand-scale process-based forest model that includes wood tissue development and labile carbon storage in trees. *Ecological Modelling*, **215**, 345-368.

dePury D.G.G. & Farquhar G.D. (1997) Simple scaling of photosynthesis from leaves to canopies without the errors of big-leaf models. *Plant Cell and Environment*, **20**, 537-557.

FAO (2016) Proportion of total water withdrawal withdrawn for agriculture.

Feddes R.A., Kowalik P.J. & Zaradny H. (1978) *Simulation of Field Water Use and Crop Yield*. Wiley.

Fereres E. & Connor D.J. (2004) Sustainable water management in agriculture In: *Challenges of the New Water Policies for the XXI Century: Proceedings of the Seminar on Challenges of the New Water Policies for the 21st Century* (eds E. Cabrera & R. Cobacho), pp. 157-170. Swets & Zeitlinger, Lisse,Netherlands.

Fereres E., Goldhamer D.A. & Parsons L.R. (2004) Irrigation water management of horticultural crops (vol 38, pg 1040, 2004). *Hortscience*, **39**, 201-201.

Fereres E. & Soriano M.A. (2007) Deficit irrigation for reducing agricultural water use. *Journal of Experimental Botany*, **58**, 147-159.

García-Tejera O. (2011) *Caracterización fenológica de variedades de girasol para siembra temprana* Master Thesis, Universidad de Córdoba.

Gimeno V., Fernández-Martínez J.M. & Fereres E. (1989) Winter planting as a means of drought escape in sunflower. *Field Crops Research*, **22**, 307-316.

Girona J., Mata M., Goldhamer D.A., Johnson R.S. & Dejong T.M. (1993) Patterns of soil and tree water status and leaf functioning during regulated deficit irrigation scheduling in peach. *Journal of the American Society for Horticultural Science*, **118**, 580-586.

Goldhamer D.A., Viveros M. & Salinas M. (2006) Regulated deficit irrigation in almonds: effects of variations in applied water and stress timing on yield and yield components. *Irrigation Science*, **24**, 101-114.

Iniesta F., Testi L., Orgaz F. & Villalobos F.J. (2009) The effects of regulated and continuous deficit irrigation on the water use, growth and yield of olive trees. *European Journal of Agronomy*, **30**, 258-265.

IPCC (2013) *Working Group II Report "Impacts, Adaptation and Vulnerability"*. IPCC.

Jarvis P.G. & McNaughton K.G. (1986) Stomatal control of transpiration - scaling up from leaf to region. *Advances in Ecological Research*, **15**, 1-49.

Javaux M., Couvreur V., Vander Borght J. & Vereecken H. (2013) Root Water Uptake: From Three-Dimensional Biophysical Processes to Macroscopic Modeling Approaches. *Vadose Zone Journal*, **12**.

Klepper B. (1991) Crop root system response to irrigation. *Irrigation Science*, **12**, 105-108.

MAGRAMA M.d.A.A.y.M.A. (2012) Anuario de estadística.

Morales A., Leffelaar P.A., Testi L., Orgaz F. & Villalobos F.J. (2016) A dynamic model of potential growth of olive (Olea europaea L.) orchards. *European Journal of Agronomy*, **74**, 93-102.

Passioura J.B. (1979) Accountability, philosophy and plant physiology. *Search*, **10**, 347-350.

Sperry J.S., Adler F.R., Campbell G.S. & Comstock J.P. (1998) Limitation of plant water use by rhizosphere and xylem conductance: results from a model. *Plant Cell and Environment*, **21**, 347-359.

Testi L., Villalobos F.J., Orgaz F. & Fereres E. (2006) Water requirements of olive orchards: I simulation of daily evapotranspiration for scenario analysis. *Irrigation Science*, **24**, 69-76.

Thornley J.H.M. & Johnson I.R. (2000) *Plant and Crop Modelling: A Mathematical Approach to Plant and Crop Physiology*. Blackburn Press.

van den Honert T.H. (1948) Water transport in plants as a catenary process. *Discussions of the Faraday Society*, **3**, 146-153.

Villalobos F.J., Hall A.J., Ritchie J.T. & Orgaz F. (1996) OILCROP-SUN: A Development, Growth, and Yield Model of the Sunflower Crop. *Agronomy Journal*, **88**, 403-415.

Villalobos F.J., Testi L., Orgaz F., García-Tejera O., Lopez-Bernal A., González-Dugo M.V., Ballester-Lurbe C., Castel J.R., Alarcón-Cabañero J.J., Nicolás-Nicolás E., Girona J., Marsal J. & Fereres E. (2013) Modelling canopy conductance and transpiration of fruit trees in Mediterranean areas: A simplified approach. *Agricultural and Forest Meteorology*, **171–172**, 93-103.

Wallace J.S. (2000) Increasing agricultural water use efficiency to meet future food production. *Agriculture, Ecosystems & Environment*, **82**, 105-119.

Williams M., Rastetter E.B., Fernandes D.N., Goulden M.L., Wofsy S.C., Shaver G.R., Melillo J.M., Munger J.W., Fan S.M. & Nadelhoffer K.J. (1996) Modelling the soil-plant-atmosphere continuum in a Quercus-Acer stand at Harvard forest: The regulation of stomatal conductance by light, nitrogen and soil/plant hydraulic properties. *Plant Cell and Environment*, **19**, 911-927.

Chapter 2

Effect of soil temperature on root resistance: implications for different trees under Mediterranean conditions

Chapter 2

Effect of soil temperature on root resistance: implications for different trees under Mediterranean conditions

Summary

The effect of temperature on radial root hydraulic specific resistance (R_p) is a known phenomenon; however, the impact of R_p variations expected from soil temperature changes over the tree root system is unknown. The present chapter analyses the relations of R_p with temperature in olive 'Picual' and a hybrid rootstock, GF677, at five different temperatures, showing that a variation of 3 and 4.5 folds exists for olive 'Picual' and GF677 in the range from 10 to 20 ºC. The functions obtained were scaled up to show the theoretical changes of total radial root system resistance (*RR*) in a common tree orchard in a Mediterranean climate at a daily and seasonal scale, using recorded soil temperature values: a difference between summer and winter of: 3.5 for olive 'Picual' and 9 folds for GF677 was observed. Nevertheless, R_p changes are not only related with temperature, but, cavitation or circadian rhythms in aquaporin expression may play a role. The results obtained from an experiment with the two cultivars submitted to constant pressure and temperature during several hours exhibited a variation in R_p, but this was of lower magnitude than that observed due to temperature changes. Finally, a comparison of R_p at 25ºC between GF677 and GN15 (another rootstock obtained from the same parental as GF677) showed significant differences. According to our results, diurnal and seasonal changes in R_p due to temperature

variations are of significant importance and it would therefore be advisable to assess them explicitly into soil-plant-atmosphere continuum (SPAC) models.

2.1. Introduction

Models of the soil plant atmosphere continuum (SPAC) are powerful tools to improve our insight into plant water relations traits. The movement of water through the plant can be compared to an electric circuit composed of a catena of resistances in series or parallel and with the differences in water potential as the driving force. This simplification of the hydraulic system was first proposed by van den Honert (1948) and is widely used in SPAC models (Williams *et al.*, 2001, Couvreur *et al.*, 2012). According to that simple approach, plant transpiration (E_p) can be written as:

$$E_p = \frac{\Psi_s - \Psi_l}{R_{soil} + R_{plant}} \quad (1)$$

Where R_{soil} is the soil resistance, i.e., the resistance of water movement from the soil to the root xylem, R_{plant} is the plant resistance that includes the resistance of the xylem of roots, stem and branches and Ψ_s and Ψ_l are soil and leaf water potential respectively. If one focuses on the soil part of the equation, R_{soil} can be divided into two resistances in series: the hydraulic specific resistance of the soil (R_s) for the movement of water from the bulk soil to the root surface and the hydraulic specific resistance of the root in the radial direction (R_p), that is, the resistance from the root surface to xylem vessels. The equation now would be

$$E_p = \frac{\Psi_s - \Psi_l}{R_s + R_p + R_{plant}} \quad (2)$$

According to equation 2, variations in R_p due to shifts in the root environment would affect plant transpiration, but how important is R_p in relation to the other terms of equation 2?

Experiments on trees have revealed that shoot and root resistances are approximately equal (Tyree & Zimmermann, 2002a). When the soil is wet, R_s is much lower than R_p (Campbell, 1985); hence R_{soil} would be approximately equal to R_p. If R_{plant} and R_{soil} are nearly the same, in theory, the changes in R_p would have a significant impact on E_p under the above-mentioned conditions.

Variations in E_p due to shifts in root temperature have been described for different species (Kramer, 1940, Running & Reid, 1980, Lee *et al.*, 2004). Still in the nineteenth century, Sachs (1870) observed that well-watered tobacco plants growing in conditions of low evaporative demand wilted when soil temperature was decreased to 3 ºC and they recovered when the soil was warmed to 12 ºC. Kramer (1940) and Ameglio *et al.* (1990) also observed a reduction in E_p of around 80% in tomato and sunflower, when the root system was cooled down to 5 and 2.7 ºC respectively, as compared to its values at 20 ºC. The changes on transpiration are not unique to herbaceous species; trees like *Populus tremuloides* Michx., *Quercus rubra* L. or *Olea europea* L., also show a reduction in transpiration when the temperature of the root system is decreased below a certain value (Pavel & Fereres, 1998, Wan *et al.*, 2001, Apostol *et al.*, 2007).

Different hypotheses have been proposed to explain the effect of low root temperature on the reduction in E_p. The increase of water viscosity as temperature decreases has been suggested as the main factor for reducing water flow from the soil to the plant (Yamamoto,

1995, Hertel & Steudle, 1997). Other authors hypothesized that the phenomenon originates from changes in membrane permeability due to modifications of its fluidity, or reductions in the activity of membrane aquaporins (Running & Reid, 1980, Ameglio *et al.*, 1990, Wan *et al.*, 2001). Leaving aside the mechanisms involved, it seems to be clear that changes in root temperature modify radial root hydraulic specific conductance, or its inverse, R_p.

Environmental factors are not the exclusive causal agents for changes in R_p, but the plant itself presents endogenous rhythms related to its ability to uptake water. Henzler *et al.* (1999) found a 24-h cycle of one order of magnitude in *Lotus japonicas* L. when the root system was submitted to a constant pressure. The authors attributed those changes to a circadian rhythm in the aquaporin expression of the root system. Besides, Tyree and Zimmermann (2002b) discovered a 24-hour cyclic pattern of the same order of magnitude in root water conductivity in plants whose roots were held at a constant pressure for three days. In their experiment, carried out with tobacco plants using a wild type and a mutant with the NtAQp1 aquaporin protein suppressed, both the mutant and the wild type showed exactly the same pattern, suggesting that no aquaporin was involved in the circadian cycle or at least that type of aquaporin.

Although variations in R_p among cultivars, soil conditions and even according to endogenous rhythms have been widely described in the literature, the value of R_p used to compute root water uptake in SPAC models is usually a fixed parameter (Doussan *et al.*, 1998, Williams *et al.*, 2001). However, Mellander *et al.* (2006) demonstrated that a significant improvement in the prediction of transpiration can be

achieved by taking into account the delayed temperature of the soil during the spring season using the empirical reduction function of E_p proposed originally by Axelsson and Ågren (1976).

As far as we know, the effect of temperature on R_p is unknown for olive and fruit tree rootstocks. For that reason the aims of the present chapter are: a) to study the variations of R_p with temperature for olive (*Olea europaea* L.) 'Picual' and *Prunus amygdalus* L. *x Prunus persica* L. 'GF677', the former being one of the more extensively grown olive oil cultivars in Spain while the latter is a widely used hybrid rootstock for peach, plum and almond trees; b) analyse the effect of the above-mentioned variations of R_p with temperature in a tree orchard, using recorded soil temperature data and scaling up from a single root to an entire root system using reported values of root length density (L_v); c) study the presence or absence of other sources of variation in R_p other than temperature, like a circadian rhythm; and finally d) compare R_p values of the above-mentioned 'GF677' rootstock with *P. amygdalus x P. persica* 'GN15', another rootstock with the same parental species.

2.2. Materials and methods

2.2.1. Plant Material

The experiment was performed with rooted cuttings of Olive 'Picual' and of two hybrid rootstocks of *P. amygdalus x P. persica*, 'GF677' and 'GN15', obtained from commercial nurseries in Spain. Hereinafter we will refer to each of the two hybrid rootstocks studied as GF677 and GN15, while the term "olive" alone is to be intended as

the cultivar 'Picual'. The one year old cuttings were transported from the nursery to the experimental greenhouse in August (both Prunus) and September 2014 (olive). Once in the experimental greenhouse, cuttings were planted in pots filled with peat moss, where they were irrigated every day in order to avoid water stress. The cuttings stayed no longer than one month in the greenhouse before starting the measurements in the growth chamber. Table 2.1 presents the mean values and the standard deviation (SD) for height and root area of the cuttings used in the experiments. Cuttings were transferred from the greenhouse to the growth chamber three days before the start of the experiments to allow for adaptation.

Table 2.1. Shoot height and total root area for the cultivars used in this study.

	Shoot height (m)	***Root area*** (m^2)
Olive	0.15 ± 0.05 (n=25)	0.012 ± 0.0040 (n=25)
GF677	0.30 ± 0.07 (n=25)	0.022 ± 0.010 (n=25)
GN15	0.28 ± 0.05 (n=5)	0.0074 ± 0.0029 (n=5)

All the measurements were done in one growth chamber with controlled temperature, monitored continuously using a datalogger (MicroLite, Fourier Systems, USA) and a fixed 14-hour photoperiod with fluorescent lights at 360 μmoles m^{-2} s^{-1}. All the necessary material to perform the experiment was left inside the growth chamber in order to keep everything at the same temperature as the plant material.

2.2.2. Experiment 1: determination of the radial root hydraulic specific resistance at different temperatures

The radial root resistance at five temperatures, namely 10, 15, 20, 25 and 30 ºC, were measured for GF677 and olive cuttings using four plants for each temperature. At each air temperature, the four cuttings were transferred from the greenhouse to the growth chamber. Values of R_p at each temperature were measured using a pressure chamber (Soil Moisture Equipment Corp., Santa Barbara, CA, USA) adapted to measure flow from a root system. To this end, a pot filled with water was set into the pressure vessel of the chamber in order to supply water to the root system. Plants were extracted from their pots and immersed in water to remove part of the substrate taking extreme care to not disturb the root system. Then the upper part of the cuttings were cut 5 cm above the plant collar; the remaining shoot stub was covered with paraffin from the collar to 1 cm below the cut in order to avoid any radial flux of water into it. The detached root system was then fixed to the specimen holder of the pressure chamber using an appropriate rubber seal, in such a way that after the chamber closure the root system was completely immersed in water. All the measurements were performed inside the growth chamber at the corresponding temperature (± 0.5 ºC) to avoid any thermal shock to the root system.

Four different pressures were applied at each temperature: 0.4, 0.6, 0.8 and 1.2 MPa. The xylem sap flowing through the root system at each pressure was collected during periods of 15 minutes using cotton-filled sample tubes previously weighted in a four decimal precision balance (model AV104, Mettler Toledo, Greifensee, Switzerland).

The mass of the sample tube plus the xylem sap after 15 minutes was obtained from the same precision balance. The flux was then calculated by dividing the difference of dry and wet mass of the tube by the time interval. The process was repeated until the difference in flux between measurements was less than 0.5 ‰. Obtaining a steady value for the flux usually took from 30 to 50 minutes.

Once the fluxes at the given temperature and at the five pressures were obtained, the root system was carefully washed with water to remove all the remaining substrate and was then scanned using a commercial scanner (HP Scanjet G3110). Values of root length average diameter and total root surface were obtained using the WinRhizo software (Regent Instruments Inc, Quebec City, Canada).

The inverse of the slope of the linear fit of flux versus pressure was taken as the total root radial resistance of the plant at the corresponding temperature. R_p of each plant was then obtained by dividing the total root radial resistance by its total root surface, assuming a maximum diameter of 1.4 mm for an absorbing root. For each temperature, R_p was averaged for the 4 plants.

The function of R_p vs. temperature in olive and GF677 cuttings was fitted using the software TableCurve 2D (SYSTAT software Inc, San Jose, California); and fitted using a power function as proposed by Ameglio et al. (1990).

2.2.3. Experiment 2: rootstocks comparisons

Values of R_p for the two rootstocks were obtained following the same method as in experiment 1. During the experiment the temperature was kept at 25 ºC. Five cuttings of both GF677 and GN15 were used.

An analysis of variance (ANOVA) was applied to compare the R_p values of the two rootstocks.

2.2.4. Experiment 3: Test of stability of radial root hydraulic specific resistance in steady conditions

The validity of the relationships from experiment 1 and 2 are subjected to the absence of other sources of variation in R_p during the measurements, such as circadian rhythms related to daily variations in the expressions of aquaporins (Henzler *et al.*, 1999), cavitation in the xylem vessels (Espino & Schenk, 2011) or any other cause of instability. The presence of such behaviours would cause errors in the measurements of experiments 1 and 2, and a consequent incorrect function of temperature. To determine the presence and magnitude of endogenous rhythms or any other variation of R_p not related to temperature changes, a stability test in cuttings of olive and GF677 was performed. The temperature of the growth chamber was fixed at 30 ºC and a constant pressure of 0.4 MPa was maintained in the pressure chamber. Values of R_p during 5 hours (from 9:00 to 14:00 UTC) were obtained for both species, following the same procedure described for experiment 1. The experiments of stability for the two species were started at the same relative circadian time as experiment 1, i.e., 8 hours after turning the chamber lights on.

2.2.5. Soil temperature and scaling-up of radial root hydraulic specific resistance

To scale the variation of the radial resistance with the soil temperature up to the whole root system, an elementary model was used. The scaling up for the entire root system can be done by invoking the

electric circuit similarity proposed by van den Honert (1948). For our purposes, the specific resistance of the electric circuit is R_p, which varies with the temperature. R_p represents the resistance per square meter of root surface. To use root length density (L_v) as a scaling factor, a conversion from square meter of root surface to square meter of soil must be done using an average root radius (a_{root}). L_v is then distributed through different layers in the soil and *RR* (the resistance per square meter of soil of the whole root system) is computed as:

$$RR = \frac{1}{\sum \frac{2\pi\, a_{root}\, d_i Lv_i}{R_p(T) i}} \quad (3)$$

Where *d* is the thickness of soil layer *i*.

Soil temperature profile data was recorded over 3 years, from June 2002 to September 2004, in an experimental olive orchard at the "Alameda del Obispo" experimental farm located in Cordoba, Spain (37°52′ N, 4°49′ W). The climate is Mediterranean, with mild and rainy winters and very hot and dry summers; in the period of data collection the maximum and minimum air temperatures were 47.1 ºC and -1.1 ºC, registered on 01/08/2003 and 20/01/2004, respectively. The soil is a "TypicXerofluvent" of sandy-loam texture. Soil thermocouples (type K) were installed at five depths: 5, 10, 20, 40, and 80 cm; the thermocouples outputs were read every minutes, and 10-min averages were recorded with a datalogger (Type CR10X, Campbell Scientific Inc., Logan, UT, USA). The orchard had a tree density of 400 trees ha^{-1} and was planted in 1995. In August 2002 the orchard had a Leaf Area Index of 2.0 (measured with a plant canopy

analyser, model LAI-2000, LI-Cor, Lincoln, NE, USA) and the canopy covered 45% of the ground; it maintained these characteristics during the entire measurement period. The profile was obtained along the row, at ¼ of the distance between two adjacent trees of average dimension and canopy shape, inside the dripper wet zone but near its edge; this position was chosen as representative of the soil volume occupied by most of the root system.

Daily variations of R_p with soil temperature were computed using recorded values every 10 minutes at each soil layer. For the seasonal variation analysis, in turn, noon temperatures were used. In order to scale from R_p vs. temperature to *RR* using equation 3, average root radius data obtained from experiment 1 was used. In addition, root length density values reported by Searles *et al.* (2009) from an intensive olive plantation and Abrisqueta *et al.* (2008) for a GF677 grafted peach orchard, have been used to compute *RR*. A summary of the input values used for *RR* calculations is presented in table 2.2.

Table 2.2. Input parameters for the model proposed in equation 4. Values for root length density have been obtained from Searles et al. (2009) for olive and from Abrisqueta et al (2008) for the GF677 rootstock. Average root radiuses have been obtained from the scanned root systems of the plants of experiment 1. In the table, L_v, d and a_{root} are root length density, layer depth and root radius.

Soil depth (m)	***L_v Olive*** ($m\ m^{-3}$)	***L_v GF677*** ($m\ m^{-3}$)	***d*** (m)	***a_{root} Olive*** (m)	***a_{root} GF677*** (m)
0.05	21200	14000	0.05	0.00027	0.0003
0.1	19800	4700	0.05	"	"
0.2	17200	4700	0.1	"	"
0.4	12500	14200	0.2	"	"
0.8	5540	9500	0.4	"	"

No extrapolation was applied outside the lower range of temperatures of experiment 1 from which the functions were obtained, meaning that soil temperatures data below 10 ºC were not considered. This rule has been applied because cell membrane functionality below this temperature could not be studied.

2.2.6. Data analysis

Statistical analysis of the data was performed using the program Statistic (Statistix9 for Windows, Analytical Software, Tallahassee, FL, USA). An ANOVA was used to compare the two almond rootstock using the Tukey test with a level of significance of $p < 0.05$.

2.3. Results

2.3.1. Experiment 1: effect of the temperature on radial root hydraulic specific resistance

The pressure-flow functions showed a linear relationship at all temperatures and for all the species (Fig. 2.1), thus a linear fit was used to compute the slope. The average R_p values obtained from the inverse of the slopes at each temperature are presented in Fig. 2.2. The average values present an increase in R_p as the ambient temperature is decreased from 30 to 10 ºC, with a 6.0 fold difference for olive and a 9.5 fold difference for GF677, between the point at 30 ºC and the one at 10 ºC.

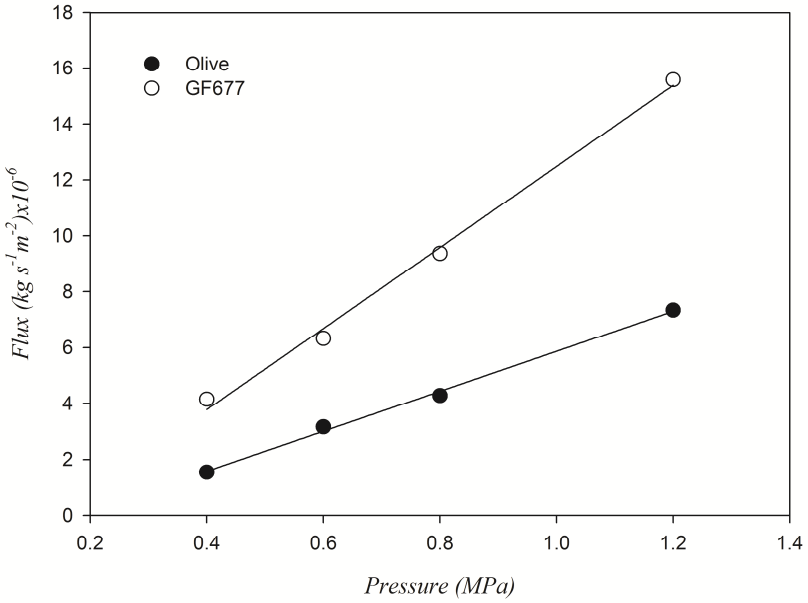

Fig 2.1. Examples of flux-pressure relations measured at 25ºC in olive and the GF677 rootstock. The lines represent the linear fits. For Olive (R^2=0.99 p<0.001) and GF677 (R^2=0.99 p<0.001).

The average R_p values obtained for the GF677 rootstock were always lower than for olive trees except at 15 ºC; at that point the value of R_p of both species is nearly the same.

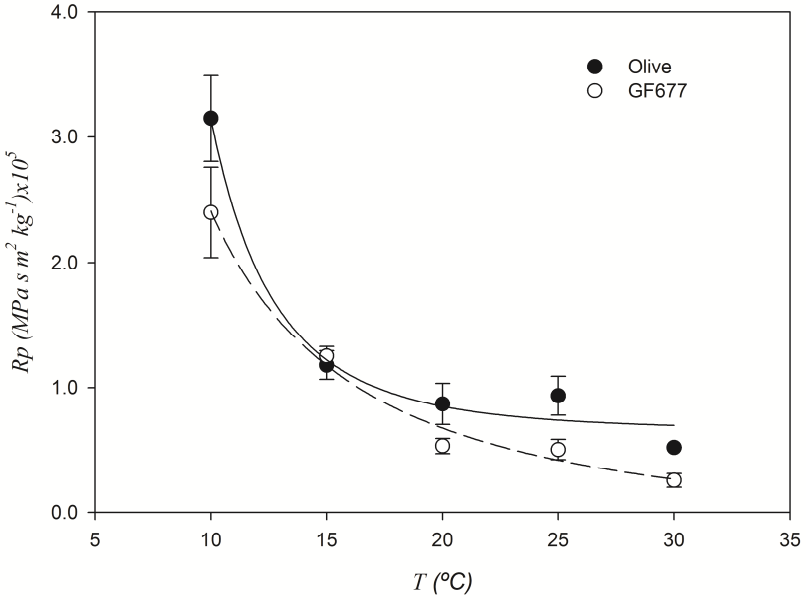

Fig 2.2. Specific root resistance (R_p) at different temperatures for olive and GF677 rootstock. Means and standard deviations (n=4) are shown. The fitted equations for olive and GF677 are: $R_p = 64934.88 + 1.09 \cdot 10^9 T^{-3.64}$(solid line) and $R_p = -19593.29 + 1.000 \cdot 10^7 T^{-1.58}$(dotted line). Adjusted R^2 and significance levels are $R^2 = 0.98$, $p < 0.016$ for olive and $R^2 = 0.99$, $p < 0.011$ for the GF677.

A three parameter power function has been fitted for the two species:

Olive:$R_p = 64934.88 + 1.09 \cdot 10^9 T^{-3.64} (R^2 = 0.98, p < 0.016)$

(4)

GF677: $R_p = -19593.29 + 1.00 \cdot 10^7 T^{-1.58} (R^2 = 0.99, p < 0.011)$

(5)

Where R_p has the dimensions of MPa s m^2 kg^{-1}

2.3.2. Experiment 2: comparison between rootstocks

R_p at 25 ºC was $5.00 \cdot 10^4 \pm 8.22 \cdot 10^3$ MPa s m^2 $kg^{-1}$for GF677 and only $1.40 \cdot 10^4 \pm 2.81 \cdot 10^3$MPa s m^2 kg^{-1} for GN15; this difference resulting highly significant ($p<0.01$).

2.3.3. Experiment 3: Stability test of radial root hydraulic specific resistance in olive and GF677

The resistance at a constant pressure changed over time in a different way for the two studied cuttings. Olive plants maintained a quasi-steady value during the whole experiment, reducing R_p less than 10%. In the GF677, on the contrary, plants showed a larger variation, increasing linearly until a maximum of 40% at the end of the experiment (Fig. 2.3). Temperature was closely monitored and recorded during both experiments; it decreased 0.9 ºC and 0.4 ºC during the olive and GF677 experimental measurements, respectively.

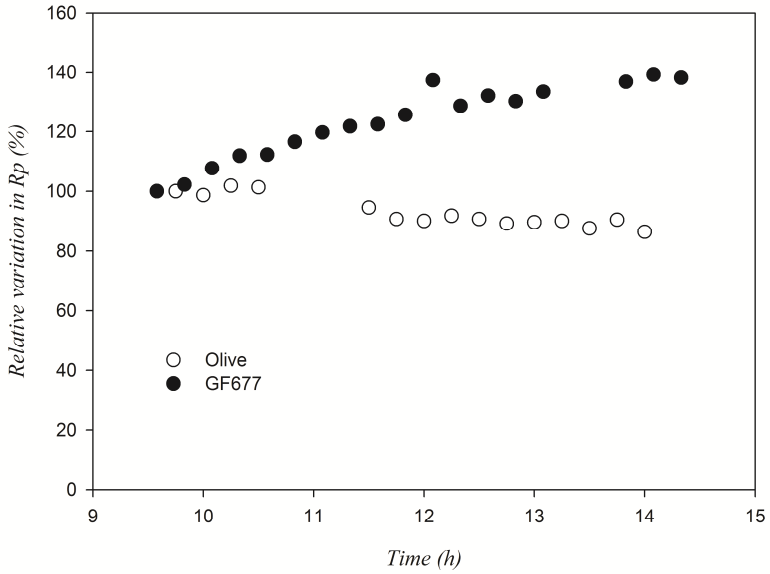

Fig 2.3. Variations in R_p at a fixed pressure (0.4 MPa) for olive (open circles) and the GF677 rootstock (closed circles) during five hours of measurements.

2.3.4. Scaling-up the radial root hydraulic specific resistance to the whole root system

Equations 3, 4 and 5 were used to compute the variations in *RR* of olive and GF677 due to the daily and seasonal cycles of soil temperature through two consecutive winters; the results are presented in Fig. 2.4 and 2.5. Gaps during winter periods correspond to soil temperatures below the range covered by equations 4 and 5, i.e., 10 ºC.

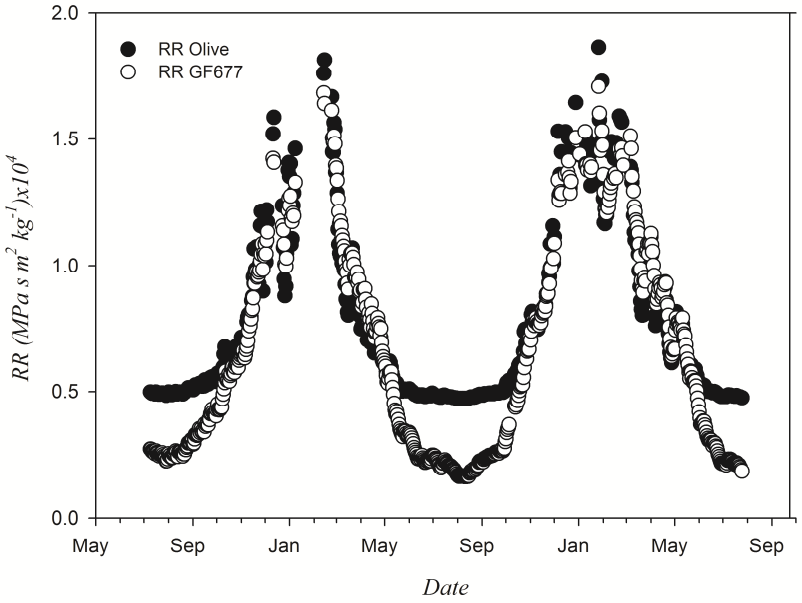

Fig 2.4. Calculated values of *RR* for olive (closed circles) and the GF677 rootstock (open circles). Each point represents the *RR* value obtained using noon temperatures at each of the five soil layers for the two consecutive winters. The gaps during the winter periods correspond to non-computed values because the temperature in one or more layers was below 10ºC.

The computations with the model using the function for olive gave rather steady *RR* values around $0.5 \cdot 10^4$ MPa s m^2 kg^{-1} for the whole summer (Fig. 2.4). *RR* increased from the first days of autumn until the end of the winter, reaching its maximum value around $1.5 \cdot 10^4$MPa s m^2 kg^{-1} (about 3.5 times the summer *RR*) in February of both years. When the winter ended, *RR* decreased quickly during the spring, reaching the summer value again at the beginning of June. GF677 showed a less stable root resistance during the summer period (Fig. 2.4), changing its *RR* from $0.2 \cdot 10^4$ MPa s m^2 kg^{-1} in early June, to

$0.15 \cdot 10^4$ MPa s m^2 kg^{-1} in early August. Fluctuations of *RR* along the season followed a similar pattern as in olive, rising from the lowest values of the summer to a peak around $1.46 \cdot 10^4$ MPa s m^2 kg^{-1} during the winter period for both years.

Fig. 2.5 compares two examples of the computed daily variations of *RR* for a winter and a summer day; air temperature is also shown. Dotted lines mark the time of dawn and twilight. Time of maximum and minimum values of *RR* appeared to be independent of the season, with the maximum value occurring one hour after dawn and the minimum value occurring between 1400 and 1500 UTC. While the time of maximum *RR* was coincident with the time of minimum air temperature, the minimum value of *RR* occurred around two hours before the time of maximum air temperature. Differences between the maximum and the minimum values of *RR* in different seasons were related to the different amplitude of soil temperature diurnal waves.

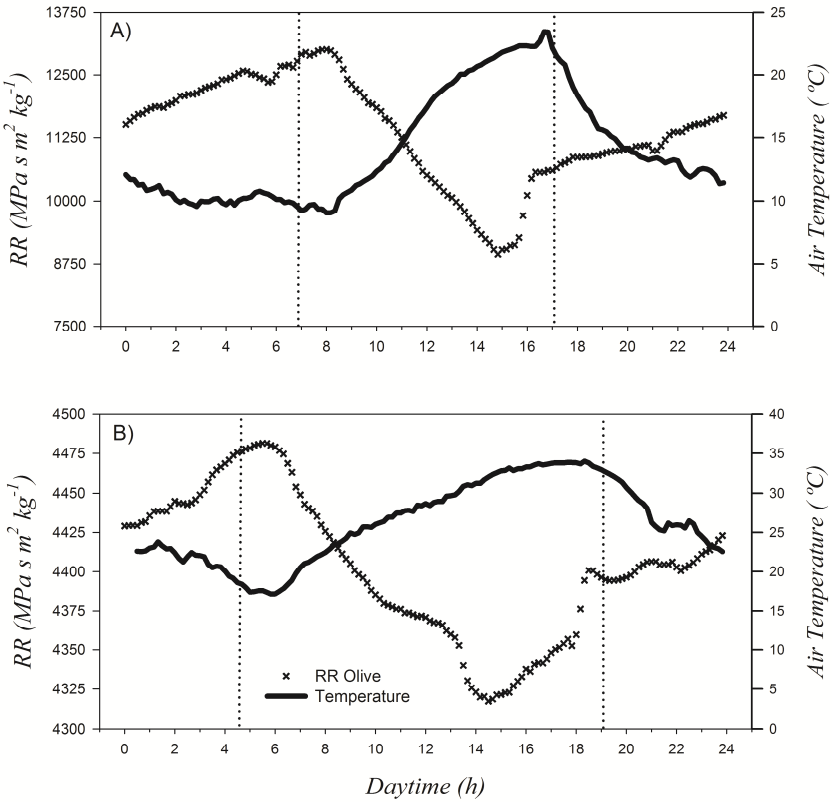

Fig 2.5. Daily variations of calculated *RR* (crosses) for olive and the corresponding air temperature (solid line) during a winter and summer day. Graph A correspond to DOY 34 (February) and graph B correspond to DOY 184 (June). Dotted lines represent dawn and twilight hours.

2.4. Discussion

The results of experiment 1 show that an increase in R_p (both for olive and the GF677 rootstock) occurs when the root system is exposed to low temperatures. Our calculations suggest that this effect would have an implication for modelling transpiration in periods when soil temperature is relatively low (Fig. 2.2, Fig. 2.4 and Fig. 2.5).

Differences in the water uptake ability of the roots between cultivars has also been exposed in experiment 2, showing that significant differences in the absolute values of R_p can be expected within the same species.

2.4.1. Variations of plant resistance

Values of R_p reported in the literature for other species refer to a single temperature, usually 20 ºC. At that temperature, large interspecific differences can be found, ranging from $3 \cdot 10^7$ MPa s m^2 kg^{-1} for maize (*Zea mays* L.), $1 \cdot 10^{10}$ MPa s m^2 kg^{-1} for *P. tremuloide*s or $1 \cdot 10^5$ MPa s m^2 kg^{-1} for sunflower (*Helianthus annuus* L.) (Frensch & Steudle, 1989, Ameglio *et al.*, 1990, Wan *et al.*, 2001). In his work with sunflower, Ameglio *et al.* (1990), reported an increase of one order of magnitude at 4 ºC regarding to its value at 20 ºC; Running and Reid (1980) in *Pinus contorta* Douglas and Norisada *et al.* (2005) in *Cryptomeria japonica* D.Don accounted for a relative variation of 4.4 and 2.2 folds for a temperature range of 20 to 0 ºC in the first case and 30 to 5 ºC in the second. The relative change on R_p with temperature found in olive and GF677 is shown in Fig. 2.6. The results are closer to those found in sunflower by Ameglio *et al.* (1990) than for the other species in the literature.

The underlying mechanism for the observed changes in R_p has been a matter of controversy since the first experiments developed by Kramer (1940) with tomato plants. In his work, variations in water viscosity were suggested as the main factor producing the increases in R_p and the observed reductions in transpiration. Later studies have shown that under low temperatures (below 15 ºC), increases in R_p do not follow the expected changes in water viscosity, and modifications in cell

membrane structure and /or aquaporin number and activity have been hinted as the responsible cause (Kaufmann, 1975, Kaufmann, 1977, Grossnickle, 1988, Wan *et al.*, 2001). Kuiper (1964), first proposed that combinations of both factors (water viscosity and modifications in the membrane structure) are involved in the phenomenon. The author pointed out that a critical threshold value exists, and the temperatures below that limit trigger changes in membrane structure, increasing R_p to a greater extent than that expected by the increase in water viscosity. Our results fully support Kuiper's hypothesis: Fig. 2.6 represents our measurements of the relative changes to R_p together with the relative variations in water viscosity, calculated following (Roderick & Berry, 2001). The change in water viscosity does not explain the observed changes in R_p when the temperature is lower than 15 ºC, a threshold that seems common to both cultivars analysed (Fig. 2.6). Wan *et al.* (2001) came to the same conclusion with *P. tremuloides,* finding a relative variation in R_p of 3.5 times when changing root temperature from 20 to 5 ^{o}C while water viscosity only varied 1.5 times for the same temperature range. Fig. 2.6 also shows that the deviation from the viscosity is not only produced at low temperatures; both olive and GF677 exhibit lower values of R_p than that expected due to viscosity changes at 30 ºC. This is in accordance with the observations made by Cochard *et al.* (2000) for *Quercus robur* L.

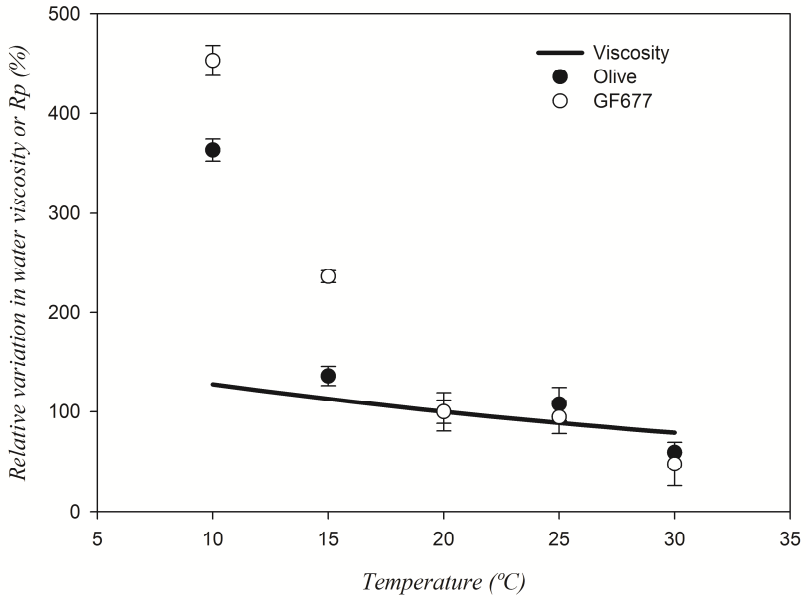

Fig 2.6. Relative variation in viscosity and R_p for olive (closed circles) and the GF677 rootstock (open circles) regarding to its value at 20 ºC. The line represents the computed variation of the viscosity with the temperature using the equation proposed by Roderick and Berry (2001). The circles are the means and the bars represents the SD (n=4).

Although these important variations of R_p with temperature have been described for various species, the practical implications of a temperature-dependent R_p in modelling E_p are unknown. Figures 2.4 and 2.5 represent an attempt of quantifying total root resistance changes as a function of soil temperature in a real orchard. The seasonal thermal regime of a given soil is determined by the climate, the degree of shading and the soil hydrological and physical characteristics. In this sense, the experimental site used to collect soil temperature profile data is reasonably representative of an irrigated,

intensive tree orchard in southern Spain on a medium texture soil, with minor or null regard to what the cultivated species actually is.

Values of *RR* presented in Fig. 2.4 exhibit variations between summer and winter around 3.5 times for olive, and 9 times for GF677. Experiments have revealed that a reduction of stomatal conductance occurs due to changes in the soil temperature environment (Kaufmann, 1982, Wan *et al.*, 2001, Apostol *et al.*, 2007). The observed reduction in stomatal conductance has been explained by the larger increase of *RR* in relation to R_{plant} when the root environment is chilled (Running & Reid, 1980, Pavel & Fereres, 1998). In fact, for olives in the field, water-stress-like behaviour under wet soil conditions (when R_s is negligible compared to R_p) is frequent under Mediterranean climates, where rain is concentrated during winter and spring. This phenomenon has been demonstrated to be related to an increase in *RR* of the tree (Lopez-Bernal *et al.*, 2015).

The *RR* increases during winter in GF677 are of course less relevant on a practical basis, as GF677 is always grafted with deciduous scions, which leafless period varies with the climate of the area and with the species/cultivar of the scion. Nevertheless, when transpiring leaves are present during spring and autumn, a significant variation in *RR* may still be expected as it can be observed in Fig. 2.4. Apostol *et al.* (2007) demonstrated that the lower soil temperatures during spring in the deciduous tree *Q. rubra* significantly reduce *Ep* and the stomatal conductance; early shooting fruit scions may well experience significantly higher *RR* than in summer with an already considerable leaf area. For example, an almond scion grafted on GF677 would have to deal with *RR* around $0.64 \cdot 10^4$ MPa s m^2 kg^{-1} at the end of April

(Fig. 2.4), meaning 3.5 folds the *RR* of July with a leaf area only 30% less than that of full summer (E. Fereres, personal communication).

It must be considered that in the simulation of Fig. 2.4 a fixed value of L_v has been applied for the entire simulation period, meaning that *RR* could be overestimated for the intervals where new root production occurs. Fernández *et al.* (1992), observed for Olives 'Manzanillo' under different irrigation regimes that root production is concentrated in late spring and in early autumn for rainfed trees, while for irrigated trees, root production occurs from spring to autumn. In a more general study on temperate tree species, McCormack *et al.* (2014) discovered that most new root production is concentrated during late spring (and also during late summer); periods where *RR* in the simulation (Fig. 2.4) is at its minimum. Hence, including L_v changes in the model simulation would likely increase the difference between the seasons.

Giving attention to the summer period, a remarkable difference in the trend of *RR* can be observed in Fig. 2.4 for both cultivars. While a reduction of 6 folds in *RR* from May to August appears in the GF677 rootstock, *RR* remains almost constant for olive at the same period. This behavioural difference can be explained by the different sensibility of R_p to higher temperatures (over 20 ºC) of both cultivars presented in Fig. 2.2. It would be expected that under the same soil water content and atmospheric demand, GF677 would have a more favourable water status than olive since a lower *RR* would leads to a higher Ψ_l. Although it is difficult to discuss the theoretical outcomes on E_p of a variable *RR* without accounting for the other components of the resistance catena with the aid of a full SPAC model, it is self-evident from Fig. 2.4 that without a specifically calibrated function of

R_p vs. temperature, the accuracy of such a model would be dramatically reduced.

Accounting for the seasonal variation in *RR* like in Fig. 2.4 is subjected to the availability of soil temperature profile records, which are rarely available. Jackson *et al.* (1996) proved that almost 50% of the roots of a tree are typically concentrated in the first 25 cm of soil. With those numbers in mind, one might consider using mean air temperature as a surrogate for soil temperature; but what error should we expect from such assumption? In the daily patterns of olive *RR* represented in Fig. 2.5 (GF677 data are not shown for clarity, but it behaves similarly) it is noteworthy that maximum and minimum values of *RR* occur respectively around 1h after dawn and between 1400 and 1500 UTC, independently of the season. Fig. 2.5 indicates that maximum *RR* is coincident with minimum air temperature, whereas minimum *RR* is not in phase with the time of maximum air temperature. In fact, when air temperature is approaching its maximum value, between 1400 and 1800 UTC, *RR* has already inverted its trend and is again increasing instead of decreasing, as expected according to equation 4 (see Fig. 2.2). This result might be associated with the fact that tree crown is intercepting part of the incoming radiation, reducing the amount of energy reaching the soil surface. Despite this phase mismatch, daily mean air temperature may still be valid as a substitute of soil temperature in order to capture the seasonal changes shown in Fig. 2.4. Table 2.3 depicts average monthly root mean square values (RMSE) between *RR* computed using average daytime (between dawn and twilight) air temperature and mean *RR* using soil temperature records. For olive, the error is expected to range between 20% during winter to less than 2% in

summer, while for GF677 the error is relatively constant and would be around 20% across all seasons. Thus, the convenience of using mean air temperature instead of soil temperature depends on the species simulated, and should be evaluated on the base of the required precision in the estimation of mean *RR*. When *RR* is critical for modelling tree E_p and no soil temperature is available, the use of a soil temperature model may be preferable to the direct use of air temperature.

Table 2.3. Average monthly RMSE from *RR* values computed using mean daytime air temperature and mean *RR* calculated using soil temperature records for olive and GF677.

	RMSE (MPa s m^2 kg^{-1})	
Month	***Olive***	***GF677***
Jan	4204.9	2790.5
Feb	3940.1	2296.7
Mar	2821.9	2589.1
Apr	1003.3	1159.5
May	461.2	730.7
Jun	104.3	331.3
Jul	84.5	304.2
Aug	70.9	270.1
Sep	121.4	315.9
Oct	744.6	892.2
Nov	1462.5	1181.2
Dec	3357.3	2069.2

2.4.2. Uncertainties in the measurement of radial root hydraulic specific resistance

Cyclic variations in R_p has been described for different plant species and variations in aquaporin expression has been proposed as a possible cause of the daily changes in root hydraulic specific resistance (Henzler *et al.*, 1999, Tsuda & Tyree, 2000, Tyree &

Zimmermann, 2002b, Caldeira *et al.*, 2014). The results of experiment 3 (Fig. 2.3) present a change in R_p during the measurement period and show two different patterns for the two studied cultivars that could not be attributed to temperature variations, since they changed less than one degree inside the growth chamber through the whole experiment.

From figure 3, one may think that the variation present in the GF677 rootstock may be due to a circadian rhythm in R_p, however, the magnitude of such change is of lower degree than those observed by Henzler *et al.* (1999) for *Lotus japonicus* L and by Tyree and Zimmermann (2002b) for tobacco plants. Besides, Caldeira *et al.* (2014) has demonstrated, when studying maize plants that non-circadian variations appear at low evaporative demand, a common condition when using growth chambers. This information led us to think that the observed increase in R_p for GF677 may well be an artifact related to the methodology applied. Espino and Schenk (2011) demonstrated that even under positive pressure, xylem cavitation can occur, resulting in an increase of measured R_p. The same authors proposed the lateral flow out from xylem vessels as another cause inducing an artificial increase in R_p (Espino & Schenk, 2011). The fact that only the GF677 rootstock presents an increase on R_p and the olive did not, could be attributed to anatomical differences between them, although we have no proof of this.

Regardless of the mechanisms implied, the increase in R_p in steady conditions of temperature and pressure that we observed in GF677 did not have an impact on the determination of R_p values obtained when changing the applied pressure. Evidence of it is the linearity of the relationship between pressure and flux (Fig. 2.1). The linear functions

fitted to the measurements, to compute R_p at the different temperatures, all have a R^2 around 0.90 (data not shown). If the variation observed in Fig 2.3 has had an impact on the measurements, a curvilinear response should have been observed in the flux-pressure relationships like that of Fig 2.1.

2.4.3. Radial root hydraulic specific resistance differences between rootstocks

The result of experiment 2 exhibits a highly significant difference between the two rootstocks studied. The experiment was performed at one temperature only and with a reduced number of plants; hence further research is needed in order to clarify if the difference we found is also present at other temperatures. If this difference has a genetic origin, measuring R_p could be an interesting trait to evaluate the performance related to water use for a variety of rootstocks under specific environments, since R_p is directly related to the water uptake capacity of a root, and can be easily incorporated into SPAC models.

2.5 Conclusion

According to our results, root hydraulic resistance can no longer be considered a steady feature of the hydraulic pathway; the transpiration rate, the water uptake and the plant water status do not depend only on canopy demand and water availability but may be heavily influenced by soil temperature. Hence, it would be advisable to include R_p variation functions with temperature in SPAC models in order to properly estimate E_p, considering that of all the resistances composing the plant system analogy, R_p is usually the highest one.

Acknowledgements

This work was supported by project AGL-2010-20766 of the Spanish Ministry of Economy and Competitiveness (former Ministry of Science and Innovation) and by the European Community's Seven Framework Programme-FP7 (KBBE.2013.1.4-09) under Grant Agreement No. 613817 (MODEXTREME, modextreme.org). The authors wish to thank both the "FPI" program of the aforementioned ministry and the JAE program of the Spanish Research Council (CSIC) for providing the Ph.D. scholarships granted to the first and the fourth author, respectively. We also thank Manolo Gonzalez, Maria Roman, Jose Luis Vazquez, Marcos Orgaz and Rafaela Gutierrez for the excellent technical assistance provided.

References

Abrisqueta J.M., Mounzer O., Álvarez S., Conejero W., García-Orellana Y., Tapia L.M., Vera J., Abrisqueta I. & Ruiz-Sánchez M.C. (2008) Root dynamics of peach trees submitted to partial rootzone drying and continuous deficit irrigation. *Agricultural Water Management*, **95**, 959-967.

Ameglio T., Morizet J., Cruiziat P. & Martignac M. (1990) The effects of root temperature on water flux, potential and root resistance in sunflower. *Agronomie*, **10**, 331-340.

Apostol K.G., Jacobs D.F., Wilson B.C., Salifu K.F. & Dumroese R.K. (2007) Growth, gas exchange, and root respiration of Quercus rubra seedlings exposed to low root zone temperatures in solution culture. *Forest Ecology and Management*, **253**, 89-96.

Axelsson B. & Ågren G.I. (1976) *Tree Growth Model (pt 1): A Development Paper*.

Caldeira C.F., Jeanguenin L., Chaumont F. & Tardieu F. (2014) Circadian rhythms of hydraulic conductance and growth are enhanced by drought and improve plant performance. *Nature Communications*, **5**.

Campbell G.S. (1985) *Soil physics with BASIC : transport models for soil-plant systems*. Elsevier, Amsterdam ; New York.

Cochard H., Martin R., Gross P. & Bogeat-Triboulot M.B. (2000) Temperature effects on hydraulic conductance and water relations of Quercus robur L. *Journal of Experimental Botany*, **51**, 1255-1259.

Couvreur V., Vanderborght J. & Javaux M. (2012) A simple three-dimensional macroscopic root water uptake model based on the hydraulic architecture approach. *Hydrol. Earth Syst. Sci.*, **16**, 2957-2971.

Doussan C., Pages L. & Vercambre G. (1998) Modelling of the hydraulic architecture of root systems: An integrated approach to water absorption - Model description. *Annals of Botany*, **81**, 213-223.

Espino S. & Schenk H.J. (2011) Mind the bubbles: achieving stable measurements of maximum hydraulic conductivity through woody plant samples. *Journal of Experimental Botany*, **62**, 1119-1132.

Fernández J.E., Martín Aranda J., Moreno Lucas F. & Fereres Castiel E. (1992) Olive-tree root dynamics under different soil water regimenes. *Agr.Med.*, **122**, 225-235.

Frensch J. & Steudle E. (1989) Axial and radial hydraulic resistance to roots of maize (*Zea mays* L). *Plant Physiology*, **91**, 719-726.

Grossnickle S.C. (1988) Planting stress in newly planted jack pine and white spruce .1. Factors influencing water-uptake. *Tree Physiology*, **4**, 71-83.

Henzler T., Waterhouse R.N., Smyth A.J., Carvajal M., Cooke D.T., Schaffner A.R., Steudle E. & Clarkson D.T. (1999) Diurnal variations in hydraulic conductivity and root pressure can be correlated with the expression of putative aquaporins in the roots of Lotus japonicus. *Planta*, **210**, 50-60.

Hertel A. & Steudle E. (1997) The function of water channels in Chara: The temperature dependence of water and solute flows provides evidence for composite membrane transport and for a slippage of small organic solutes across water channels. *Planta*, **202**, 324-335.

Jackson R.B., Canadell J., Ehleringer J.R., Mooney H.A., Sala O.E. & Schulze E.D. (1996) A global analysis of root distributions for terrestrial biomes. *Oecologia*, **108**, 389-411.

Kaufmann M.R. (1975) Leaf water stress in engelmann spruce - influence of root and shoot environments. *Plant Physiology*, **56**, 841-844.

Kaufmann M.R. (1977) Soil temperature and drying cycle effects on water relations of Pinus radiata. *Canadian Journal of Botany*, **55**, 2413-2418.

Kaufmann M.R. (1982) Evaluation of season, temperature, and water-stress effects on stomata using a leaf conductance model. *Plant Physiology*, **69**, 1023-1026.

Kramer P.J. (1940) Root resistance as a cause of decreased water absorption by plants at low temperatures. *Plant Physiology*, **15**, 63-79.

Kuiper P. (1964) Water uptake of higher plants as affected by root temperature. *MededLandbouwhogeschWageningen*, **64**, 1:11.

Lee S.H., Singh A.P., Chung G.C., Ahn S.J., Noh E.K. & Steudle E. (2004) Exposure of roots of cucumber (Cucumis sativus) to low temperature severely reduces root pressure, hydraulic conductivity and active transport of nutrients. *Physiologia Plantarum*, **120**, 413-420.

Lopez-Bernal A., Garcia-Tejera O., Testi L., Orgaz F. & Villalobos F.J. (2015) Low winter temperatures induce a disturbance of water relations in field olive trees. *Trees-Structure and Function*, **29**, 1247-1257.

McCormack M.L., Adams T.S., Smithwick E.A.H. & Eissenstat D.M. (2014) Variability in root production, phenology, and turnover rate among 12 temperate tree species. *Ecology*, **95**, 2224-2235.

Mellander P.E., Stahli M., Gustafsson D. & Bishop K. (2006) Modelling the effect of low soil temperatures on transpiration by Scots pine. *Hydrological Processes*, **20**, 1929-1944.

Norisada M., Hara M., Yagi H. & Tange T. (2005) Root temperature drives winter acclimation of shoot water relations in Cryptomeria japonica seedlings. *Tree Physiology*, **25**, 1447-1455.

Pavel E.W. & Fereres E. (1998) Low soil temperatures induce water deficits in olive (Olea europaea) trees. *Physiologia Plantarum*, **104**, 525-532.

Roderick M.L. & Berry S.L. (2001) Linking wood density with tree growth and environment: a theoretical analysis based on the motion of water. *New Phytologist*, **149**, 473-485.

Running S.W. & Reid C.P. (1980) Soil Temperature Influences on Root Resistance of Pinus contorta Seedlings. *Plant Physiology*, **65**, 635-640.

Sachs J. (1870) Movement of water in plants. In: *Textbook of botany Morphological and Physiological Book III* (ed J. Sachs), pp. 598-614. Cambridge University press.

Searles P.S., Saravia D.A. & Rousseaux M.C. (2009) Root length density and soil water distribution in drip-irrigated olive orchards in Argentina under arid conditions. *Crop and Pasture Science*, **60**, 280-288.

Tsuda M. & Tyree M.T. (2000) Plant hydraulic conductance measured by the high pressure flow meter in crop plants. *Journal of Experimental Botany*, **51**, 823-828.

Tyree M.T. & Zimmermann M. (2002a) Variable hydraulic conductance: temperature, salts and direct plant control. In: *Xylem structure and the ascent of sap* (eds M.T. Tyree & M. Zimmermann), pp. 205-214. Springer, Heidelberg.

Tyree M.T. & Zimmermann M.H. (2002b) Hydraulic architecture of whole plants and plant performance. In: *Xylem Structure and the Ascent of Sap*, pp. 175-205. Springer-Verlag Berlin Heidelberg.

van den Honert T.H. (1948) Water transport in plants as a catenary process. *Discussions of the Faraday Society*, **3**, 146-153.

Wan X.C., Zwiazek J.J., Lieffers V.J. & Landhausser S.M. (2001) Hydraulic conductance in aspen (Populus tremuloides) seedlings exposed to low root temperatures. *Tree Physiology*, **21**, 691-696.

Williams M., Law B.E., Anthoni P.M. & Unsworth M.H. (2001) Use of a simulation model and ecosystem flux data to examine carbon-water interactions in ponderosa pine. *Tree Physiol*, **21**, 287-298.

Yamamoto R. (1995) Dependence of water conductivity on pressure and temperature in plant stems. *Biorheology*, **32**, 421-430.

Chapter 3

A soil-plant-atmosphere continuum (SPAC) model for simulating tree transpiration with a soil multi-compartment solution

Chapter 3

A soil-plant-atmosphere continuum (SPAC) model for simulating tree transpiration with a soil multi-compartment solution

Summary

A soil-plant-atmosphere continuum (SPAC) model for simulating tree transpiration (E_p) with variable water stress and water distribution in the soil is presented. The model couples a sun/shade approach for the canopy with a discrete representation of the soil in different layers and compartments. To test its performance, the outputs from the simulations are compared to those from an experiment using trees of olive 'Picual' and almond 'Marinada' with the root system split into two. Trees are subjected to different irrigation phases in which one side of the root system is dried out while the other is kept wet. The model is able to accurately predict E_p (R^2 and the efficiency factor (EF) around 0.9) in the two species studied. The use of a function that modulates the uptake capacity of a root according to the soil water content was necessary to track the fluxes observed from each split part. It was also appropriate to account for root clumping to match the measured and modelled leaf water potential. Coupling the sun/shade approach with the soil multi-compartment solution provides a useful tool for exploring tree E_p for different degrees of water availability and distribution.

3.1. Introduction

Hillel (2003) made an effective simile to illustrate the cohesion-tension theory of water flow through plants: "plants can be compared to a wick in an old fashioned Kerosene lamp" moving water from the soil to the atmosphere. The same author also recognized the crudeness of this simplification, since plants can actively regulate transpiration (E_p) through the stomata (Hillel, 2003). Globally, the magnitude of water flow through plants is paramount: more than half of the global precipitation falling onto the earth is returned to the atmosphere through plant transpiration (Jackson *et al.*, 2000). As critical actors in the water cycle, a better understanding of the processes involved in root water uptake and E_p are crucial to efficiently understanding and managing global water resources (Green *et al.*, 2006). This challenge can be achieved with the aid of models which serve to study not only the complicated interactions between plants and their environment, but to highlight the knowledge gaps that need to be filled.

Traditionally, E_p has been viewed as a process modulated either by the canopy or the roots, depending on the area of research. Micrometeorologists, for example, view the regulation of E_p of a plant or a stand of plants as being mediated by the available energy reaching the leaves and the atmospheric demand (Jarvis & McNaughton, 1986), whereas for soil scientists, it is the rate of water withdrawn by the roots that controls transpiration (Javaux *et al.*, 2013). The few studies in the literature which have set up the available equations describing the demand of water from the canopy and its supply provided by the roots, have demonstrated that all the elements contribute to the

regulation of E_p; particularly when some degree of water stress is present (Williams *et al.*, 1996, Tuzet *et al.*, 2003).

In modelling E_p, not only the integration of the relevant equations describing demand and supply is important, but also the recognition of the variability. Nature is heterogeneous, and the reliability of the predictions made with a model will often depend strongly on how this heterogeneity is handled (Campbell & Norman, 1998). For example, accounting for the radiation intercepted by canopies (a paramount driver for plant photosynthesis and stand primary production) needs to deal with radiation attenuation described by Beer's law (Monsi & Saeki, 1953, dePury & Farquhar, 1997). To do so, the canopy can be divided into different layers with distinct characteristics (leaf angle, leaf density or nitrogen content) (Wit, 1965, Lemon *et al.*, 1971, Whisler *et al.*, 1986). The layered approach successfully simulates light interception and canopy photosynthesis but the complexity of the parametrisation and the number of calculations required limit its use (dePury & Farquhar, 1997). As a solution, the canopy can be divided into categories of sunlit and shaded leaves, thus taking into account variability while lowering the parameter number and requiring simpler equations (Sinclair *et al.*, 1976, dePury & Farquhar, 1997).

Soil environment is even more heterogeneous in nature, especially when anthropic effects like irrigation or other agronomic practices are present; in which case, the approaches to simulating root water extraction should depend on the situation to be modelled. While simple one-dimensional models may be suitable when the soil is uniformly wetted and the roots evenly distributed, in many field conditions, and particularly for crops watered with localised irrigation

systems, they are not. In these vegetation systems, very large variations in soil water content (θ_{soil}) throughout the root zone are present, generating a significant variability in root density as roots tend to grow faster in portions of the soil whose conditions are favourable to their function. In this case, the use of one-dimensional models to compute root water extraction would fail to account for preferential water uptake from the wetted areas or the differences in root activity (Clothier & Green, 1997). Alternatively, one could use models that work in more than one dimension. Doussan *et al.* (1998) for example, developed a detailed three dimensional maize root water uptake model combining an explicit representation of the root system with the catenary hypothesis, allowing them to study the so called "hydraulic architecture of the root system". But as for the canopy multilayer approach, the computational requirements and its complex parametrization reduce its applicability (Couvreur *et al.*, 2012).

A solution between the simple one dimensional approach to compute water extraction and the more complicated explicit models is proposed. The soil is not only divided into different layers, but also into compartments to capture local variations in θ_{soil} and root density, using an approach which is simple enough to be easily implemented with measurable parameters, but with a sufficient degree of complexity to correctly compute the different water uptake from each single compartment.

The present chapter describes a SPAC model for trees which makes use of a soil multi-compartment as well as a sun/shade approach. Plant transpiration water potential at leaf and root collar, photosynthesis and stomatal conductance are calculated when heterogeneous conditions of

soil water content or root density are present. Outputs of the model have been compared with the results of a split-root experiment using olive 'Picual' (*Olea europea L.*) and almond 'Marinada' (*Prunus dulcis L.*) grafted onto GF677 rootstock (*Prunus dulcis* L. *x Prunus persica* L.), where the fluxes of water extracted from each split part of the root system were continuously recorded using sap flow and time domain reflectometry (TDR) probes. The model performance and the main conclusion from the experiments are discussed.

3.2. Model Description

Since van den Honert (1948), transport of water through the plant has been depicted as an electric circuit analogy composed of a set of resistances in parallel or in series and the differences in water potential as the driving force. For steady-state conditions, E_p, can be calculated as the difference in soil water potential (Ψ_s) minus water potential at the xylem collar (Ψ_c) and divided by the resistance of the soil (R_s) plus the resistance of the root (R_r); or Ψ_c minus leaf water potential (Ψ_l) divided by the resistance of the xylem vessels (R_x), if no capacitance is considered.

$$E_p = \frac{\Psi_c - \Psi_l}{R_x} = \frac{\Psi_s - \Psi_c}{R_s + R_r} \quad (1)$$

This simple equation represents the basis on which most of the SPAC models are developed (Williams *et al.*, 1996, Sperry *et al.*, 1998). On the right hand of eq. 1 a supply function of the system describing the

water withdrawn by the roots is given, while the left hand side describes the demand function that accounts for the water being transported through the trunk and branches. The following paragraphs of this section describes how the sun/shade and the soil multi-compartment approach have been integrated into the supply and demand parts of eq. 1, and how both parts have been linked to computing total tree E_p. Figure 3.1 provides a visual scheme of the model. A detailed description of the mathematical derivations and the structure of the model are presented in appendix I.

3.2.1. The supply function

To derive the uptake capacity of a group of roots, Gardner (1960), defined them, as being infinite long cylinders, uniformly distributed, withdrawing water in the radial direction from a volume of soil surrounding them. The volume of soil could be inferred from root length density (L_v) (Gardner, 1960, Cowan, 1965, Newman, 1969). Gardner's equation was derived for the path from the mid space between two consecutive roots towards the root surface; so that, the resistance of the soil surrounding a root could be computed as:

$$R_s = \frac{\ln\left(\frac{1}{\pi Lv\ {a_{root}}^2}\right)}{Lv\ d\ 4\pi k} \quad (2)$$

Symbols, a_{root}, d and k in equation 2, represent: root radius, root depth and soil hydraulic unsaturated conductivity, while L_v refers to the root length density of the absorbing roots. It is often difficult to describe an absorbing root because, although the highest rates of water uptake are

found in the thin, unsuberized portions, the contributions of the woody suberized root parts can be significant in trees with large root systems (Kramer, 1969). In the present model, only roots with a diameter of under 1.4 mm are considered to be active in water uptake.

The other resistance present in the supply function can be derived by simply upscaling the specific hydraulic resistance of a root (r_r) to the entire root system using L_v and d:

$$R_r = \frac{r_r(\theta, T)}{Lv\ d} \tag{3}$$

The value of r_r integrates, for a root section in the radial direction, the degree of permeability of the different tissues arranged in series that conform the root cylinder (Steudle & Peterson, 1998).This, however, is usually a fixed value in most of the models. Nevertheless, permeability might well vary due to changes in the root environment like temperature or soil water content by: modifications in the degree of suberification of the exo and endodermis, aquaporine activity, or a loose contact between the root surface and the soil, among others (Herkelrath *et al.*, 1977, North & Nobel, 1992, North & Nobel, 1997, Steudle & Peterson, 1998, Steudle, 2000) . In the present model, r_r was obtained as a function of the temperature using the approach developed by Garcia-Tejera et al. (2016), and then modified according to θ_{soil} using Bristow's model (Bristow *et al.*, 1984).

Tree E_p must equal the sum of all the fluxes coming from each soil layer (i) of each soil compartment (j) if tree capacitance is not taken into account. Once that the total resistance from root and soil are

derived using equations 2 and 3, the water withdrawn by the roots from each soil layer (i) at each soil compartment (j) is obtained by applying to the supply function the water potential gradient between the soil ($\Psi_{si,j}$) and the root xylem ($\Psi_{rxi,j}$). The integration of all those fluxes to obtain tree E_p would read:

$$E_p = \sum \frac{\Psi_{si,j} - \Psi_{rxi,j}}{R_{si,j} + R_{ri,j}} \quad (4)$$

Equation 4 can be further simplified. Unless cavitation is present, root xylem resistance is negligible compared to R_s and R_r (Sperry *et al.*, 1998, Tyree & Zimmermann, 2002b). Considering a negligible root xylem resistance necessarily implies a common xylem water potential throughout the root xylem system; in other words, Ψ_c is assumed to be the same throughout the whole conductive system. With this simplification in mind, equation 4 can be rearranged as a function of Ψ_c as:

$$\Psi_c = \frac{\sum \frac{\Psi_{si,j}}{R_{si,j} + R_{ri,j}} - E_p}{\sum \frac{1}{R_{si,j} + R_{ri,j}}} \quad (5)$$

3.2.2. The demand function

The specific hydraulic conductance of the xylem has been estimated by adding up the conductivities of the conduits found in a cross-section of wood using a modified version of the Hagen–Poiseuille equation, in which the quarter-power diameters are substituted by

mean vessel diameter and vessel density (Tyree & Ewers, 1991). The specific hydraulic resistance of the xylem is then calculated as the inverse of the specific hydraulic conductance. However, the use of the Hagen-Poiseuille equation to model water transport through the stems consistently underestimates the specific resistance measured experimentally on wood segments. This deviation has been attributed to the resistance of inter-conduit pit pores, as sap has to cross a porous membrane to flow from one conduit to the next. Some studies including several angiosperm species have estimated that, on average, those pits contribute 56 % to total xylem specific resistance regardless of wood porosity (ring or diffuse) (Wheeler *et al.*, 2005, Hacke *et al.*, 2006). The present model uses the Hagen–Poiseuille equation to compute specific conduit resistance; pit specific resistance is then obtained by multiplying 1.27 (56% of the total xylem specific resistance) to the specific conduit resistance. Finally, the total specific hydraulic resistance (r_t) is calculated by adding up conduit and pit specific resistances. Upscaling to total xylem hydraulic resistance (R_x) can be done by considering the path from the mean root depth (Z_{root}) to shoot height (Z_{shoot}) and the cross-sectional area of sapwood per square meter of soil (SWA) as:

$$R_x = \frac{r_t(Z_{root} + Z_{shoot})}{SWA} \quad (6)$$

In computing the demand function, tree canopy is discretized into sunlit and shaded leaves to upscale from leaf to tree photosynthesis (dePury & Farquhar, 1997). If the canopy is divided into sunlit and

shaded leaves, total transpiration must be computed as the sum of E_p from each leaf class

$$E_p = E_{psun} + E_{pshade} \quad (7)$$

For well coupled canopies, like forests or tree crops, E_p can be directly related to the stomatal conductance using a simplified version of the Penman-Monteith equation, assuming that, the aerodynamic conductance is much higher than the stomatal conductance due to the "roughness" of the canopy surface (Villalobos *et al.*, 2000, Orgaz *et al.*, 2007). In that case, E_p is called "imposed" and is estimated as a function of the vapour pressure deficit (*VPD*) and the stomatal conductance for CO2 (g_{co2}) (Jarvis & McNaughton, 1986):

$$E_{psun} = g_{co2sun} 1.6 \frac{VPD}{P} LAI_{sun} \quad (8)$$

Where P is atmospheric pressure and LAI_{sun} and g_{co2sun} are leaf area index and stomatal conductance for CO2 of the sunlit leaves. LAI_{sun} is computed hourly as a function of the zenith angle, the G projection function and the solar radiation reaching the canopy, assuming a spheroidal canopy shape. Equation 8 (and the following eqs. 9 and 10) refers only to sunlit leaves for the sake of concision; those for shaded leaves are analogous.

Equation 8 can be further developed using the adaptation of Leuning's equation proposed by Tuzet (2003), in which, g_{co2} is related to leaf assimilation, the concentration of CO2 at the substomatal cavities (C_i),

the light compensation point (Γ), and reduced by leaf water potential through an empirical function (see Tuzet et al. (2003) for a detailed description). For a sunlit leaf, Tuzet's equation reads:

$$g_{co2sun} = g_0 + \frac{mA'_{sun}}{C_{isun} - \Gamma} f(\Psi_{lsun}) \quad (9)$$

$$f(\Psi_{lsun}) = \frac{1 + \exp[s_f \Psi_f]}{1 + \exp[s_f(\Psi_f - \Psi_{lsun})]} \quad (10)$$

In eq.9, the symbol g_0 is the night time conductance (i.e. for zero gross assimilation) and m is a proportionality factor between photosynthesis and stomatal conductance, while in eq. 10 Ψ_f is a reference water potential which marks the initial value of Ψ_{lsun} at which g_{co2sun} is affected and s_f modulates the rate of the reduction. The present model uses gross assimilation (A') computed using the Farquhar et al. (1980) approach instead of net assimilation as was originally proposed by Tuzet (2003). Parameters for Farquhar's model are assumed to change with temperature following the exponential function developed by Bernacchi et al. (2001).

3.2.3. Coupling supply and demand

In eq. 1 Ψ_c appears in the demand and the supply functions. On the other hand, in eq. 5, an expression to obtain Ψ_c was developed for the supply part. Now substituting eq. 5 in the demand function of eq. 1 and rearranging for Ψ_l yields:

$$\Psi_l = \frac{\sum \frac{\Psi_{si,j}}{R_{si,j} + R_{ri,j}} - E_p}{\sum \frac{1}{R_{si,j} + R_{ri,j}}} - E_p R_x$$

(11)

For a canopy discretized into sunlit and shade leaves, eq. 11 turns into:

$$\Psi_{lsun} = \frac{\sum \frac{\Psi_{si,j}}{R_{si,j} + R_{ri,j}}}{\sum \frac{1}{R_{si,j} + R_{ri,j}}} - g_{co2sun} 1.6 \frac{VPD}{P} 0.018 \left(\frac{\sum \frac{1}{R_{si,j} + R_{ri,j}} + R_x}{f_{sun}} \right) LAI_{sun}$$

(12)

Where f_{sun} is the ratio LAI_{sun}/LAI and f_{shade} would be 1- f_{sun}. The coefficients transform the conductance for CO_2 in mmol m^{-2} s^{-1} to conductance for H_2O in kg m^{-2} s^{-1}. As in eq. 8, 9 and 10, eq. 11 is formally the same for Ψ_{lshade}, simply changing the values of the corresponding parameters to those of the shaded leaves.

Equation 12 assumes that the tree is split into two parts according to the fractional area of sun and shade leaves. In other words, the model assumes that each leaf class will be sustained by a proportion of roots and trunk equal to f_{sun} and f_{shade}, respectively.

To find the values for Ψ_l and g_{co2} for each leaf class an iterative procedure is followed using C_i as a convergence criterion. Once an equilibrium point for C_i is attained, values for E_p and Ψ_c are then obtained from eq. 8, 7 and 5. Appendix I provides a detailed description of the iterative procedure to match Ψ_l and g_{co2}.

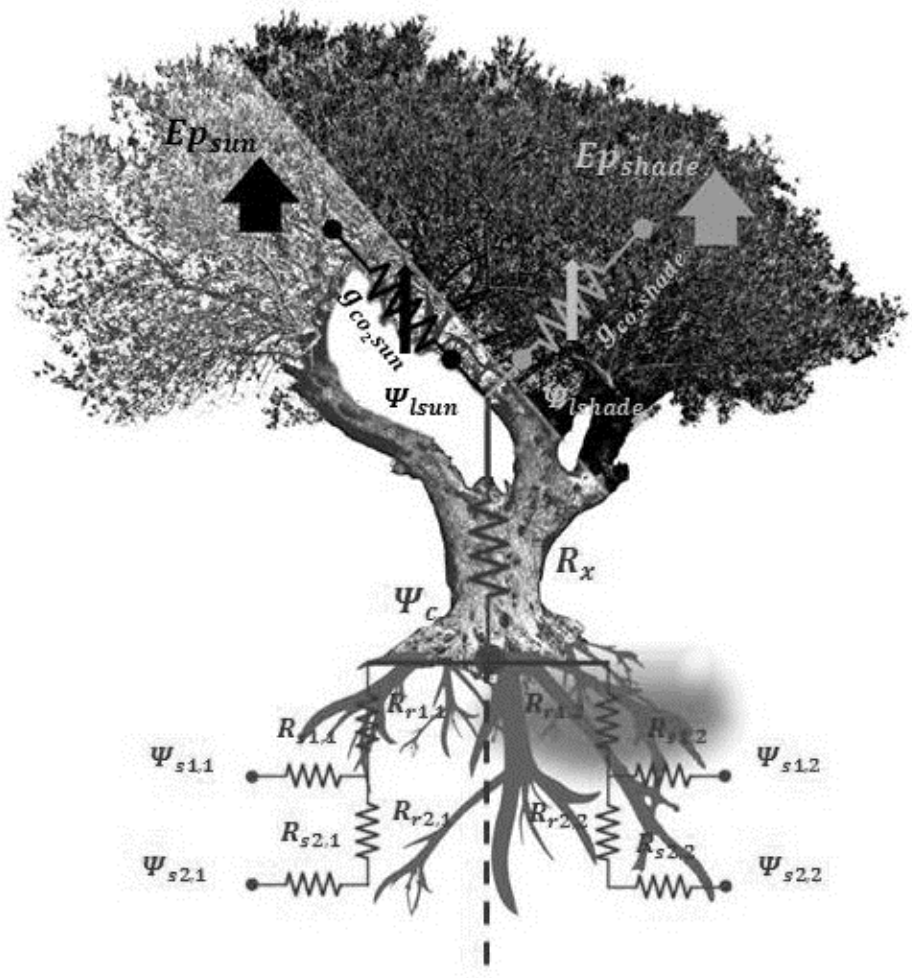

Fig 3.1. Schematic representation of the model. The figure represents the sun/shade approach for a tree with two soil layers and two soil compartments with different L_v and θ_{soil}. The dotted line placed at the tree collar represents the virtual separation between soil compartments.

3.3. Split root Experiment

Model results were compared to the data obtained from an experiment with two 1-year old almond 'Marinada' grafted onto GF677 rootstock and two 2-year old olive 'Picual'. The four trees were received in the spring of 2012. The root system of the cuttings was carefully divided into two equal halves and then placed in individual 25-liters pots. As a result of the dividing process, each cutting occupied two pots with one half of the root system in each.

The cuttings stayed in the pots until the winter of 2013. At the end of that season, plants were transferred to specially designed lysimeters with transparent walls (Fig 3.2). The lysimeters consisted of a metal frame of 0.2 x 0.8 m and with a depth of 0.8 m, covered with 6 transparent polymethyl methacrylate sheets (4-mm thick) on all the vertical walls. The volume of each lysimeter was divided by another plastic wall into two isolated parts of 0.2 x 0.4 x 0.8 m. At the bottom, each part had its own drainage collector system, while at the top a plastic cover was fitted to prevent evaporation from the soil substrate. The cuttings were placed on top of the division sheet with the split roots on the two sides of the lysimeter. The substrate used was a sterilised mix of 50:50% sand:vermiculite.

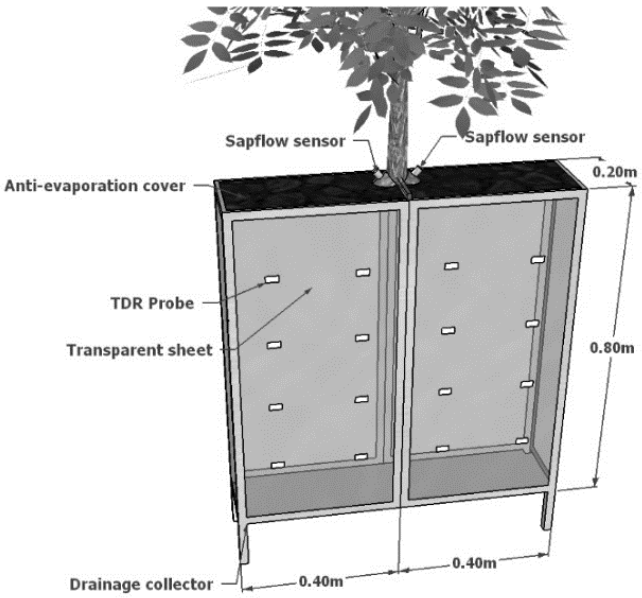

Fig 3.2. Lysimeter design

3.3.1. Measurements

The experiment was conducted in a shadehouse covered with an anti-trip mesh at the facilities of the Institute of Sustainable Agriculture (IAS) in Cordoba, Spain (37°52′N, 4°49′W) from May to September, 2014. In one tree at a time, an irrigation sequence was imposed consisting of two phases, one with full irrigation (F, irrigation given each morning to both sides of the root systems until the occurrence of steady drainage), followed by dry one half (D, one side of the root system receiving water like F and the other one receiving none). Throughout the irrigation cycles, the flux of water coming from each

half and the soil moisture variations in the lysimeter were recorded every 10 min. Whereas for almond trees only one irrigation sequence was imposed, olive trees received two consecutive sequences, inverting the irrigated and dried sides during phase D namely D_1 and D_2. Figure 3.3 presents a diagram of the different irrigation phases.

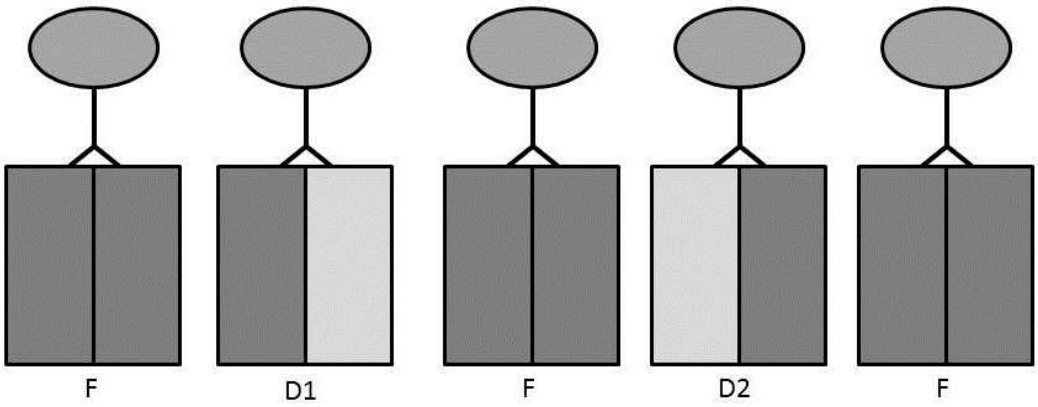

Fig 3.3. Diagram showing the different irrigation phases for the experiment with olive trees. F represents phases where both sides were watered while D1 and D2 are the phases in which one side was dried out.

To impose different levels of stress, olive tree no. 1 was submitted to a period without irrigation (i.e. neither side receiving water during one day) at the end of D_1 and at the beginning of D_2; also, phase F between D_1 and D_2 was shorter than for olive tree no. 2. Almond trees were subjected to the same water stress level as olive tree no. 2, with at least one side of the root system always receiving water.

Irrigation in each half was applied using 3 emitters with a discharge rate of 4 l h^{-1}. Variations in soil water content were monitored with 8 TDR probes per half (model CS645, Campbell Scientific Inc. Logan

UH, USA) distributed in two columns of four sensors at 0.10, 0.30, 0.50, 0.70 m depth from the soil surface and spaced 0.2 m between them. TDR probes were 75 mm long and were previously calibrated using the method suggested in Regalado *et al.* (2001). All the 16 TDR probes were monitored at a 10-min frequency with a multiplexed TDR (model TDR100 + two SDMX50, Campbell Scientific Inc. Logan UH, USA). Total soil moisture variation in the lysimeter was also monitored continuously at the same frequency of the TDR using a +/- 1g precision scale (model Kern DSK150, Kern & Sohn GmbH, Balingen, Germany).

The water flux through each half of the root system was recorded using two sap flow sensors per plant, installed in each of the two branches of the split collar at the beginning of the experiment. The sap flow measurement system was based on the Compensated Heat Pulse method (Swanson & Whitfield, 1981) and the Calibrated Average Gradient method at low convective velocities (Testi & Villalobos, 2009). The probes consisted of three stainless steel rods 2 mm in diameter, one being a linear heater and the other two temperature sensors, installed 10 and 5 mm down- and upstream of the heater, respectively. Each temperature sensor contained two thermocouple junctions that were sampled separately to obtain heat-pulse velocities at 5 and 15 mm depths below the cambium. The system was controlled by a datalogger (CR1000, Campbell Scientific Inc., Logan, UT, USA) and sampled at 10-min interval. Heat-pulse velocities were corrected for wounding reaction (Green *et al.*, 2003) and the sap flow was obtained by integrating sap flux densities across the radius of the collar branches (Green *et al.*, 2003).The two collar branches of each plant originated from splitting the root system, so that the exact

anatomy of their conductive system could differ substantially from the assumptions normally made in the flux density integration of normal trunks, due to their expected cicatrisation tissue. Therefore, the final flux in each branch was obtained as the apparent flux from sap flow measurements times a calibration coefficient (specific for each probe) obtained from mass balance calculations using total mass from the scale, θ_{soil} variations on each side from TDR differential values for one day and the drainage collected. These coefficients ranged between 0.3 and 0.8 and they remained stable during the experiments.

Temperature and relative humidity inside the shadehouse were monitored every 10 minutes using a sheltered temperature and humidity probe (HMP45AC, Vaisala, Wantaa, Finland). Global radiation data were collected from a silicon cell pyranometer (model SKS 1110, Skye Instruments Ltd, Llandrindod Wells, Powys, UK) at 1.7 m height from an automatic weather station at the IAS facilities. Radiation data from the weather station were corrected for the shadehouse according to mesh transmissivity values provided by the manufacturer.

Root dynamics during the irrigation cycles were monitored using the root intersection method in the lysimeters with olive trees. The two frontal transparent sheets were divided into squares of 5 x 5 cm and roots in contact with the transparent sheet of each square were counted at the beginning of the irrigation cycle (phase F), at maximum stress (end of phase D_1) and several days after phase D_1 (second phase F).

In olive tree no.2, measurements of leaf water potential at the end of phase D_2 (maximum stress) were made at 7:00, 9:00 and 11:00 GMT

using a pressure probe chamber (model 3000, Soil Moisture Equipment, California, USA).

At the end of the experiment, the trees were extracted from the lysimeters and processed as follows. All the leaves were removed to measure leaf area using a leaf area meter (LI-3100 Area Meter, Licor inc, Nebraska USA). Roots were carefully extracted and then washed on a 1mm mesh sieve to remove the substrate and then dried in an oven at 60ºC for three days, after taking a subsample of 10% in mass from each side of the root system. The subsamples were digitally scanned using a commercial scanner (HP Scanjet G3110) and the resultant image files were then analysed with root image analysis software (WinRhizo, Regent Instruments Inc, Quebec City, Canada) to obtain the total root length of the subsample and average root radius (a_{root}). Once analysed, the subsamples were dried in the oven at the same temperature and for the same time as the rest of the root systems. The dry weight of the subsamples was obtained using a four decimal precision balance (model AV104, Mettler Toledo, Greifensee, Switzerland) while root dry mass of the total root systems was measured using another balance (Kern FCB 8K0.1, KERN & SOHN GmbH, Balingen Germany). Finally, the average specific root length (SRL) for each tree, used to convert from root biomass to L_v, was calculated as the ratio of mean root length to mean root dry mass of the corresponding subsamples.

3.3.2. Substrate hydraulic properties

The soil water retention curve was derived from six samples of soil substrate with different water contents, using a Dewpoint Potentiometer (WP4-T, Decagon Devices, Washington, USA); a more

detailed description of the procedure is available at http://www.decagon.com/education/ . For the saturated water conductivity (k_s), the Philip-Dunne permeameter method was used following the protocol developed by Muñoz-Carpena et al. (2002). The data collected were then fitted using a curve fitting software package (Curve Fitting toolbox Matlab R2010b, MathWorks Inc, Massachusetts, USA) applying the empirical relationships proposed by Campbell (1985a), which represent the water release characteristic curve and the unsaturated soil water conductivity.

3.3.3. Model parameters and calibration

Because the model was tested using small trees (maximum measured leaf area of 4.97 m^2); it was assumed that the fraction of shaded leaves was negligible compared to that of sunlit ones. Therefore the simulations were made considering that all the leaves were illuminated. The parameters for the biochemical photosynthesis model of Farquhar et al. (1980) for olive trees were obtained from Diaz-Espejo et al. (2006) while for almond trees, reported values from Egea et al. (2011b) for the summer period were used.

All the parameters of the Tuzet model, except m and Γ, that was obtained from Moriana et al. (2002), were derived directly from this experiment. Tuzet's empirical relation (eq. 10) was calibrated in one tree of each species using the recorded sap flow values from the first day of the experiment (when the two parts of the lysimeters were well watered). The calibrated parameters were used on the remaining days and for the experiment with the other tree of the same species. For the same tree and the same period as for the calibration of the Tuzet's function, the value for g_0 was obtained from the conductance derived

by inverting eq. 9, and using the calibrated sap flow records at two hours before dawn. Soil water content was daily initialized using recorded TDR values.

3.3.4. Statistical analysis

Regression analyses were performed comparing: measured E_p from each tree, calculated as the sum of the calibrated fluxes recorded from the sap flow probes inserted on each side of the split collar, against the E_p derived from the model. The efficiency factor of the model was computed as:

$$EF = 1 - \frac{\sum(Xmeas - Xmod)^2}{\sum(Xmeas - \bar{X}meas)^2} \quad (13)$$

Where Xmeas and Xmod correspond to measured and modelled values. EF was calculated using the same data set as for the regression analyses.

3.4. Results

3.4.1. Model parameters

Table 3.1 presents a summary of: L_v, leaf area (LA), a_{root} and specific root length (SRL) for the four trees used in the experiment. In relation to olive trees, the almond plants presented a lower LA and a similar or higher L_v. The mismatch in $LA{:}L_v$ relation between the two species is related to the differences in SRL, which were almost double for almond.

Table 3.1. Measured root and shoot characteristics. L_{v1} and L_{v2} : root length densities for each lysimeter compartment. SRL, LA and a_{root} are: specific root length, leaf area and average root radius.

Tree	L_{v1} (m m^{-3})	L_{v2} (m m^{-3})	a_{root} (m)	*SRL* (m g^{-1})	*LA* (m^2)
Olive 1	156076	141304	0.00016	6.48	4.97
Olive 2	115828	95053	-	-	3.62
Almond 1	91274	91236	0.0001	15.79	3.1
Almond 2	177267	177230	-	-	2.8

Calibration of Tuzet's empirical parameters (Table 3.2), gave different values for almond and for olive trees. The sensitivity factor (s_f) was smaller for almond than for olive, meaning a lower susceptibility of g_{co2} to Ψ_l. The reference water potential (Ψ_f), however, was very similar for both species with a reduction threshold for g_{co2} close to zero. Unlike Tuzet's function parameters, olive g_0 was one order of magnitude lower than that for almond.

Table 3.2. Values for the parameters used in the photosynthesis and stomatal conductance models Parameters for photosynthesis obtained from (Diaz-Espejo *et al.*, 2006) for olive trees and from (Egea *et al.*, 2011a) for almond trees are: the degree of curvature of the response to PAR of the electron transport rate (θ), the quantum efficiency (α) and values of activation energy (ΔH_a) and the scaling constants (c) for: Michaelis constant for CO_2 (K_c) and O_2 (K_o), CO_2 compensation point (Γ), maximum catalytic activity of Rubisco in the presence of saturating amounts of ribulose biphosphate and CO_2 (V_{cmax}), maximum ratio of electron transport (J_{max}), and the rate of CO_2 evolution in the light resulting from process other than photorespiration (R_d). Parameters for stomatal conductance have been obtained from the recorded sap flow values through a calibration procedure, those are: a proportionality factor between photosynthesis and stomatal conductance (m), the stomatal conductance for null net photosynthesis (g_0) and the parameters for the empirical model of Tuzet, namely, reference water potential (Ψ_f) and a sensitivity factor (s_f).

Parameter	Olive	Almond
	Photosynthesis	
θ	0.9	0.9
α	0.2	0.2
cK_c	38.05	38.05
$\Delta H_a K_c$	79430	79430
cK_o	20.3	20.3
$\Delta H_a K_o$	36380	36380
$c\Gamma$	19.02	19.02
$\Delta H_a \Gamma$	37830	37830
cV_{cmax}	33.99	31.58
$\Delta H_a V_{cmax}$	73680	78100
cJ_{cmax}	18.88	13.77
$\Delta H_a J_{cmax}$	35350	34110

cR_d	17.91	17.91
$\Delta H_a R_d$	44790	44790
Stomatal conductance		
Ψ_f	-463	-327
sf	0.0061	0.0031
m	4.5	4.5
g_o	0.005	0.02

Soil substrate parameters for Campbell's function are presented in Table 3.3. Two things characterized the substrate used in the experiment. One was the high k_s, and the other the low value of air entry potential (Ψ_e), when compared to data for different soil types from the literature (Campbell, 1985a, Campbell & Norman, 1998).

Table 3.3. Parameters to describe soil substrate hydraulic properties measured during the experiment. Symbols represent: depth layer (d), soil water content at permanent wilting point (θ_{ll}), field capacity (θ_{ul}) and saturation (θ_{sat}), air entry soil water potential (Ψ_e), saturated hydraulic conductivity (k_s) and a shape factor (b).

d (m)	θ_{ll} ($m^3\ m^{-3}$)	θ_{ul} ($m^3\ m^{-3}$)	θ_{sat} ($m^3\ m^{-3}$)	Ψ_e (kPa)	b	k_s ($kg\ s\ m^{-3}$)
0.2	0.03	0.29	0.38	-16.65	1.9	0.01478

3.4.2. Model test

The model was tested against total tree E_p computed as the sum of the calibrated fluxes recorded from the two sap flow sensors installed in each tree (Fig. 3.4). To facilitate the visibility of the data, only hourly values of modelled versus observed E_p are presented. Regression analysis produced R^2 values of around 0.9 for all trees except for almond no. 2 (R^2=0.82), and EF close to 1 (Table 3.4). According to Fig. 3.4, the model tends to under-predict almond E_p in the mid-range, while maximum E_p is slightly over-predicted; this is more evident for almond no. 2. For olive trees, instead, an over prediction of the mid-range values of E_p was observed.

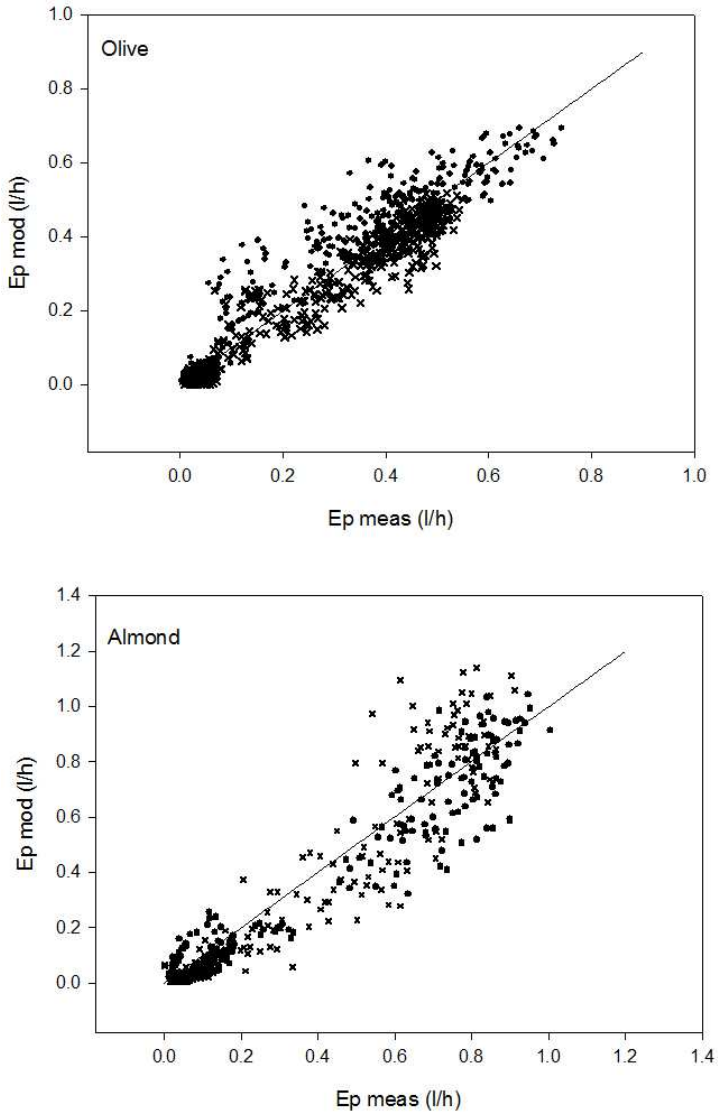

Fig 3.4. Measured transpiration (E_p meas) computed as the sum of the calibrated fluxes from each side of the lysimeter against the transpiration obtained with the model (E_p mod) on an hourly basis for olives and almonds. Dots represent tree number one and crosses refers to tree number two in both species.

In Fig. 3.5 the time series of modelled and recorded root water extraction fluxes from each split root branch of the two olive trees are presented. The model was able to capture the tendencies in both parts of the split root system not only during the periods in which both sides were irrigated (phases F), but also when one side of the root system was dried out (phases D). In general, for the four trees during phase D, the model tended to under-predict the flux of the dried side while the flux of the wetted one was overestimated (see Fig. 3.5 for olive trees and appendix II for almond trees). We also found a lag in the recovery of the flux after phase D of the side that had been previously dried (see doy 181 and 182 in olive tree no. 2 as an example). Also noticeable was the deviation in olive tree no. 1, in the modelled water extraction flux from one of the two root branches on the last four days of the experiment, with an over prediction as high as 44% with respect to the measured flux.

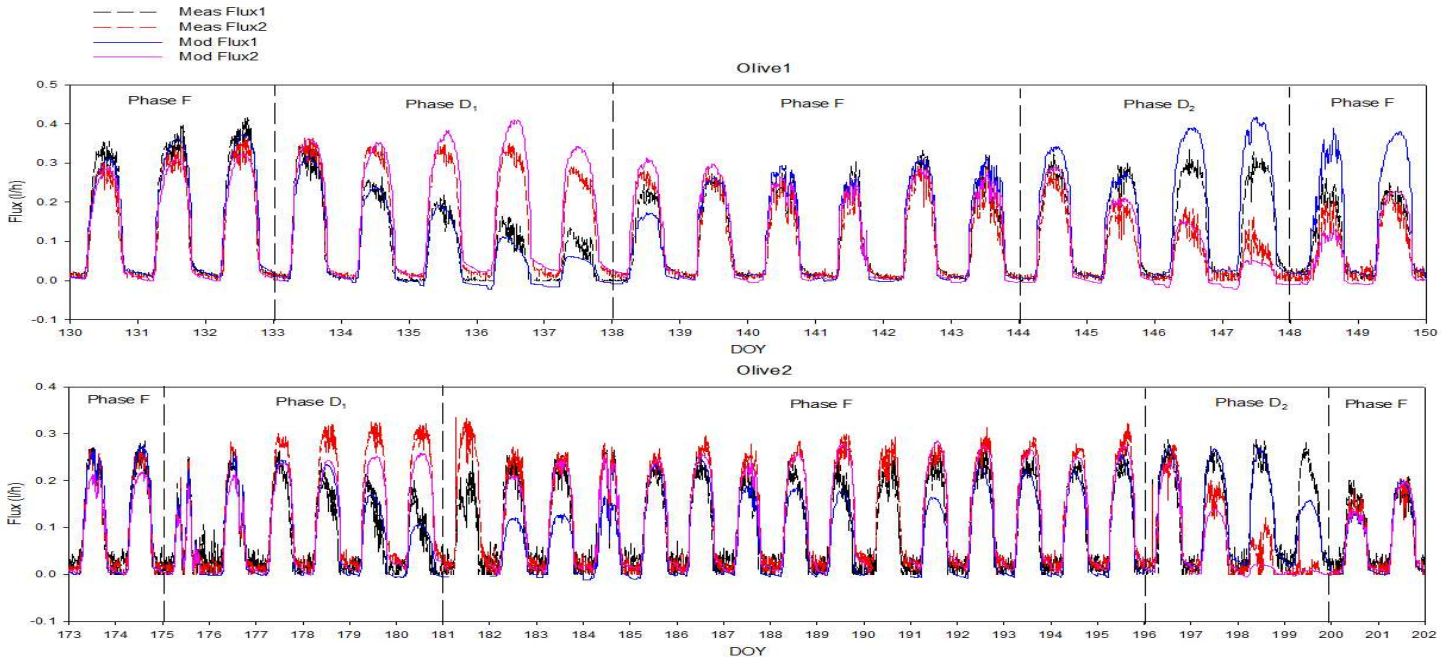

Fig 3.5. Time span of measured and modelled fluxes for olive trees no. 1 and no. 2 at different irrigation phases. Black and red lines are the fluxes measured from sides one and two, while blue and purple lines correspond to modelled fluxes from sides one and two.

3.4.3. Root dynamics

Root counts on both sides of the two olives trees highlighted root dynamics when a reduction in soil water content occurred in one part of the root system (Fig. 3.6). During the period of maximum stress, at the end of phase D_1, a decrease in the root counts on the water-deprived side was observed for both olives trees, with a reduction of 80% and 40% with respect to the value at the beginning of the drying cycle for olive trees no. 1 and no. 2. Surprisingly, for the same period, the irrigated side also underwent a 20% reduction in both olive trees. Counts after phase D_1, gave different results: while there was an increase in root appearance in olive tree no. 2; olive tree no. 1, which experienced a higher reduction in root counts on the dry side at the time of maximum stress (Dry (D)), was not able to reach the values at the beginning of the counting period (Irri (F2)).

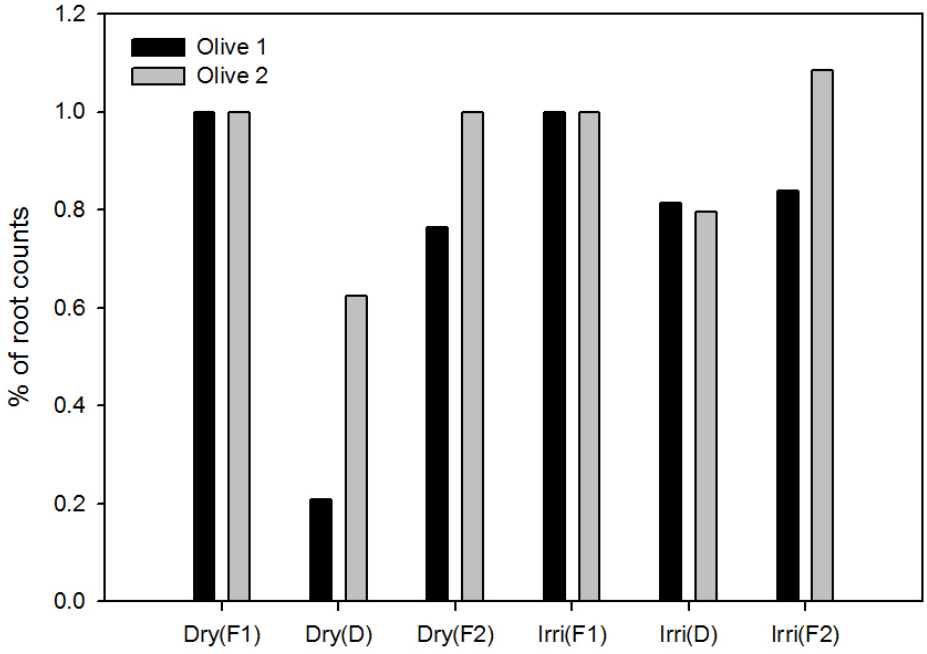

Fig 3.6. Root counts on both sides of the lysimeter for olive no. 1 (black) and no. 2 (grey) during their first drying phases, expressed as % of the initial (F1). Counts were made after the beginning of phase D_1 (F1), at the end of phase D_1 (D) and several days before the end of phase D_1 (F2). The dried and the irrigated side are indicated as "Dry" and "Irri".

3.4.4. Leaf water potential estimations

Fig.3.7 presents measured and modelled Ψ_l at the end of phase D_2 in olive tree no. 2, using two L_v values, one derived from root biomass measurements at the end of the experiment, and another where the root biomass was artificially reduced until modelled E_p and Ψ_l matched the measured values. When measured root biomass was used, a twelve bar difference between measured and modelled Ψ_l was

observed. However, when root biomass was reduced by 40% and Tuzet's empirical function was recalibrated, the model was able to match measured Ψ_l and E_p.

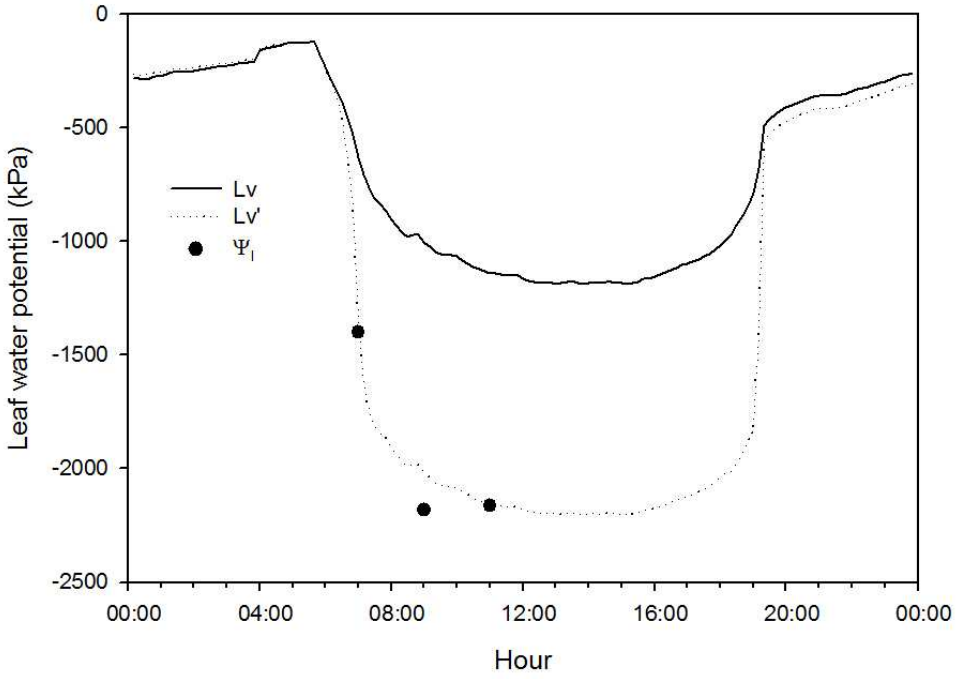

Fig 3.7. Measured (points) and modelled (lines) leaf water potential (Ψ_l). The solid line corresponds to modelled leaf water potential for measured L_v while the dotted line is the leaf water potential when effective L_v is assumed to be 60% of the measured value (L_v').

3.5. Discussion

3.5.1. Model performance

The fluxes during the different irrigation phases were successfully simulated (Fig 3.5). Nevertheless, some deviations were observed,

particularly after the end of the drying phases in both olive trees and also at the end of phase D_2 in olive tree no. 1. Those biases are probably associated with different phenomena. The deviation observed in olive tree no. 1 at the end of the experiment, might well be related to the root dynamics observed during the different phases of the experiment (Fig. 3.6). Unlike olive tree no. 2, olive tree no. 1 showed a reduction in root counts on both sides after phase D_1 (Fig. 3.6, column Dry F2 and Irri F2). This meant a lower L_v value than that used in the model at the start of the simulation period. As a result, L_v in the model was higher during the recovery period after phase D_2, leading to an overestimation of the modelled fluxes. On the other hand, the divergence observed immediately after the end of D phases, particularly in olive tree no. 2 (doy 181 and 182, Fig. 3.5) was related to a faster redistribution of water between layers than that predicted by the model (see appendix II). If the water applied to a previously dried side is less uniformly distributed by the model, increases in θ_{soil} associated with irrigation would be restricted to the top layers thus reducing the amount of roots with access to water and, as a result the predicted fluxes would be lower. However, those deviations have had a minor effect on the simulation of tree E_p, as can be deduced from the high R^2 (around 0.9) and the high efficiency factor (close to 1) for the four trees presented in Table 3.4.

Table 3.4. Coefficients for linear regressions, root mean square error (RMSE), model efficiency factor (EF) and regression coefficient (R^2).

	Olive1	***Olive2***	***Almond1***	***Almond2***
EF	0.92	0.94	0.90	0.84
RMSE	0.06	0.05	0.1	0.12
$\boldsymbol{R^2}$	0.93	0.95	0.91	0.89

For field conditions one would expect those errors to be smaller. Lifespan of roots growing in the field is prolonged during periods of water stress thanks to a redistribution of the water throughout the root system from the wetted zones to the driest areas, allowing the maintenance of the membrane integrity and root turgor (Bauerle *et al.*, 2008). On the contrary, in the set up used in the present experiments, the root system was completely divided into two parts preventing the redistribution of water from the wet to the dry compartments, leading to a faster root mortality (Bauerle *et al.*, 2008).

A mismatch between measured and modelled leaf water potential for olive tree no. 2 at the end of phase D_2 was observed (Fig. 3.7). One might argue that the absence of capacitance in the model was responsible for the differences observed. However under the climate conditions experienced during the experiment, with a high evaporative demand and clear days, the inclusion of the capacitance would only have served to improve the simulation of E_p at the beginning and end of the day, but it would not have had any implications in the estimation of daytime Ψ_l especially at noon. The mismatch observed between measured and modelled Ψ_l is more related to the

underestimation of tree resistance. Xylem failure could be a possible cause of the mentioned underestimation since the model does not include cavitation, but Sperry *et al.* (1998) demonstrated that the E_p of a tree with a root area/leaf area ratio (A_r:A_l) below 10 and growing in a sandy soil would be limited by rhizosphere resistance, meaning that R_s +R_r would be the main resistances controlling the tree water relations. The A_r:A_l ratios computed from Table 3.1 for olive and almond trees were 7.64 and 4.52, which suggests that cavitation, if it occurred, played a minor role.

Roots growing in a confined media tend to overlap producing clumping (see appendix II.). Root clumping has important effects on the determination of rhizosphere resistance since for its computation, it is assumed that roots are evenly distributed occupying soil cylinders of the same volume (Passioura, 1988, Tardieu *et al.*, 1992). To cope with this problem Passioura (1988) proposed the use of an effective L_v (L_v') as a substitute for the observed L_v. This author assumed that clumped roots would behave as a single one, with access to a given volume of soil; so that measured L_v should be reduced to L_v' to account for clumping when computing R_s and R_r. In our experiment, the use of an L_v' obtained from a 40% reduction of the L_v measured led us to match modelled Ψ_l and E_p with the data observed for olive tree no. 2 after the recalibration of Tuzet's parameters (Fig. 3.7). Unfortunately, Ψ_l was only measured for olive no tree. 2, so it was impossible to determine the L_v' for the other trees studied. However, that fact only had implications in the determination of Ψ_l and not in the simulation of the water extracted from each side of the split root system and tree transpiration (figs. 3.4 and 3.5). Under field conditions, where L_v is much lower than the values observed in the

present experiment, the effect of root clumping should be much smaller, although experimental confirmation is required.

3.5.2. The importance of a variable radial resistance

During the drying phases, the model was able to reproduce the reduction in flux of the dried side as water was withdrawn, and the maintenance or the increase on the wetted side. The same extraction patterns have been reported in other experiments with different species, in which only a fraction of the root system was watered (Green & Clothier, 1995, Ameglio *et al.*, 1999). Ameglio *et al.* (1999), studying partially irrigated walnut trees, observed a reduction in the flux and an increase in the total hydraulic resistance of the dried compartment. The author proposed two possible explanations for the observed increase: one related to a rise in R_s and another related to an increment in R_r. When the soil dries out, there is a sharp decrease in k, so R_s increases (eq. 2). In addition, changes in root morphology or the presence of air gaps between the root surface and the soil have been reported as the soil dries, with R_r increasing as a consequence (Herkelrath *et al.*, 1977, Bristow *et al.*, 1984, North & Nobel, 1992, Stirzaker & Passioura, 1996, North & Nobel, 1997). It is generally accepted that R_r is the major resistance of the plant if no cavitation occurs (Tyree & Zimmermann, 2002b). When θ_{soil} is reduced below a certain value, R_s is greater than R_r, and controls root water uptake (Gardner, 1960). However, as Newman (1969) demonstrated, this is only true when L_v is low (less than 5000 m m^{-3}); at higher values (more than 10000 m m^{-3}), R_s would hardly be of any significant importance, even when the soil is completely dry. To illustrate this idea, one can use the L_v data obtained from the experiment with olive

tree no. 1 to compute R_s and R_r (eqs. 2 and 3). While R_r at θ_{ul} is $3.3 \cdot 10^6$ kPa s m^2 kg^{-1} the value for R_s at θ_{ll} is $9.7 \cdot 10^4$ kPa s m^2 kg^{-1}, two orders of magnitude lower. The observed reduction in L_v at the end of phase D_1 (Fig. 3.6, Dry (D) column) does not change the aforementioned relation between R_s and R_r when the soil is dried out. Although a decrease in L_v would not affect both resistances to the same extent, the two orders difference is still maintained between them even with the reduced L_v observed (data not shown). Looking at the numbers in the example, it would seem that, given the high L_v values measured (Table 3.1), R_r is the main regulator of the rate of water uptake on both sides, even under dry conditions.

The Bristow equation (appendix II) includes the effect of a drying soil on r_r and its incorporation into the model significantly improved the simulations during the drying phases. Values of L_v above the threshold of 10000 m $m^{-3}$are commonly observed in the field (Jackson *et al.*, 1996), which means that situations in which R_r controls root water uptake are not restricted to potted plants. Yet, the Bristow equation is an empirical function, so the development of a more mechanistic model should be a priority in future studies.

The model presented here does not include chemical signaling like ABA in the control of stomatal conductance. In theory, the ABA generated in the roots as a response to a drying soil, would amplify the feedback of water potential on stomatal conductance, thereby reducing transpiration (Tardieu & Davies, 1992). However, that reduction was not observed when one side was dried out (Fig. 3.8). The daily relative flux (the ratio of measured flux and reference evapotranspiration) of the wetted side increased during drying phase D_2. The decay observed

at the beginning of phase D_2 is related to a one day interruption of the irrigation on both sides whereupon the wetted side recovered almost instantly after that day without irrigation. The evidences reported here does not imply the absence of ABA during phase D_2 , but a possible lack of control over the stomata under the conditions of the present experiment, as Holbrook *et al.* (2002) reported for split-root tomato plants.

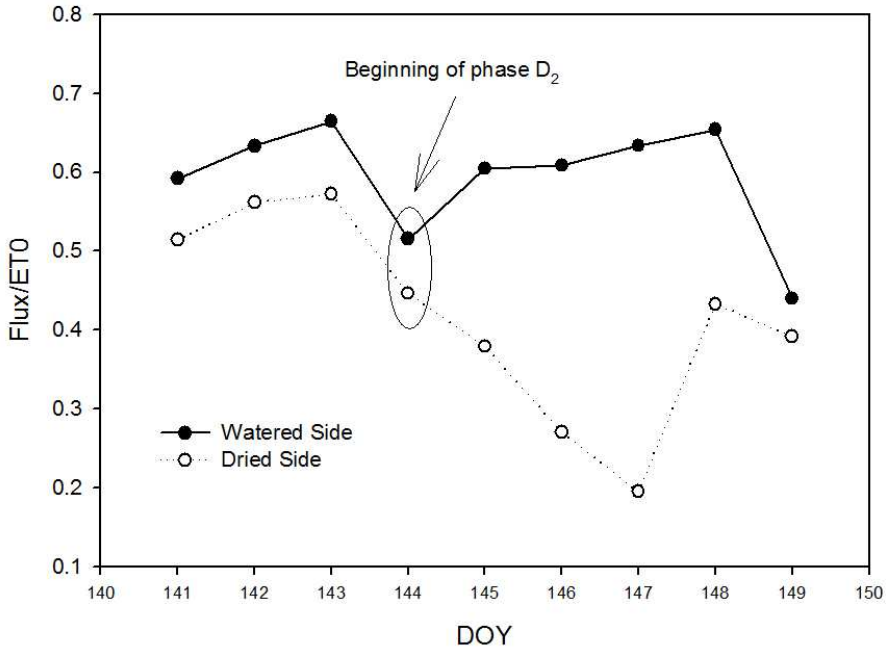

Fig 3.8. Relative measured fluxes from olive tree no. 1 from three days after the beginning of phase D_2 until the end of the experiment. The relative values correspond to the fluxes measured with sap flow probes divided by the reference evapotranspiration (ET0). The circle indicates the beginning of phase D in which the irrigation was cut off on both sides of the lysimeter. Filled dots relates to the watered side whilst the empty dots represent the side that has been dried out.

3.5.3. Species-related parameters and their implications

Table 3.1 presents a summary of the parameters measured for the two species studied that showed a large difference in specific root length while the root radius was almost the same. The root bulk density, i.e. the ratio of dry mass and root volume (ρ_{root}, g cm^{-3} *)* can be calculated as:

$$\rho_{root} = \frac{1}{\pi\, a_{root}{}^2 SRL} \quad (14)$$

The value for olive (2.1 10^3 kg m^{-3}) doubled the one for almond (1.1 10^3 kg m^{-3}) in parallel with differences in root radial resistance. García-Tejera *et al.* (2016) found the same difference in r_r for the two species used here at 20 and 25ºC. The relation between root density and r_r might be related to the deposition of compounds like lignin in the exo- and endodermis of the root, thus reducing its permeability (North & Nobel, 1992). Future work should test the feasibility of using root density to predict root radial resistance for different species or genotypes, which could be used as a selection index in breeding programmes. The model presented here couples the water supply and demand of the tree so it could be used to study the implications of the variability in the parameters between and within species in water uptake under limited water supply for different current and future environments.

3.6. Conclusions

The SPAC model presented here can simulate tree transpiration when a contrasting water content situation exists in the soil by using a soil multi-compartment approach. The model was able to simulate the tendencies in the fluxes of both sides when different levels of stress were applied to olive and almond trees. The inclusion of a variable R_r was essential for simulating the water extracted from each soil compartment, and it was necessary to account for root clumping (through an effective root length density) to match the measured Ψ_l and E_p. The model integrates the whole plant response to water availability using a mechanistic approach to describe the supply and demand functions using measurable parameters. This provides a useful tool for exploring the interaction between the plant and the environment in the cases in which a non-uniform water content is present in the root zone. The inclusion of physiological and anatomical parameters of the roots may be useful as a help in breeding programmes for tree crops.

Acknowledgements

This work was supported by project AGL-2010-20766 of the Spanish Ministry of Economy and Competitiveness (former Ministry of Science and Innovation) and by the European Community's Seven Framework Programme-FP7 (KBBE.2013.1.4-09) under Grant Agreement No. 613817 (MODEXTREME, modextreme.org). The authors wish to thank both the "FPI" programme of the aforementioned ministry and the JAE programme of the Spanish Research Council (CSIC) for providing the Ph.D. scholarships granted to the first and the second author, respectively. We also thank Manolo Gonzalez, Jose Luis Vazquez, Ignacio Calatrava and Rafael del Río for the excellent technical assistance provided.

References

Ameglio T, Archer P, Cohen M, Valancogne C, Daudet FA, Dayau S, Cruiziat P (1999) Significance and limits in the use of predawn leaf water potential for tree irrigation. Plant and Soil 207: 155-167.

Bauerle TL, Richards JH, Smart DR, Eissenstat DM (2008) Importance of internal hydraulic redistribution for prolonging the lifespan of roots in dry soil. Plant Cell and Environment 31: 177-186.

Bernacchi CJ, Singsaas EL, Pimentel C, Portis Jr AR, Long SP (2001) Improved temperature response functions for models of Rubisco-limited photosynthesis. Plant, Cell & Environment 24: 253-259.

Bristow KL, Campbell GS, Calissendorff C (1984) The effects of texture on the resistance to water-movement within the rhizosphere. Soil Science Society of America Journal 48: 266-270.

Campbell GS (1985) Soil physics with BASIC : transport models for soil-plant systems. Elsevier, Amsterdam ; New York.

Campbell GS, Norman JM (1998) Introduction to environmental biophysics. Springer, New York.

Clothier BE, Green SR (1997) Roots: The big movers or water and chemical in soil. Soil Science 162: 534-543.

Couvreur V, Vanderborght J, Javaux M (2012) A simple three-dimensional macroscopic root water uptake model based on the hydraulic architecture approach. Hydrol Earth Syst Sci 16: 2957-2971.

Cowan IR (1965) Transport of Water in the Soil-Plant-Atmosphere System. Journal of Applied Ecology 2: 221-239.

dePury DGG, Farquhar GD (1997) Simple scaling of photosynthesis from leaves to canopies without the errors of big-leaf models. Plant Cell and Environment 20: 537-557.

Diaz-Espejo A, Walcroft AS, Fernandez JE, Hafridi B, Palomo MJ, Giron IF (2006) Modeling photosynthesis in olive leaves under drought conditions. Tree Physiol 26: 1445-1456.

Doussan C, Pages L, Vercambre G (1998) Modelling of the hydraulic architecture of root systems: An integrated approach to water absorption - Model description. Annals of Botany 81: 213-223.

Egea G, Gonzalez-Real MM, Baille A, Nortes PA, Diaz-Espejo A (2011a) Disentangling the contributions of ontogeny and water stress to photosynthetic limitations in almond trees. Plant Cell Environ 34: 962-979.

Egea G, Gonzalez-Real MM, Baille A, Nortes PA, Diaz-Espejo A (2011b) Disentangling the contributions of ontogeny and water stress to photosynthetic limitations in almond trees. Plant Cell and Environment 34: 962-979.

Farquhar GD, von Caemmerer S, Berry JA (1980) A biochemical model of photosynthetic CO2 assimilation in leaves of C3 species. Planta 149: 78-90.

García-Tejera O, López-Bernal Á, Villalobos FJ, Orgaz F, Testi L (2016) Effect of soil temperature on root resistance: implications for different trees under Mediterranean conditions. Tree Physiology.

Gardner WR (1960) Dynamic aspects of water availability to plants. Soil Science 89: 63-73.

Green S, Clothier B, Jardine B (2003) Theory and Practical Application of Heat Pulse to Measure Sap Flow. Agronomy Journal 95.

Green SR, Clothier BE (1995) Root water uptake by kiwifruit vines following partial wetting of the root zone. Plant and Soil 173: 317-328.

Green SR, Kirkham MB, Clothier BE (2006) Root uptake and transpiration: From measurements and models to sustainable irrigation. Agricultural Water Management 86: 165-176.

Hacke UG, Sperry JS, Wheeler JK, Castro L (2006) Scaling of angiosperm xylem structure with safety and efficiency. Tree Physiology 26: 689-701.

Herkelrath WN, Miller EE, Gardner WR (1977) Water Uptake By Plants: II. The Root Contact Model. Soil Science Society of America Journal 41: 1039-1043.

Hillel D (2003) Plant uptake of soil moisture. Introduction to Environmental Soil Physics. Elsevier Science,, Burlington.

Holbrook NM, Shashidhar VR, James RA, Munns R (2002) Stomatal control in tomato with ABA-deficient roots: response of grafted plants to soil drying. Journal of Experimental Botany 53: 1503-1514.

Jackson RB, Canadell J, Ehleringer JR, Mooney HA, Sala OE, Schulze ED (1996) A global analysis of root distributions for terrestrial biomes. Oecologia 108: 389-411.

Jackson RB, Sperry JS, Dawson TE (2000) Root water uptake and transport: using physiological processes in global predictions. Trends in Plant Science 5: 482-488.

Jarvis PG, McNaughton KG (1986) Stomatal control of transpiration - scaling up from leaf to region. Advances in Ecological Research 15: 1-49.

Javaux M, Couvreur V, Vander Borght J, Vereecken H (2013) Root Water Uptake: From Three-Dimensional Biophysical Processes to Macroscopic Modeling Approaches. Vadose Zone Journal 12.

Kramer PJ (1969) Plant & Soil Water Relationships: A Modern Synthesis.

Lemon E, Stewart DW, Shawcroft RW (1971) The Sun's Work in a Cornfield. Science 174: 371-378.

Monsi M, Saeki T (1953) Uber den Lichtfaktor in den Pflanzengesellschaften und seine Bedeutung fur die Stoffproduktion. Japanese Journal of Botany 14: 22-52.

Moriana A, Villalobos FJ, Fereres E (2002) Stomatal and photosynthetic responses of olive (Olea europaea L.) leaves to water deficits. Plant, Cell & Environment 25: 395-405.

Muñoz-Carpena R, Regalado CM, Álvarez-Benedi J, Bartoli F (2002) Field evaluation of the new philip-dunne permeameter for measuring saturated hydraulic conductivity. Soil Science 167: 9-24.

Newman EI (1969) Resistance to Water Flow in Soil and Plant. I. Soil Resistance in Relation to Amounts of Root: Theoretical Estimates. Journal of Applied Ecology 6: 1-12.

North GB, Nobel PS (1992) Drought-induced changes in hydraulic conductivity and structure in roots of ferocactus-acanthodes and opuntia-ficus-indica. New Phytologist 120: 9-19.

North GB, Nobel PS (1997) Root-soil contact for the desert succulent Agave deserti in wet and drying soil. New Phytologist 135: 21-29.

Orgaz F, Villalobos FJ, Testi L, Fereres E (2007) A model of daily mean canopy conductance for calculating transpiration of olive canopies. Funct Plant Biol 34: 178-188.

Passioura JB (1988) Water Transport in and to Roots. Annual Review of Plant Physiology and Plant Molecular Biology 39: 245-265.

Regalado C, Muñoz Carpena R, Socorro AR, Hernández Moreno JM (2001) ¿Por qué los suelos volcánicos no siguen la ecuación de Topp? Universidad Pública de Navarra: 75-82.

Sinclair TR, Murphy CE, Knoerr KR (1976) Development and Evaluation of Simplified Models for Simulating Canopy Photosynthesis and Transpiration. Journal of Applied Ecology 13: 813-829.

Sperry JS, Adler FR, Campbell GS, Comstock JP (1998) Limitation of plant water use by rhizosphere and xylem conductance: results from a model. Plant Cell and Environment 21: 347-359.

Steudle E (2000) Water uptake by roots: effects of water deficit. Journal of Experimental Botany 51: 1531-1542.

Steudle E, Peterson CA (1998) How does water get through roots? Journal of Experimental Botany 49: 775-788.

Stirzaker RJ, Passioura JB (1996) The water relations of the root-soil interface. Plant Cell and Environment 19: 201-208.

Swanson RH, Whitfield DWA (1981) A Numerical Analysis of Heat Pulse Velocity Theory and Practice. Journal of Experimental Botany 32: 221-239.

Tardieu F, Bruckler L, Lafolie F (1992) Root clumping may affect the root water potential and the resistance to soil-root water transport. Plant and Soil 140: 291-301.

Tardieu F, Davies WJ (1992) Stomatal Response to Abscisic Acid Is a Function of Current Plant Water Status. Plant Physiology 98: 540-545.

Testi L, Villalobos FJ (2009) New approach for measuring low sap velocities in trees. Agricultural and Forest Meteorology 149: 730-734.

Tuzet A, Perrier A, Leuning R (2003) A coupled model of stomatal conductance, photosynthesis and transpiration. Plant Cell and Environment 26: 1097-1116.

Tyree MT, Ewers FW (1991) The hydraulic architecture of trees and other woody plants. New Phytologist 119: 345-360.

Tyree MT, Zimmermann MH (2002) Hydraulic architecture of whole plants and plant performance. Xylem Structure and the Ascent of Sap. Second edn. Springer-Verlag Berlin Heidelberg.

van den Honert TH (1948) Water transport in plants as a catenary process. Discussions of the Faraday Society 3: 146-153.

Villalobos FJ, Orgaz F, Testi L, Fereres E (2000) Measurement and modeling of evapotranspiration of olive (Olea europaea L.) orchards. European Journal of Agronomy 13: 155-163.

Wheeler JK, Sperry JS, Hacke UG, Hoang N (2005) Inter-vessel pitting and cavitation in woody Rosaceae and other vesselled plants: a basis for a safety versus efficiency trade-off in xylem transport. Plant, Cell & Environment 28: 800-812.

Whisler FD, Acock B, Baker DN, Fye RE, Hodges HF, Lambert JR, Lemmon HE, McKinion JM, Reddy VR (1986) Crop Simulation Models in Agronomic Systems. In: NC Brady (ed) Advances in Agronomy. Academic Press.

Williams M, Rastetter EB, Fernandes DN, Goulden ML, Wofsy SC, Shaver GR, Melillo JM, Munger JW, Fan SM, Nadelhoffer KJ (1996) Modelling the soil-plant-atmosphere continuum in a Quercus-Acer stand at Harvard forest: The regulation of stomatal conductance by light, nitrogen and soil/plant hydraulic properties. Plant Cell and Environment 19: 911-927.

Wit CTd (1965) Photosynthesis of leaf canopies. Wageningen,NL. Pudoc, Wageningen.

Chapter 4

Field validation of the multi-compartment SPAC model for olive trees and analysis of the effect of wetted area on tree transpiration

Chapter 4

Field validation of the multi-compartment SPAC model for olive trees and analysis of the effect of wetted area on tree transpiration

Summary

In the present chapter the multi-compartment SPAC model is tested in a drip irrigated hedgerow olive tree plantation. Modelled transpiration (E_p) is compared with 2 years of calibrated sap flow records for two different irrigation treatments, a control (C) that is watered using a crop coefficient of 0.75 and a regulated deficit irrigation (RDI) in which the irrigation applied is gradually reduced in relation to that of the control during midsummer. Midday leaf water potential (Ψ_l) from the simulations is also compared with measurements performed twice a month in each treatment and for both years. The model accurately predicts E_p in both years for the two treatments (R^2=0.81 and RMSE= 0.29 mm) while, Ψ_l is slightly underestimated. Analysis performed using the model shows that the use of drip irrigation systems limits the maximum attainable E_p for a given environment, and that the degree of limitation would depends on the ratio of areas of roots and leaves and the vapour pressure deficit (VPD). The model proved to be a tool robust enough to capture the trend in E_p and Ψ_l for trees submitted to different irrigation regimes and allows the study of the interactions among irrigation, tree E_p and the environment.

4.1. Introduction

Irrigation is applied in periods when soil available water in the root zone cannot meet the evaporative demand from the atmosphere, minimizing the impact that water limitation might have on crop production (Loomis & Connor, 2002). In general, an efficient irrigation practice should increase the fraction of water devoted to transpiration (E_p) as it is proportional to biomass production (De Wit, 1958), reducing the losses by evaporation, drainage and runoff. If water is limited, it will also be necessary to reduce irrigation amounts when the vapour pressure deficit (VPD) is high and the impacts on yield are minimal. The VPD modulates the rate of E_p allowing the plant to fix more or less carbon per unit of water transpired (transpiration efficiency), thus, reducing E_p by limiting the water supplied to the crop during the periods of high atmospheric demand should increase the transpiration efficiency (Tanner & Sinclair, 1983). The use of drip irrigation along with regulated deficit irrigation (RDI) meets both objectives. The former reduces soil evaporation by restricting the soil wetted area and ensuring a high uniformity of application (Tanji & Hanson, 1990). The latter implies concentrating the water deficit in periods where evaporative demand is high and yield is less sensitive to stress, increasing as a consequence the transpiration efficiency while maintaining the harvest index (Chalmers *et al.*, 1981).

Drip irrigation systems and deficit irrigation strategies have been more successful on fruit trees than on annual crops (Fereres & Soriano, 2007). First, because in general, on tree crops, the soil is not completely covered by tree canopies, leaving a soil surface

permanently exposed for evaporation (E_s) (Fereres & Soriano, 2007). As an example, Villalobos *et al.* (2000) calculated a 24% annual loss of E_s from an olive plantation representing an average irrigated orchard in Andalusia, Spain (fraction of ground cover equal to 0.4). Second because the effect of a reduction in stomatal conductance due to water deficit has a greater impact on canopies coupled to the atmosphere (Jarvis & McNaughton, 1986), as is the case of trees composed of tall, rough canopies. Finally, because the returns from tree production are more related, to crop quality than biomass production, as for annual crops (Fereres & Soriano, 2007). However, the adoption of RDI together with drip irrigation is not a guarantee of success when one tries to increase water use efficiency unless a good combination between the management of the drip irrigation system, the soil hydraulic properties and the crop water requirements is attained (Andreu *et al.*, 1997).

Models can provide a useful tool to explore the relations among the elements composing the system by highlighting the knowledge gaps that require stronger research efforts. Using a model we can also speed up and reduce the cost of research. By way of illustration, Testi *et al.* (2006) developed a model to simulate olive evapotranspiration (ET) that accounted for leaf area index (LAI) variations successfully, allowing the estimates of olive ET for well-watered trees of any size and in any location. The model created by Testi *et al.* (2006) permitted the quick analysis of different orchards typologies, that otherwise will take decades of research using the traditional methods based on field experiments.

In modelling the plant-water relations one should be aware of the interaction and the scales at which the different elements of the system work. Transpiration and photosynthesis occur in the leaves and are influenced by the local microclimate conditions, but the demand of water from the leaves must be matched by the uptake from the roots which in turns depends on their spatial distribution and on the soil water content (θ_{soil}) (Clothier & Green, 1994, Williams *et al.*, 1996). Only few models in the literature integrate the demand and the supply functions to simulate transpiration and photosynthesis when some degree of water stress is present (Williams *et al.*, 1996, Sperry *et al.*, 1998, Tuzet *et al.*, 2003). Yet, while they discretized the canopy to account for nitrogen variability or the light environment, the soil is simply modelled using a multi-layered one-dimensional approach. This might well lead to important errors when large spatial heterogeneities in root length density (L_v) and/or θ_{soil} are present, as might happen when using drip irrigation (Clothier & Green, 1997).

In this chapter the multi-compartment SPAC model described in chapter 2 is tested in a drip irrigated, hedgerow olive orchard (~1666 trees ha^{-1}) for two different irrigation strategies. Then, the model is used to analyse the effect of different combinations of irrigation volumes and soil wetted areas to establish rational criteria for selecting optimum irrigation managements.

4.2. Materials and methods

4.2.1. Model description

Simulations of E_p and leaf water potential (Ψ_l) were performed with the multi-compartment SPAC model described in chapter 2. The model uses an electric circuit analogy to simulate water movement from soil through roots, trunk and branches and it release to the atmosphere across the stomata. The canopy is split in two leaf classes, sunlit and shaded and the soil is also divided into several layers and in two different compartments to account for heterogeneity on root length density (L_v) and soil water content (θ_{soil}). A brief description of the model with the most relevant equations and the operational procedure is presented here. A detailed description is given in the supplementary material one at the end of the present document.

4.2.1.1. Leaves

Following dePury and Farquhar (1997), the canopy is split into sunlit and shaded leaves. The area of sunlit and shaded leaves of the tree crown is computed at 10-minute intervals using a simple geometric model while the fractions of diffuse and direct radiations are estimated using Spitters et al. (1986) and corrected for Mie and Rayleigh scattering. Then, for each leaf class, stomatal conductance is calculated using Tuzet et al. (2003) equation, in which the stomatal conductance is a function of leaf assimilation, computed using Farquhar et al. (1980), the concentration of CO_2 in the sub stomatal cavities (C_i) and Ψ_l:

$$g_{co2sun} = g_0 + \frac{mA'_{sun}}{C_{isun} - \Gamma} f(\Psi_{lsun})$$

(1)

where:

$$f(\Psi_{lsun}) = \frac{1 + \exp[s_f \Psi_f]}{1 + \exp[s_f(\Psi_f - \Psi_{lsun})]}$$

(2)

where g_{co2} and g_0 (mmol m^{-2} s^{-1}) are the stomatal conductance for CO_2 and the night time conductance (i.e. for zero gross assimilation), m (dimensionless) is a proportionality factor between photosynthesis and stomatal conductance, A' (µmol photons m^{-2} s^{-1}) is the gross assimilation and Γ is the light compensation point. In equation 2, Ψ_f (kPa) and s_f (kPa^{-1}) are shape factors related to the point at which Ψ_l begins to limit the stomatal conductance and the rate at which this limitation take place. The suffix 'sun' in both equations indicates that the results will correspond to sunlit leaves. For the shaded ones the expressions are exactly the same except for the suffix which should be changed by 'shade'.

4.2.1.2. Roots

Root water uptake depends on two main resistances, soil (R_s) and root (R_r) resistances. R_s is related to water flow from the soil to the root surface and is calculated using the analytical expression developed by Gardner (1960). R_r is the resistance to water flow from the root

surface to the root xylem. One of the main features of the present model is that the global resistance of the root-soil system can vary with θ_{soil} and the soil temperature (T_{soil}). Soil drying results in an increase in R_s induced by a strong reduction of hydraulic conductivity. On the other hand, R_r is a function of T_{soil} and is calculated using the empirical equation developed by García-Tejera et al. (2016) for olive and corrected then for θ_{soil} using the empirical function of Bristow et al. (1984). If T_{soil} records are not available, García-Tejera et al. (2016) demonstrated that mean air temperature can be used as a surrogate for soil temperature. In the model, the root xylem resistance is considered negligible respect to R_s and R_r.

$$R_s = \frac{\ln\left(\frac{1}{\pi Lv\ {a_{root}}^2}\right)}{Lv\ d\ 4\pi k} \quad (3)$$

$$R_r = \frac{r_r(\theta, T)}{Lv\ d} \quad (4)$$

Where a_{root} is the root radius (m), d is the depth of the soil layer (m), k is the soil unsaturated conductivity (kg s m^{-3}) and r_r is the root specific hydraulic resistance (kPa s m kg^{-1}) that is a function of soil water content and temperature (Bristow *et al.*, 1984, García-Tejera *et al.*, 2016).

4.2.1.3. Linking roots and leaves

The demand (leaves) and the supply (roots) structures are connected through xylem vessels. The transport of water through trunk xylem

vessels (R_x) is modelled using a modified version of the Hagen-Poiseulle function to account for pit resistance (see appendix I).

Once the areas of sunlit and shaded leaves and each of the resistances of the tree (R_r, R_s and R_x) are known, the model computes leaf water potential (Ψ_l) of sunlit leaves as:

$$\Psi_{lsun} = \frac{\sum \frac{\Psi_{si,j}}{R_{si,j} + R_{ri,j}}}{\sum \frac{1}{R_{si,j} + R_{ri,j}}} - g_{co2sun} 1.6 \frac{VPD}{P} 0.018 \left(\frac{\sum \frac{1}{R_{si,j} + R_{ri,j}} + R_x}{f_{sun}} \right) LAI_{sun} \quad (5)$$

As for equations 1 and 2 the suffix 'sun' refers to sunlit leaves. The expression being the same for the shaded ones. In the equation, Ψ_s is the soil water potential (kPa), LAI_{sun} (m^2 leaf m^{-2} ground) is the leaf area index of sunlit leaves, and f_{sun} is the ratio of sunlit to total leaf area. The coefficients transform the conductance for CO_2 in mmol m^{-2} s^{-1} to conductance for H_2O in kg m^{-2} s^{-1}. The suffix *i* and *j* represent the soil layer and compartment number, respectively. Equation 5 implies that the tree is split in two parts according to the fractional area of sun and shade leaves, i.e. sunlit and shaded leaves will be sustained by a proportion of roots and xylem area in the trunk equal to f_{sun} and f_{shade}, respectively.

The model iterates for g_{co2sun} and Ψ_{lsun} until an equilibrium in internal CO_2 concentration is reached. Finally, E_p is computed as the sum of transpiration of sunlit and shaded leaves.

$$E_{psun} = 1.6\, g_{co2sun} \frac{VPD}{P} LAI_{sun}$$

(6)

$$E_{pshade} = 1.6\, g_{co2shade} \frac{VPD}{P} LAI_{shade}$$

(7)

Where P is the atmospheric pressure (kPa).

In equations 6 and 7 the canopy is assumed to be fully coupled to the atmosphere, thus transpiration is calculated using the imposed evaporation version of the Penmman-Monteith equation (Villalobos *et al.*, 2000, Orgaz *et al.*, 2007).

4.2.1.4. Soil

The relationships between soil hydraulic conductivity and matric potential are those proposed by Campbell and Norman (1998). The approach developed by Bonachela *et al.* (2001)for calculating soil evaporation in row crops have been added to the model to simulate field plants.

4.2.2. Model validation

4.2.2.1. Site description

The outputs of the model were compared to field measurements in a commercial hedgerow olive (*Olea europeaea* 'Arbequina') orchard in Cordoba (37.8 ºN, 4.8 ºW, 170 m altitude), Spain from 2012 to 2013. Trees were planted on 2005 at a 4 x 1.5 m spacing (~1667 trees ha^{-1}) and were drip irrigated with three emitters per plant with a discharge

rate of 2.2 Lh^{-1}. The soil was classified as a Vertisol with a depth around 0.6 m.

In order to test the model under different water regimes, two irrigations treatments composed of plots of 40 trees in four adjacent rows were established in one corner of the orchard. The treatments were:

- Control irrigation (C): Irrigation amounts were estimated as the difference between ET and rainfalls, computing ET as the product of ET0 and a crop coefficient. The crop coefficient was set to 0.75, a value high enough to ensure a good tree water status as it was confirmed by the water potential measurements.
- Regulated deficit irrigation (RDI): Each year, irrigation amounts for this treatment were exactly the same as those for the C except for a period running from June to August in which the water applied was monthly reduced to 50, 25 and 20 % of that of the control.

In both treatments irrigations were performed 3 times a week. Fig. 4.1 presents annual values of ET0 and rainfall together with the cumulative irrigation for each treatment.

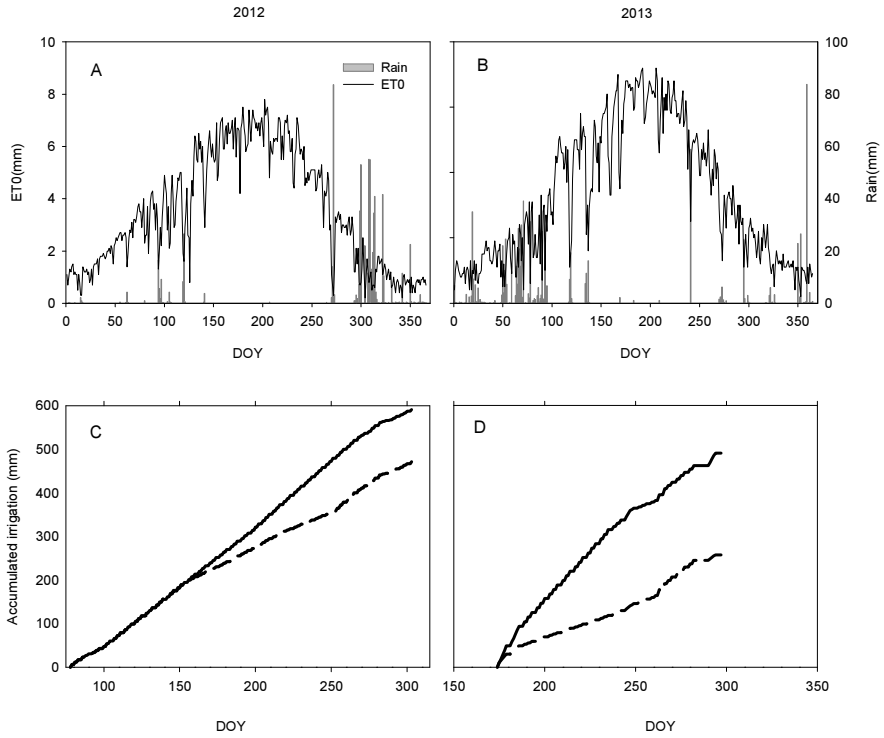

Fig 4.1. Annual evolution of reference evapotranspiration (ET0, black lines) and precipitation for years 2012 and 2013 (graphs A and B), and accumulated irrigation for years 2012 and 2013 for C (straight line) and RDI (dashed line) treatments (graphs C and D).

Meteorological variables were recorded at 10-min intervals from an automated weather station located near one of the orchard borders. The station was composed of a sheltered air temperature and humidity probe (model HMP35, Vaisala, Helsinki, Finland), placed at 1.7 m height; a silicon cell pyranometer (model SKS 1110, Skye Instruments LTD, Llandrindod Wells, Powys, UK), at 1.7 m height, a propeller wind monitor (model 05103, RM Young, Traverse City, MI, USA) at 2 m height and a tipping bucket rain gauge produced in the IAS-CSIC laboratories (Cordoba, Spain) placed at 0.4 m height.

4.2.2.2. Plant measurements

During the experiment, determinations of canopy structure, Ψ_l and E_p were performed. Measurements were concentrated in two trees from each treatment selected as representative of the plot. L_v records were also carried out on 2013 in three different trees of the same plot corresponding to the repetition of the treatment. The sections below describe in detail each of the plant measurements carried out.

4.2.2.3. Transpiration Measurements

Transpiration (E_p) was derived from sap flow records obtained from two of the central trees in the plot from each irrigation treatment using the compensated heat-pulse method (Swanson & Whitfield, 1981) and the Calibrated Average Gradient method (Testi & Villalobos, 2009). Each tree was monitored with one probe placed at a height of 30 cm above soil ground and below the main branches. The probes were covered with a shelter to avoid errors related due to heating of the wires. Probes, developed at the IAS-CSIC laboratory, consist of a 4.8-W stainless steel heater of 2mm diameter and two temperature sensors located 10 and 5 mm down and upstream of the heater respectively (Testi & Villalobos, 2009). Each temperature probe has four embedded type E (chromel-constantan wire) thermocouple junctions, spaced 10 mm along the needle, that were sampled separately to obtain heat-pulse velocities at 5, 15, 25 and 35 mm below the cambium. The system was controlled by a datalogger (CR1000, Campbell Scientific Inc., Logan, UT, USA) and sampled at 15-min intervals. Heat-pulse velocities were corrected for wounding reactions (Green *et al.*, 2003). The sap flow values were finally derived by

integration of sap flux densities first across the trunk radius and then around the azimuth angle (Green *et al.*, 2003).

Sap flow records need to be corrected for the azimuthal variability of sap flow rates (López-Bernal *et al.*, 2010). To do so, they were calibrated using the model of Villalobos *et al.* (2013), which allows the estimation of tree transpiration (E_{ps}) as a function of daily solar radiation (S_G) and the mean daytime VPD (VPD_{mean}):

$$E_{ps} = 37.08\ 10^{-3} \frac{QS_G}{a + b\,VPD_{mean}} \frac{VPD_{mean}}{P} \quad (8)$$

Where Q is the fraction of photosynthetically active radiation (PAR) intercepted by the canopy and parameters 'a' and 'b' are related to the radiation use efficiency and the specific response to VPD_{mean}. The coefficient 37.08 10^{-3} converts from Jules of solar radiation to µmol quanta and from mol to kg of H_2O. Values for a and b for olive were obtained from Villalobos *et al.* (2013). Radiation interception was derived from a simplified version of the model of Mariscal *et al.* (2000b).

The calibration coefficients for each tree in each treatment were determined at the beginning of summer, before the start of the divergence in their water status, and assumed constant throughout the season. The calibration data corresponded to a clear day in which leaf water potential showed no differences among treatments and good tree water status.

4.2.2.4. Canopy Structure

Ground cover (GC) was derived from canopy volume (V) measurements deduced from tree silhouette, dividing the tree in trapezoids and revolved them around the vertical axis computing the resulting volume with the second Pappus-Guldinus theorem (Selby & Company, 1974) . Each trapezoid was determined by measuring, at different points on a regular grid, the limits of the foliage at top and bottom of the canopy on a vertical large ruler. The grid was composed of three transects perpendicular to the planting row separated at a 0.75m interval. Each transect was divided into 10 segments of 20 cm. Leaf area (LA), was calculated as the product of leaf area density (LAD) and V using the procedure described in Iniesta *et al.* (2009). Leaf area density was estimated from measurements of vertical transmisivity with a plant canopy analyser (LAI-2000, Li-Cor, Lincoln, NE) either on cloudy days or just before sunrise.

4.2.2.5. Water potential measurements

Midday leaf water potential was measured using a pressure chamber (Soil Moisture Equipment Corp., Santa Barbara, CA) from June to October. Each measurement consisted on the collection of four sun exposed leaves at canopy top from each treatment in one of the trees instrumented with sap flow probes.

4.2.2.6. Root length density

Root length density (L_v) was obtained from soil cores on August 2013 (DOY 233). Cores were extracted using an auger sampler with a 0.04 m diameter from C and RDI in three trees which corresponded to the repetitions of the same treatment. The selected trees were adjacent to

the ones monitored with sap flow probes and had a similar canopy size. Measurements were performed in a transect perpendicular to the dripper line at 0.25, 0.75 and 1.5 m from the emitter and at a soil depth of 0.15, 0.3 and 0.6 m. Once collected, the cores were stored in refrigerators at 5ºC until they were processed. The time between the collection of the samples and their analysis never exceeded more than one month.

To analyse the samples, the roots were first separated from the soil by putting the cores at the top of a column made from three screen mesh of 3, 2 and 1 mm under free running water. The soil was washed and the roots remaining in each screen mesh were manually collected and stored in a 50:50 % ethanol : water solution at 5ºC for later determinations. Clean roots in the solution were digitally scanned using a commercial scanner (HP Scanjet G3110) and analysed using the WinRhizo software (Regent Instruments Inc, Quebec City, Canada) to obtain root length and average root radius. Root length density was derived dividing the measured root length by the sampling volume.

4.2.2.7. Soil water content

The soil water content was monitored in each treatment every 15 days with a neutron probe (model 503, Campbell Pacific Nuclear Corp, Pacheco, CA). Six access tubes per treatment were installed in one of the trees monitored with a sap flow probe. Access tubes were buried in two lines of three points perpendicular to the planting row at a distance of 0.25, 0.75 and 1.5m from the drip line; one line in front of a dripper and the other in the mid-distance between two drippers.

4.2.3. Model parametrization and calibration

A list of the parameters together with a detailed description of the model is provided in supplementary material one. The inputs required were measured during the experiment or taken from the literature when necessary except s_f, Ψ_f and g_0 (eq. 1 and 2), that were calibrated at the end of the experiment. The parameters of the Farquhar *et al.* (1980) biochemical model of photosynthesis were taken from Diaz-Espejo *et al.* (2006) and Moriana *et al.* (2002) while the parameters related to canopy structure were obtained from Mariscal *et al.* (2000b). The inputs required to calculate the resistance of the xylem were obtained from López-Bernal *et al.* (2010). The parameters to compute R_r were obtained from Bristow *et al.* (1984) and García-Tejera *et al.* (2016). Finally, values for the soil characteristic curve and the unsaturated conductivity models were taken from Campbell and Norman (1998).

Calibration of Tuzet's parameters s_f and Ψ_f (eq. 2) was performed on year 2014 (DOY 234) on C treatment, giving that this day, additional measurements of Ψ_l from predawn to noon were carried out. For the calibration, values of LAD, V and GC were obtained following the procedures described in 2.2.2. The Ψ_l measurements during the day were performed like in 2.2.3 while the predawn values were obtained from four leaves randomly selected throughout the canopy. The values of L_v for the Tuzet's calibration, were acquired from an intensive sampling in one of the two trees monitored with sap flow on DOY 240 (year 2014). Soil cores were taken from three transects parallel to the planting row at a 0.25, 0.75 and 1.5 m from the drip line. Cores were extracted from six points separated 0.25 m between them for the

transect at 0.25 m while the spacing for the other two transects at 0.75 and 1.5 m was 0.5m. In each sampling position, cores at a depth of 0.15, 0.30 and 0.6 m were extracted. Fig 4.2 presents a diagram with the sampling design. Records from neutron's probe measurements were used as initial values of θ_{soil}. During the calibration, s_f and Ψ_f were allow to vary freely until differences in E_p and Ψ_l between measured and simulated values were at its minimum. The value for g_0 was obtained from the conductance derived by inverting eq. 7, and using the calibrated sap flow records at two hours before dawn for the same day and tree.

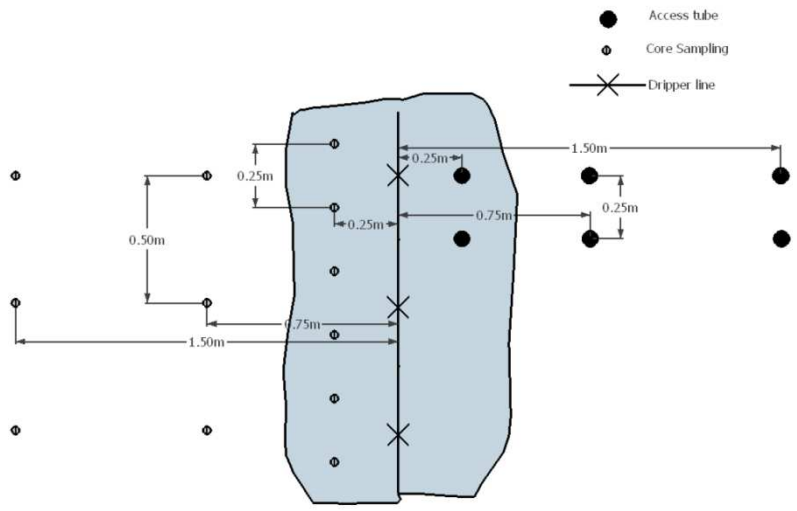

Fig 4.2. Schematic diagram of root sampling on 2014 for model calibration and access tubes to measure soil water content in one tree. Black points represent the access tubes, crosses constitute the drippers and grey circles are the sampling position of the cores. The core sampling during 2013 for model validations was set following the same distribution of the access tubes but only in one transect in front of the dripper.

Table 4.1 presents a summary of the calibrated values used in the photosynthesis model of Farquar and in the Tuzet's equation (eq. 1 and 2).

Table 4.1. Values for the parameters used in the photosynthesis and stomatal conductance models. Parameters for photosynthesis obtained from (Diaz-Espejo *et al.*, 2006) for olive trees are: the degree of curvature of the response to PAR of the electron transport rate (θ), the quantum efficiency (α) and values of activation energy (ΔH_a) and the scaling constants (c) for: Michaelis constant for CO_2 (K_c) and O_2 (K_o), CO_2 compensation point (Γ), maximum catalytic activity of Rubisco in the presence of saturating amounts of ribulose biphosphate and CO2 (V_{cmax}), maximum ratio of electron transport (J_{max}), and the rate of CO_2 evolution in the light resulting from process other than photorespiration (R_d). Parameters of the stomatal conductance for null net photosynthesis (g_0) and the parameters for the empirical model of Tuzet, namely, reference water potential (Ψ_f) and a sensitivity factor (s_f), have been obtained from the recorded sap flow values through a calibration procedure. The proportionality factor between photosynthesis and stomatal conductance (m) was acquired from (Moriana *et al.*, 2002).

Parameter	**Value**
Photosynthesis	
θ	0.9
α	0.2
cK_c	38.05
$\Delta H_a K_c$	79430
cK_o	20.3
$\Delta H_a K_o$	36380
$c\Gamma$	19.02
$\Delta H_a \Gamma$	37830
cV_{cmax}	33.99
$\Delta H_a V_{cmax}$	73680

cJ_{cmax}	18.88
$\Delta H_a J_{cmax}$	35350
cR_d	17.91
$\Delta H_a R_d$	44790
Stomatal conductance	
Ψ_f^*	-1000
s_f^*	0.0023
m	4.5
g_o^*	0.005

* Parameters obtained during model calibration

4.2.4. Soil compartmentalization

In order to capture the variability in L_v and θ_{soil} associated to drip irrigation, the soil system in the model was divided into two compartments named wet and dry. This classification was maintained for the validation and the calibration exercises using the L_v profiles measured in 2013 for the validation and the ones obtained in 2014 for the calibration. The L_v values used for the wet compartment corresponded to those measured at a distance of 0.25 m from the drip line, and they were assumed to represent the soil fraction covered by the wet bulb. Because in 2014 several cores were extracted at 0.25m from the drip line, for the calibration, each depth in the model compartment constituted the average of all the samplings at that corresponding depth. In the dry compartment, the L_v profile was taken from the average values of the measurements at 0.75 and 1.5 m on

2013 and 2014. The dry compartment was assumed to represent the fraction of soil not influenced by the wet bulb.

4.2.5. Case studies

Two simulations experiments were performed. For the first one, the effect of wetted area (by drip irrigation) on daily olive transpiration was studied in two environments for two different root distributions in the wet compartment. The two root distributions were those measured in 2013 for the C treatment on the one hand and the highest root length density values found in the literature for drip irrigated olive trees (Fernández *et al.*, 1991) on the other. The dry compartment in both cases had a fixed L_v profile equal to that measured in 2013 outside the wet bulb in the C treatment. The system was simulated for different values of fraction wetted (F_{wet}) by drippers ranging from 5 to 40 % of the area per tree. The application of water in the wet compartment was distributed throughout the day applying a volume which was high enough to maintain the soil in the wet compartment slightly over field capacity. The L_v in both compartments was assumed the same independently of wetted area; in other words, total root length increased along with wetted area in the wet compartment and decreased in the dry one. Values for the initial soil water content were obtained from neutron's probe measurements on DOY 211 (year 2013). For each L_v profile, two weather datasets were used. One from Cordoba, Spain (Mediterranean semi-arid) on DOY 211 (year 2013) corresponding to a clear day of summer that had a VPD_{mean} equal to 3 kPa. The other one from Güimar, in the Canary Islands (sub-tropical) (28.3ºN, 16.4ºW, 500m altitude) for a clear summer day (DOY 207, year 2015) that had a VPD_{mean} around 1.7 kPa. The analysis was

performed in relative terms comparing actual E_p with the maximum attainable transpiration for the given wetted area (E_{pmax}), i.e. considering that both, the wet and the dry compartment are at field capacity and watered. For each wet-dry compartment relation, E_{pmax}, was calculated assuming that the two compartments were at field capacity and watered.

The second simulation experiment consisted of the distribution of the same total irrigation applied to the C and RDI treatments into different wetted areas (5, 10, 15, 20, 25, 30, 35 and 40%). The frequency of irrigation was one day per week. Again, root length density was assumed constant for each compartment as the wetted fraction varied. The simulations were run for 2013 using the corresponding values of LAD, V, GC and L_v for each treatment.

4.3. Results

4.3.1. Model test

Table 4.2 presents the values measured in both treatments during the validation period. LAI and GC were almost the same for C and RDI on 2012, but on 2013, there is a reduction in the values for RDI. This is because a pruning was performed on that treatment by the farmer.

Table 4.2. Initial parameters used in the simulations for both irrigation treatments in 2012 and 2013. $Root_{wet}$ and $Root_{dry}$ represents the total length of roots per square meter of soil in the wet and the dry compartment, a_{root} is the root radius, LAI is the leaf area index and GC is the percentage of ground cover. The root distribution measured in both compartments in 2013 was applied to the simulations in 2012.

	Control		***RDI***	
	2012	***2013***	***2012***	***2013***
$Root_{wet}$ $(m\ m^{-2})$	6555	6555	6525	6525
$Root_{dry}$ $(m\ m^{-2})$	3948	3948	4389	4389
LAI $(m^2\ m^{-2})$	1.56	1.61	1.59	1.26
a_{root} (m)	0.0027	0.0027	0.0027	0.0027
GC $(\%)$	0.44	0.46	0.45	0.36

Fig. 4.3 shows the time course of daily measured and simulated transpiration in 2012 and 2013. Measured E_p corresponds to the average value of the two monitored trees per treatment. For year 2012, the model was able to match E_p of C and RDI with only minor deviation in some irrigation periods (more evident on RDI from DOY 208 to DOY 238) and after a rain period on DOY 275. In 2013, an unusual rain of nearly 60 mm in August (on DOY 240) had different effects on the two treatments. While simulated E_p in C overestimated the measured values during the irrigation periods from DOY 241 to DOY 270, the simulated RDI did not reach measured transpiration even when irrigation occurred after the rain, and this situation remained for the rest of the measurement period. The linear regression analysis presented in Fig. 4.4 showed a good fit, with a slope close to one, $R^2 = 0.82$, EF = 0.7 and RMSE = 0.29 mm day^{-1}.

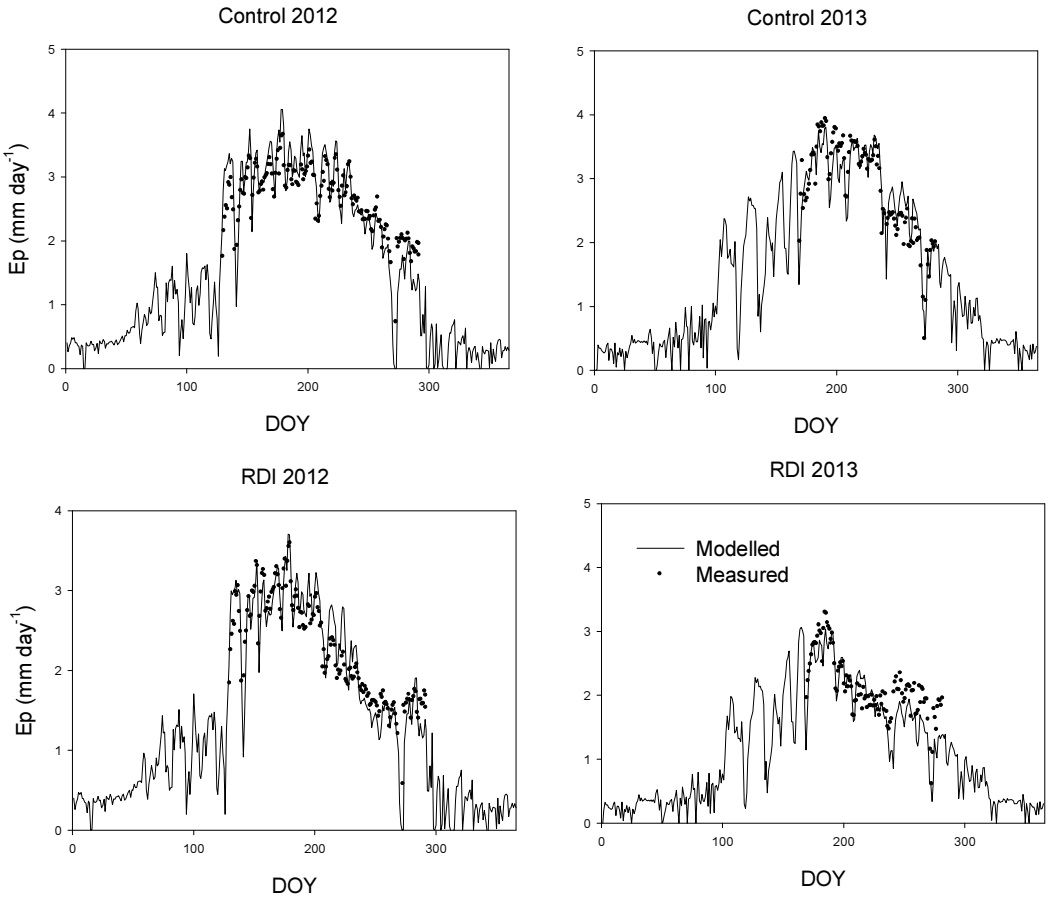

Fig 4.3. Time course of measured E_p (black dots) and simulated E_p (straight line) for control (C) and regulated deficit irrigation (RDI) on years 2012 and 2013.

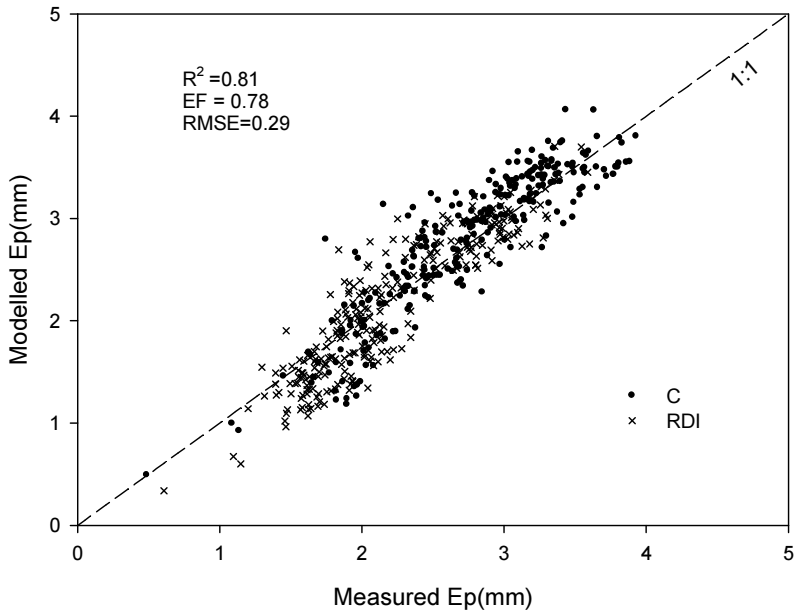

Fig 4.4. Measured and modelled daily transpiration E_p for treatments C (dots) and RDI (crosses) for years 2012 and 2013. The dash line represents the fitted 1:1 line. The adjusted R^2 from the linear regression was 0.81. The efficiency factor (EF) was 0.78 and the root mean square error (RMSE) 0.29 mm.

Measured midday leaf water potential Ψ_l for the two treatments and the two years are compared with the outputs of the model in Fig 4.5. The points represent the Ψ_l values of sunny leaves. Generally, the model underestimated Ψ_l in both treatments with some exceptions. For instance, there was nearly 1 MPa difference between simulated and observed Ψ_l for RDI on DOY 226 in 2012. When comparing both years, the deviations observed in 2012 for the two treatments were higher than those found in 2013. Values of average RMSE yielded 0.3 and 0.2 MPa in 2012 and 2013, respectively.

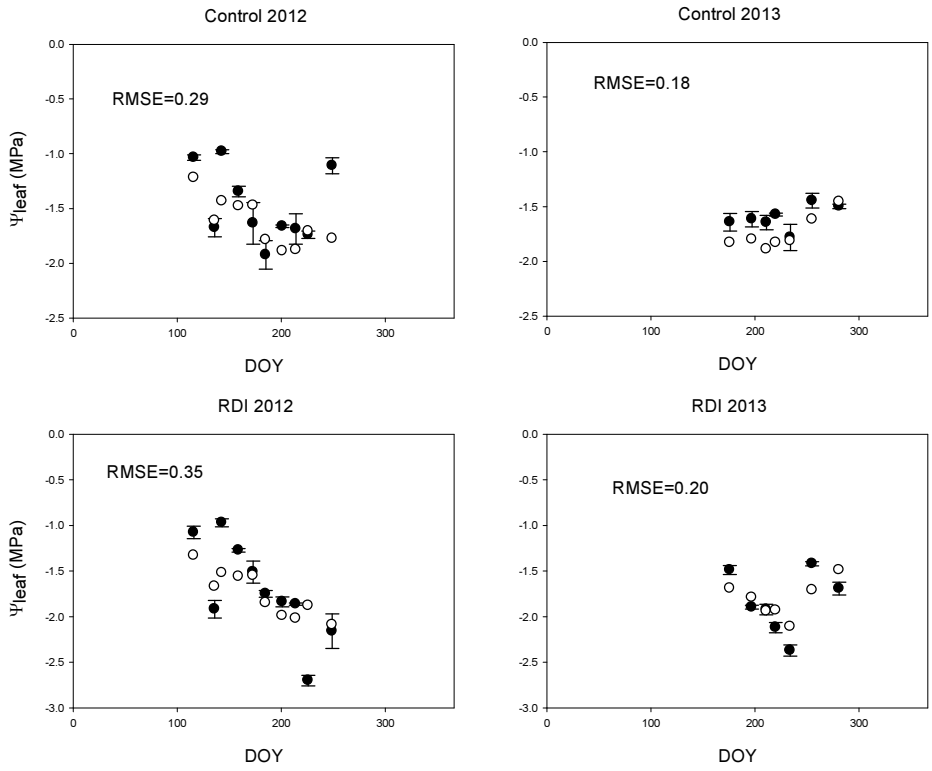

Fig 4.5. Midday measured (black dots) and simulated (white dots) leaf water potential for the control and the regulated deficit irrigation (RDI) treatments on years 2012 and 2013. The measured values correspond to the averages of the recorded values in four sun exposed leaves and the bars represent the standard error.

4.3.2. Case Studies

Fig. 4.6 shows the ratio of daily transpiration and daily maximum transpiration (when all the soil is at field capacity), of the hedgerow olive orchard when the area of the wet compartment is varied from 5 to 40% for two different L_v distributions and in two environments differing in VPD_{mean}. The series with low L_v (i.e. with the L_v values measured in the C treatment) showed a nearly linear increase in

relative E_p in both environments when the wet compartment was increased, while the series with high L_v values (i.e. those in which L_v in the wet zone was taken from Fernández *et al.* (1991)) presented a more curvilinear shape. The maximum relative E_p in each situation was attained at the highest percent of wetted area tested (40%) and was always slightly higher for the low VPD_{mean} environment. Simulations with high L_v showed a larger difference between the two environments as the percent of the wetted area increased. It is worthy to note that the Y axis starts with a relative E_p of 0.75, meaning that the maximum expected change in relative E_p is only of 0.14 when moving from 5 to 40 % of the wetted area for the measured L_v. The fraction of wetted soil surface (F_{wet}) of the C treatment during the experiment was 22 %, which, according to the simulations, should correspond to a value of relative E_p around 0.8.

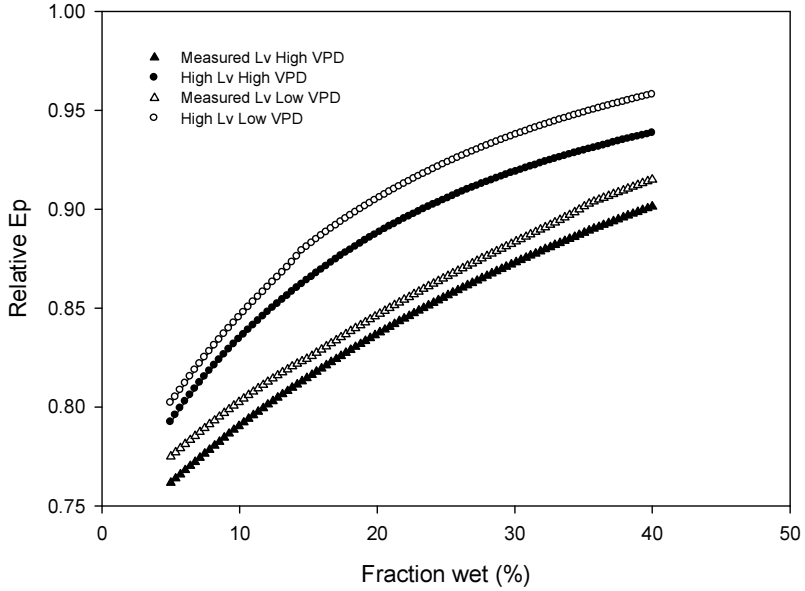

Fig 4.6. Variation of the relative E_p defined as ratio of actual E_p and E_{pmax} on a clear summer day, when the wet compartment is varied from 5 to 40% of total root space. Triangles: simulations assuming L_v profile for the wet compartment measured in the present experiment; circles: simulations with the maximum values reported for olive trees. Filled symbols: results for a clear day of August in Cordoba, Spain (VPD_{mean} = 3kPa) empty symbols: result from a clear day of August in a sub-tropical environment with lower VPD_{mean} (Güimar, Spain. VPD_{mean} = 1.7 kPa)

Regarding the second case study, Fig. 4.7 shows the cumulative E_p during the irrigation period from DOY 175 to DOY 294 in 2013 for a variable F_{wet} ranging from 5 to 40% in the two treatments. Varying the wet compartment had two opposite effects on annual E_p. In the control the cumulative E_p increased with the wet fraction, while in the RDI the value was slightly decreasing with the rise in the wetted area.

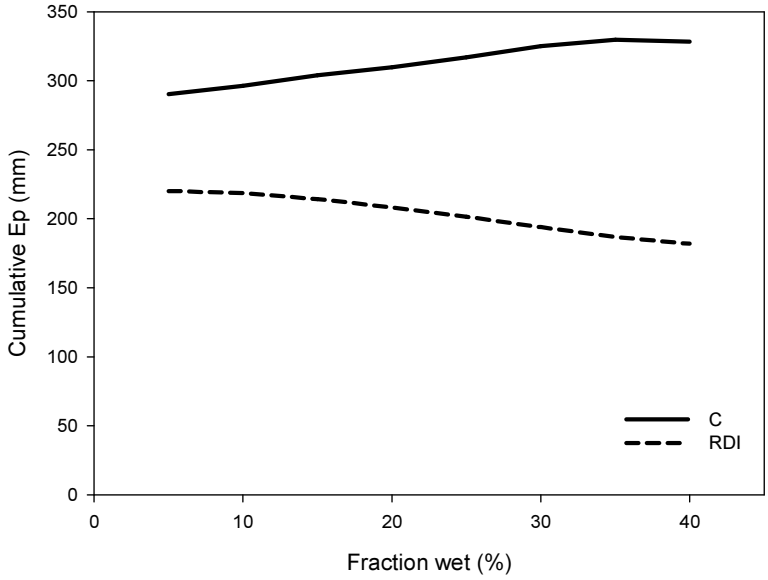

Fig 4.7. Effect on accumulated E_p during the irrigation campaign in 2013 (DOY 175 to DOY 294) on control (C, solid line) and the regulated deficit irrigation (RDI, dashed line) when the same amount of water devoted to each treatment is applied to different wetted surfaces expressed as percentages of total plant area.

4.4. Discussion

4.4.1. Model performance

The model successfully simulated tree E_p and Ψ_l in both years and for both irrigation treatments (Figs. 4.3, 4.4 and 4.5). The changes in E_p throughout the measurement period were well described, with some bias, particularly after rainy days. On the other hand, the average error in Ψ_l was 0.35 MPa which, giving the expected error in water potential measurements can be considered a satisfactory result. The observed discrepancies may be partly explained by the fact that the model is

static and the formation of new roots or leaves is not considered. Little is known about growth dynamics in olive trees. For roots, Fernández *et al.* (1992) working on olive trees under drip irrigation showed a step increase in L_v at the end of summer in the area influenced by the wet bulb and at a shallow depths. The effect of new roots appearance should have an impact on plant resistances as R_s and R_r changes when L_v is modified (see supplementary material one). This might explain why the major discrepancies between simulated and measured values happened during late summer and autumn after the rainfalls. Despite those disagreements, the regression analysis showed a good correlation between modelled and observed transpiration (Fig. 4.4), meaning that the model is able to capture the variations in E_p for different levels of water stress.

4.4.2. The problem of the minimum wet area

To clearly understand the graph presented in Fig. 4.6, one should first define what E_{pmax} is. According to the model, E_{pmax} for a given environment would be attained when the total resistance of the plant is at its minimum; this statement can be explained from equation 5, where a feedback response is described between g_{co2} and Ψ_l for each leaf class. The interaction between both is modulated by the resistances of soil, root and xylem (R_s, R_r and R_x), the VPD and LAI (eq. 5). If the period considered is short and the water status of the tree does not induce xylem cavitation, values of LAI and R_x should remain almost constant (Sperry *et al.*, 1998), leaving VPD, R_s and R_r as the main regulators of the feedback response. The VPD is imposed by the environment, but the resistances depend among others on θ_{soil}, its value increasing when the soil dries out. As a consequence, if the soil

is partially wetted the root water uptake capacity would be limited by R_s and R_r values higher than the ones obtained when the whole soil is completely wetted, giving a value of E_p below E_{pmax}. This implies that under systems with limited wet area, like drip irrigation, some reduction of E_{pmax} is always present. That is the reason why relative E_p does not reaches 1 in Fig. 4.6 even at 40% of F_{wet}. However, it is worthy to note that even for the worst scenario (i.e. low L_v, high VPD and low F_{wet}), relative E_p remains high (around 75%) and increasing F_{wet} does not lead to substantial increases irrespective of the L_v and VPD considered.

In Fig. 4.6 it is showed that the level reduction on E_{pmax} is not only dependent on the percentage of wetted surface but on the environment and the L_v. To describe the effect of L_v on relative E_p one could examine Fig. 4.6 from another perspective. Fig. 4.6 can be seen like the representation of the weight of the wet compartment over tree E_p. This contribution would depend among others on total root length present in the compartment giving that the total root length is a function of L_v and the volume of soil. For example at a 5% of F_{wet}, the measured total root length of the wet compartment is 1966.5 m while in the dry compartment is 22503.6 (computed from root values on table 4.2). When a higher L_v is used in the wet compartment the differences in total root length between compartments are reduced resulting in a bigger contribution from the wet one. As a consequence the relative E_p increases when the L_v is raised for every F_{wet}

The effect of the environment can be explained in terms of VPD keeping in mind the idea of the contribution of the wet compartment mentioned above. For the simulation experiment it was selected a

clear day of summer in both locations to ensure that radiation was not limiting the assimilation, the only difference was in VPD_{mean}, i.e. the atmospheric demand. The atmospheric demand drives the transpiration requirements of the plant (Tanner & Sinclair, 1983), and as a consequence the amount of water that roots should uptake. When the VPD is lowered, E_p is also reduced resulting in a decrease of the amount of roots required to sustain plant E_p. This explains why for the low VPD environment, relative transpiration is always higher for the same wetted percentage.

The assumption of a constant L_v in the wet compartment is critical in the results shown in Fig. 4.6. One might argue that this supposition is not correct as an increase in the wet fraction does not necessary imply the formation of new roots, overriding the analysis. Nevertheless, it has been demonstrated that in drip irrigated trees, roots will grow preferentially inside the wet bulb at a shallowest depths (Fernández *et al.*, 1991, Soar & Loveys, 2007). These results are reasonable because roots will tend to grow in places where soil water content is more favourable, the soil strength is minimal and the oxygen diffusion rate is adequate (Klepper, 1991), all conditions meet in the wet bulb. Working on Avocado (*Persea Americana* Mil) Michelakis *et al.* (1993) showed that as the wetted surface of the dripper increased, so it did it the root density expressed as the number of roots per 100 cm^2. Even if the L_v in the wet compartment is not maintained but still new root growth takes place when the wetted surface is increased, the results would be similar to those presented in Fig. 4.6, and the conclusions would still be the same, i.e. E_{pmax} will only be achieved when the entire absorbing area is at its minimum resistance, and the degree of reduction in E_p respect to E_{pmax} would be related to the aerial

environment (VPD) and to the relation between the supply (roots) and the demand (leaves).

4.4.3. Interaction between wetted area and water volumes

The plots shown in Fig. 4.7 represent the effect of a variable wet surface on the experimental orchard when the same volume of water is applied into the two irrigation treatments.

When water is not limited (C treatment), annual transpiration increases in proportion to wetted area. Nevertheless, the differences in E_p among fractions vary seasonally which may be explained by the variations in the resistances. Table 4.3 shows mean transpiration for April, August and October and the corresponding resistances in each soil compartment for the simulations with 10 and 40% wetted area. The table also shows the ratio of root area:leaf area (*Ar:Al*) for each wetted fraction and the relations of root areas for the wet and the dry compartment (Ar_{wet}:Ar_{dry}). The values of *Ar:Al* were similar for the two wetted fractions. The main difference relied in the surface relation of the wet and the dry compartment for each fraction. According to eq. 2 and 3 more roots would result in a lower R_s and R_r. As the season progresses and water from the dry compartment is withdrawn, the effect of a reduced Ar_{wet} starts to play a greater role on tree E_p giving in August a two order difference in the resistances between 0.1 and 0.4 fractions (Table 4.3) thus limiting more tree E_p than in other months.

Table 4.3. Monthly averages of tree transpiration (E_p) and resistances of the wet (R_{wet}) and the dry compartment (R_{dry}), together with the surface relations of roots and leaves (*Ar:Al*) and of roots in the dry and the wet compartment (Ar_{wet}:Ar_{dry}).

	E_p (mm)		R_{dry} (MPa s m^2 kg^{-1})		R_{wet} (MPa s m^2 kg^{-1})		*Ar:Al*		Ar_{wet}:Ar_{dry}	
F_{wet}	***0.1***	***0.4***	***0.1***	***0.4***	***0.1***	***0.4***	***0.1***	***0.4***	***0.1***	***0.4***
April	1.25	1.39	23.3	34.9	82.9	20.1	1.46	1.73	0.18	1.11
August	2.94	3.28	765	129	1140	23.5	"	"	"	"
October	1.37	1.45	78	61	78.1	19.5	"	"	"	"

On the RDI treatment the trend changes compared to that of C, and annual transpiration decreases as the wet fraction is increased. The result of this inversion is related to three different effects. One is very obvious: as the wetted fraction is increased so it does the surface exposed for evaporation leaving less water available for E_p. The other is related to the infiltration depth: as the same volume of water is spread into a larger area, the infiltration depth is lower and less root area is being wetted. The last effect is more subtle, and is related to the relation between L_v and the resistance. As *Ar:Al* becomes smaller, the soil resistance gets higher. This produces a lower rate of water extraction and a more conservative use of water for the higher resistance situation. The result is a lower E_p when water is available but a more sustained E_p as the dry period progresses.

The main result from the simulations presented on Fig. 4.7 relates to the irrigation strategies that should be followed according to the available water. According to the model, if sufficient water is

available to meet tree transpiration demand, one should wet a soil volume high enough to ensure that E_p is as close as possible to E_{pmax}. On the other hand, if a deficit is imposed, the strategy should be to reduce the wetted area in order to maximize the water routed to E_p.

4.5. Conclusions

The model was able to predict transpiration and leaf water potential for drip irrigated olive trees at different levels of water supply. This model represents a step forward with regard to those that focus only in one part of the system (leaves or roots) or do not account for soil and canopy variability. The simulation experiments showed that transpiration of drip irrigated olive trees is likely to be limited by wetted soil volume. According to the model, irrigation management would depend on the available water supply: under no restrictions, irrigation should be applied trying to wet the maximum possible soil volume, whereas if deficit irrigation is imposed, irrigation should be managed to reduce the wet area.

Acknowledgements

This work was supported by project AGL-2010-20766 of the Spanish Ministry of Economy and Competitiveness (former Ministry of Science and Innovation) and by the European Community's Seven Framework Programme-FP7 (KBBE.2013.1.4-09) under Grant Agreement No. 613817 (MODEXTREME, modextreme.org). We wish to thank the "FPI" programme of the aforementioned ministry for providing the Ph.D. scholarships to Omar García Tejera. We also thank Manolo Gonzalez, Jose Luis Vazquez, Ignacio Calatrava, Rafael del Río, Rafael Luque and Marcos Orgaz for the excellent technical assistance provided.

References

Andreu L., Hopmans J.W. & Schwankl L.J. (1997) Spatial and temporal distribution of soil water balance for a drip-irrigated almond tree. *Agricultural Water Management*, **35**, 123-146.

Bonachela S., Orgaz F., Villalobos F.J. & Fereres E. (2001) Soil evaporation from drip-irrigated olive orchards. *Irrigation Science*, **20**, 65-71.

Bristow K.L., Campbell G.S. & Calissendorff C. (1984) The effects of texture on the resistance to water-movement within the rhizosphere. *Soil Science Society of America Journal*, **48**, 266-270.

Campbell G.S. & Norman J.M. (1998) *Introduction to environmental biophysics*. (2nd ed.). Springer, New York.

Clothier B.E. & Green S.R. (1994) Rootzone processes and the efficient use of irrigation water. *Agricultural Water Management*, **25**, 1-12.

Clothier B.E. & Green S.R. (1997) Roots: The big movers or water and chemical in soil. *Soil Science*, **162**, 534-543.

Chalmers D.J., Mitchell P.D. & Vanheek L. (1981) Control of peach-tree growth and productivity by regulated water-supply, tree density, and summer pruning. *Journal of the American Society for Horticultural Science*, **106**, 307-312.

De Wit C.T. (1958) *Transpiration and Crop Yields*. Institute of Biological and Chemical Research on Field Crops and Herbage.

Diaz-Espejo A., Walcroft A.S., Fernandez J.E., Hafridi B., Palomo M.J. & Giron I.F. (2006) Modeling photosynthesis in olive leaves under drought conditions. *Tree Physiol*, **26**, 1445-1456.

Farquhar G.D., von Caemmerer S. & Berry J.A. (1980) A biochemical model of photosynthetic CO2 assimilation in leaves of C3 species. *Planta*, **149**, 78-90.

Fereres E. & Soriano M.A. (2007) Deficit irrigation for reducing agricultural water use. *Journal of Experimental Botany*, **58**, 147-159.

Fernández J.E., Martín Aranda J., Moreno Lucas F. & Fereres Castiel E. (1992) Olive-tree root dynamics under different soil water regimenes. *Agr.Med.*, **122**, 225-235.

Fernández J.E., Moreno F., Cabrera F., Arrue J.L. & Martín-Aranda J. (1991) Drip irrigation, soil characteristics and the root distribution and root activity of olive trees. *Plant and Soil*, **133**, 239-251.

García-Tejera O., López-Bernal Á., Villalobos F.J., Orgaz F. & Testi L. (2016) Effect of soil temperature on root resistance: implications for different trees under Mediterranean conditions. *Tree Physiology*.

Green S., Clothier B. & Jardine B. (2003) Theory and Practical Application of Heat Pulse to Measure Sap Flow. *Agronomy Journal*, **95**.

Iniesta F., Testi L., Orgaz F. & Villalobos F.J. (2009) The effects of regulated and continuous deficit irrigation on the water use, growth and yield of olive trees. *European Journal of Agronomy*, **30**, 258-265.

Jarvis P.G. & McNaughton K.G. (1986) Stomatal control of transpiration - scaling up from leaf to region. *Advances in Ecological Research*, **15**, 1-49.

Klepper B. (1991) Crop root system response to irrigation. *Irrigation Science*, **12**, 105-108.

Loomis R.S. & Connor D.J. (2002) *Ecología de cultivos: Productividad y manejo en sistemas agrarios*. Mundi-Prensa.

López-Bernal Á., Alcántara E., Testi L. & Villalobos F.J. (2010) Spatial sap flow and xylem anatomical characteristics in olive trees under different irrigation regimes. *Tree Physiology*, **30**, 1536-1544.

Mariscal M.J., Orgaz F. & Villalobos F.J. (2000b) Modelling and measurement of radiation interception by olive canopies. *Agricultural and Forest Meteorology*, **100**, 183-197.

Michelakis N., Vougioucalou E. & Clapaki G. (1993) Water use, wetted soil volume, root distribution and yield of avocado under drip irrigation. *Agricultural Water Management*, **24**, 119-131.

Moriana A., Villalobos F.J. & Fereres E. (2002) Stomatal and photosynthetic responses of olive (Olea europaea L.) leaves to water deficits. *Plant, Cell & Environment*, **25**, 395-405.

Orgaz F., Villalobos F.J., Testi L. & Fereres E. (2007) A model of daily mean canopy conductance for calculating transpiration of olive canopies. *Functional Plant Biology*, **34**, 178-188.

Selby S.M. & Company C.R. (1974) *CRC Standard Mathematical Tables and Formulae*. CRC Press.

Soar C.J. & Loveys B.R. (2007) The effect of changing patterns in soil-moisture availability on grapevine root distribution, and viticultural implications for converting full-cover irrigation into a point-source irrigation system. *Australian Journal of Grape and Wine Research*, **13**, 2-13.

Sperry J.S., Adler F.R., Campbell G.S. & Comstock J.P. (1998) Limitation of plant water use by rhizosphere and xylem conductance: results from a model. *Plant Cell and Environment*, **21**, 347-359.

Swanson R.H. & Whitfield D.W.A. (1981) A Numerical Analysis of Heat Pulse Velocity Theory and Practice. *Journal of Experimental Botany*, **32**, 221-239.

Tanji K.K. & Hanson B.R. (1990) Drainage and return flow in relation to irrigation management. In: *Irrigation of Agricultural Crops* (eds B.A. Stewart & D.R. Nielsen). ASA, Madison,WI.

Tanner C.B. & Sinclair T.R. (1983) Efficient water use in crop production research or re-search. In: *Limitations to Efficient Water Use in Crop Production* (eds H.M. Taylor, W.R. Jordan, & T.R. Sinclair), pp. 1-27. ASA,CSSA,SSSA, Madison, WI.

Testi L. & Villalobos F.J. (2009) New approach for measuring low sap velocities in trees. *Agricultural and Forest Meteorology*, **149**, 730-734.

Testi L., Villalobos F.J., Orgaz F. & Fereres E. (2006) Water requirements of olive orchards: I simulation of daily evapotranspiration for scenario analysis. *Irrigation Science*, **24**, 69-76.

Tuzet A., Perrier A. & Leuning R. (2003) A coupled model of stomatal conductance, photosynthesis and transpiration. *Plant Cell and Environment*, **26**, 1097-1116.

Villalobos F.J., Orgaz F., Testi L. & Fereres E. (2000) Measurement and modeling of evapotranspiration of olive (Olea europaea L.) orchards. *European Journal of Agronomy*, **13**, 155-163.

Villalobos F.J., Testi L., Orgaz F., García-Tejera O., Lopez-Bernal A., González-Dugo M.V., Ballester-Lurbe C., Castel J.R., Alarcón-Cabañero J.J., Nicolás-Nicolás E., Girona J., Marsal J. & Fereres E. (2013) Modelling canopy conductance and transpiration of fruit trees in Mediterranean areas: A simplified approach. *Agricultural and Forest Meteorology*, **171–172**, 93-103.

Williams M., Rastetter E.B., Fernandes D.N., Goulden M.L., Wofsy S.C., Shaver G.R., Melillo J.M., Munger J.W., Fan S.M. & Nadelhoffer K.J. (1996) Modelling the soil-plant-atmosphere continuum in a Quercus-Acer stand at Harvard forest: The regulation of stomatal conductance by light, nitrogen and soil/plant hydraulic properties. *Plant Cell and Environment*, **19**, 911-927.

Chapter 5

General conclusions and final remarks

Chapter 5

General conclusions and final remarks

5.1. General Conclusions

1. The SPAC model developed in the present thesis is able to simulate tree transpiration and leaf water potential when parts of the root system are in contrasting soil water content and/or have different root length density, using a soil multi-compartment approach. The model (tested at pot and field scale and for two different species) demonstrated to be a useful tool to explore the interactions among the different elements that compose the SPAC system, providing new insights into the mechanisms behind the regulation of tree transpiration. All the parameters of the model can be derived from plant measurements.

2. Soil temperature influences the water uptake capacity of the root through its effects over the root hydraulic resistance. The results presented on chapter 2 showed that at 15 ºC the radial root specific hydraulic resistance of the GF677 rootstock and olive (*Olea europaea*) tree starts to increase respect to its value at 20 ºC, meaning that the plant water status is not only dependent on the canopy demand and the available water in the soil but also on seasonal changes in soil temperature.

3. The radial root hydraulic specific resistance can no longer be considered a steady feature of the SPAC system. Consequently the use of a variable function of the radial root hydraulic specific

resistance with the temperature, will significantly improve the estimations of tree transpiration, giving that, from all the specific resistances composing the system, the radial root hydraulic specific resistance is usually the highest one. If soil temperature records are not available, mean air temperature can be used as a surrogate.

4. The importance of soil and root resistances in each layer and each compartment is not a unique function of the soil water content but it depends on the soil texture and the root length density. When the root length density is high (over 10000 m m^{-3}) soil resistance will be lower than root resistance even at low soil water contents, meaning that, the main controller of total plant water uptake will be the root hydraulic specific resistance.

5. Root clumping can induce significant underestimation of the real plant root resistance, which translates into deviations in the simulations of transpiration and leaf water potential in soils where the presence of cracks or pores creates places for preferential grow; or in confined media like pots or lysimeters in which root overlap might happen due to excessive density. To overcome this problem, the measured root length density should be substituted by an effective one, which assumes that roots clumped will act like a single root.

6. To reach the maximum attainable transpiration for a given environment, the resistances composing the SPAC system have to be at its minimum possible value. This means that transpiration of drip irrigated trees is likely to be limited by the volume of soil wetted by the emitters, as the roots outside the wet bulb have a higher resistance than the ones inside during dry periods. The

degree of such limitation would depend on the relations between the leaf and the root areas and with the aerial environment.

7. According to the simulations performed in chapter 4, the management of irrigation would depend on water reservoirs. If no restrictions are imposed and enough water is available to meet crop transpiration requirements, water should be supplied to wet the maximum possible volume of soil. On the contrary if deficit irrigation is imposed, irrigation should be managed to wet the minimum possible surface in order to maximize the water devoted to transpiration.

5.2. Final remarks

The integrations of the demand and the supply function to model tree transpiration resulted in a new vision of the performance of the tree under water stress. Once all the pieces composing the soil-plant-atmosphere continuum system were putted together, it was obvious that the regulation of transpiration by the stomata not only depends on the microclimate that is sensed by the leaf but also on the water that can be supplied by the roots.

Roots have been named the hidden half (Waisel *et al.*, 2002); nevertheless, giving the importance that roots have on the regulation of plant water relations, particularly during stress conditions, there is a need to make them visible. The increase in the research efforts aimed to provide new insight into the interactions of the roots with their natural environment, will allow a great leap forward into our understanding of the plant system with the aid of integrative models like the one derived in the present thesis.

Reference

Waisel Y, Eshel A, Beeckman T, Kafkafi U (2002) Plant Roots: The Hidden Half, Third Edition. Taylor & Francis.

Appendix I: Model Description

1. Introduction

In this appendix the multi-compartment SPAC model is described. The text is divided following the same structure of the paper. First a general overview of the model is presented, then, the equations related to the supply and the demand functions are provided with the procedure used to link both. Finally, the equations used to compute the intercepted radiation and to calculate the fraction of sunlit and shaded leaves is presented. At the end of the document a summary table with the symbols, their descriptions and units is provided

2. Model overview

The multi-compartment SPAC model can be divided in two different parts. The demand section deals with the equations related to the interception of radiation by the canopy, the assimilation and the stomatal conductance functions, and the transport of water through trunk and branches for two leaf classes, shaded and sunlit. On the other hand, the supply part provides the equations necessary to describe the water redistribution throughout the soil layers and the uptake of water from roots placed in different compartments.

3. The Supply function

3.1 Soil water redistribution

Water may be redistributed in the soil following gradients of water potential. Water potentials are not calculated explicitly in the model but relative water contents are used instead. The flow (mm) between

two adjacent layers (*i* and *i+1*) is computed according to (Ritchie, 1998):

$$flow_{(i)} = 0.16\left[\frac{\theta soil(i)+\theta soil(i+1)}{2} + 0.5\right]^2 \frac{\theta soil(i+1)-\theta soil(i)}{0.5\left(\Delta L_{(i+1)}+\Delta L_{(i)}\right)}100$$

(A1)

where the factor 1000 accounts for the conversion from m to mm. Note that, according to this equation, a positive/negative value of flow implies water reaching/leaving the layer *i* from/towards the layer *i+1*.

The magnitude of the flow between layers calculated with Eq. A17 is subsequently modified when it leads to water contents exceeding either saturation or upper limit levels in the layer *i* (positive flow) or in the layer *i+1* (negative flow):

$$flow_{(i)} = \begin{cases} \left[\theta_{sat\,(i)} - \theta_{soil(i)}\right]\Delta L_{(i)}1000 & \text{if } flow_{(i)} > 0 \text{ and } \theta_{soil(i)} + \frac{flow_{(i)}}{1000\Delta L_{(i)}} > \theta_{sat\,(i)} \\ \left[\theta_{UL\,(i)} - \theta_{soil(i)}\right]\Delta L_{(i)}1000 & \text{if } flow_{(i)} > 0 \text{ and } \theta_{soil(i)} + \frac{flow_{(i)}}{1000\Delta L_{(i)}} > \theta_{UL\,(i)} \\ \left[\theta_{sat\,(i+1)} - \theta_{soil(i+1)}\right]\Delta L_{(i+1)}1000 & \text{if } flow_{(i)} < 0 \text{ and } \theta_{soil(i+1)} + \frac{flow_{(i)}}{1000\Delta L_{(i+1)}} > \theta_{sat\,(i+1)} \\ \left[\theta_{UL\,(i+1)} - \theta_{soil(i+1)}\right]\Delta L_{(i+1)}1000 & \text{if } flow_{(i)} < 0 \text{ and } \theta_{soil(i+1)} + \frac{flow_{(i)}}{1000\Delta L_{(i+1)}} > \theta_{UL\,(i+1)} \end{cases}$$

(A2)

Then, θ_{soil} is updated as:

$$\theta_{soil(i)} = \theta_{soil(i)} + \frac{flow_{(i)}}{1000\Delta L_{(i)}}$$

(A3)

3.2 Soil characteristic curve and unsaturated conductivity

Soil water potential Ψ_s and soil unsaturated conductivity k can be related to soil water content θ_{soil} according to the empirical relationships (Campbell, 1985a):

$$\Psi_s = \Psi_e \left(\frac{\theta_{sat}}{\theta_{soil}}\right)^b$$

(A4)

$$k = k_{sat} \left(\frac{\theta_{soil}}{\theta_{sat}}\right)^{2b+3}$$

(A5)

Where Ψ_e is the air entry water potential (kPa), k_{sat} is the soil saturated conductivity (kg s^{-1} m kPa^{-1}) and b is a shape factor.

3.3 Soil evaporation

The evaporation from the soil is computed using the model developed by Bonachela *et al.* (2001).

3.4 Soil resistance

The resistance for the movement of water from the mid-distance between two adjacent roots towards the root surface is derived from the analytical solution proposed by Gardner (1960).The equation relates the difference in matric potential between the soil and the root surface to the flux of water that passes through the root under steady state conditions (Gardner, 1960).

$$\Psi_s - \Psi_r = \frac{q}{4\pi k} \ln\left(\frac{b'^2}{a^2}\right)$$

(A6)

Where Ψ_r and Ψ_s are the water potential at root surface and the soil water potential (kPa), k is the unsaturated soil water conductivity (kg s^{-1} m kPa^{-1}), q is the water flux from the soil to a single root (kg m^{-1} s^{-1}),b' is the half distance between roots (m) and a is the root radius (m). If roots are assumed to be evenly distributed in the soil, b' can be derived from the root length density Lv like (Newman, 1969):

$$b' = \sqrt{\frac{1}{\pi Lv}}$$

(A7)

The flux coming from a group of roots (J, kg s^{-1}) can be derived from Lv and the soil depth (d, m) as (Cowan, 1965):

$$J = qLvd$$

(A8)

J can be also derived from the ratio of the difference between Ψ_r and Ψ_s and the soil resistance (Rs, kPa m^2 s kg^{-1})(Campbell, 1985a):

$$J = \frac{\Psi_s - \Psi_r}{R_s}$$

(A9)

Equation A9 can be rearranged as a function of the differences in water potential and substituted in eq. A4

$$R_s J = \frac{q}{4\pi k} \ln\left(\frac{b'^2}{a^2}\right)$$

(A10)

If terms *J* and *b'* in eq. A10 are substituted using equations A7 and A9, an expression for soil water resistance is obtained:

$$R_s = \frac{\ln\left(\frac{1}{\pi L v a^2}\right)}{4\pi k L v d}$$

(A11)

3.5 Root radial resistance

The total resistance in the radial direction from the root surface towards the root xylem is computed like:

$$R_r = \frac{r_r(\theta, T)}{Lv\ d}$$

(A12)

The value of r_r integrates, for a root section, the degree of permeability of the different tissues arranged in series that conform the root cylinder (Steudle & Peterson, 1998). The value of r_r is usually

a fixed parameter in most of the models. Nevertheless, the permeability might well vary according to changes in the root environment like temperature or soil water content by: modifications in the degree of suberification of the exo and endodermis, the activity of the aquaporines, or a loose contact between the root surface and the soil among others (Herkelrath *et al.*, 1977, North & Nobel, 1992, North & Nobel, 1997, Steudle & Peterson, 1998, Steudle, 2000) . In the present model, r_r is obtained as a function of the temperature using the approach developed by Garcia-Tejera et al. (2016); and then modified according to θ_{soil} using Bristow's model (Bristow *et al.*, 1984).

For a soil temperature ranging from 10 to 30ºC, the empirical functions developed for olive 'Picual' and the GF677 rootstock are(García-Tejera *et al.*, 2016):

$$r_{r(T)olive} = 64934.88 + 1.09 \cdot 10^{9} T_s^{-3.64}$$

(A13)

$$r_{r(T)GF677} = -19593.29 + 1.00 \cdot 10^{7} T_s^{-1.58}$$

(A14)

Where T_s is the soil temperature (ºC). Correction of r_r according to θ_{soil} is later done using the empirical function of Bristow *et al.* (1984).

$$r_r(\theta) = r_r(T)\left(1 + \alpha' e^{\left[-\beta\prime\left(\theta_{soil}/\theta_{sat} - \delta\prime\right)\right]}\right)$$

(A15)

Where *δ', α'* and *β'*, are empirical parameters related to: the critical value of $\theta_{soil}/\theta_{sat}$ at which $r_r(\theta)$becomes limiting, the value at which $\theta_{soil}/\theta_{sat}$ equals δ and the velocity at which $r_r(\theta)$approaches infinity.

3.6 Tree collar water potential

Tree *Ep* must equal the sum of all the fluxes coming from each soil layer (i) of each soil compartment (j) if tree capacitance is not taken into account. Once the total resistances from root and soil are derived using equations A11 and A12, the water withdrawn by the roots from each soil layer (i) at each soil compartment (j) is obtained applying the water potential gradient between the soil ($\Psi_{si,j}$) and the root xylem ($\Psi_{rxi,j}$). The integration of all those fluxes to obtain *Ep* would read:

$$Ep = \sum \frac{\Psi_{si,j} - \Psi_{rxi,j}}{R_{si,j} + R_{ri,j}}$$

(A15)

Equation A15 can be further simplified. Unless cavitation is present, root xylem resistance is negligible compared to R_s and R_r (Sperry *et al.*, 1998, Tyree & Zimmermann, 2002). Considering a negligible xylem resistance necessarily implies a common xylem water potential throughout the xylem system; in other words, Ψ_c is assumed the same throughout all the conductive system. With this simplification in mind, equation A15 can be rearranged as a function of Ψ_c like:

$$\Psi_c = \frac{\sum \frac{\Psi_{si,j}}{R_{si,j} + R_{ri,j}} - Ep}{\sum \frac{1}{R_{si,j} + R_{ri,j}}}$$

(A16)

4. The demand function

4.1 Transport of water through the xylem

The theoretical specific conductivity (K_t) of the xylem is classically estimated by adding up the conductivities of the conduits found in a cross-section of wood, using the Hagen–Poiseuille equation to calculate the conductivity of each conduit, which is usually written as follows:

$$K_{te} = \frac{\pi\rho}{128\eta} \sum_{i=1}^{n} \Phi_{v,i}^4$$

(A17)

Where ρ and η are density and dynamic viscosity of sap respectively (whose values can be set as those of the water: 1000 kg/m^3 and 10^{-9} MPa s) and $\Phi_{v,i}$ is the diameter of the *i*th xylem vessel (m) and n the total number of vessels in the cross section considered (Tyree & Ewers, 1991). The sum of the quarter-power diameters can be simplified as a function of both mean vessel diameter (Φ_v, m) and vessel density (VD, vessels/m^2):

$$K_{te} = \frac{\pi\rho}{128\eta} VD\ \Phi_v^4$$

(A18)

Where K_t is expressed in kg m^{-1} s^{-1} MPa^{-1}. Theoretical specific resistivity (R_{te}) is obtained inverting Kt.

The use of Hagen-Poiseuille equations to model water transport through stems consistently overestimates the conductances measured experimentally on wood segments. The discrepancy has been attributed to the resistance of inter-conduit pit pores as sap has to cross a porous membrane to flow from one conduit to the next. The overall hydraulic resistance is thus considered to be the sum of lumen resistance and inter-conduit resistance in series:

$$r_t = r_{te} + r_{pit} = \frac{1}{k_{te}} + r_{pit}$$

(A19)

Some studies including several angiosperm species have estimated that, on average, end-walls (r_{pit}) contribute 56 % to total xylem resistance regardless of wood porosity -ring or diffuse- (Wheeler *et al.*, 2005, Hacke *et al.*, 2006). As a result, we may write:

$$R_t = \frac{1}{K_t} = \frac{R_{te}}{1 - 0.56} = \frac{1}{0.44\ K_{te}}$$

(A20)

The final step computes root-to-leaf hydraulic resistance considering the pathway length (that we take as the sum of mean root depth ($Z_{root,}$,

m) and shoot height (Z_{shoot}, m) and the cross-sectional area of sapwood per m^2 soil (SWA):

$$R_x = \frac{r_t(Z_{root} + Z_{shoot})}{SWA}$$

(A21)

4.2 Canopy transpiration and photosynthesis

In computing the demand function, tree canopy is discretized into sunlit and shaded leaves to upscale from leaf to tree photosynthesis (dePury & Farquhar, 1997). If the canopy is divided into sunlit and shaded leaves, total transpiration must be computed as the sum of *Ep* from each leaf class

$$Ep = E_{psun} + E_{pshade}$$

(A22)

For well coupled canopies, like forests or tree crops, *Ep* can be directly related to the stomatal conductance using a simplified version of the Penman-Monteith equation, assuming that, the aerodynamic conductance is much higher than the stomatal conductance due to the "roughness" of the canopy surface (Villalobos *et al.*, 2000, Orgaz *et al.*, 2007). In that case, *Ep* is called "imposed" and is estimated as a function of the vapor pressure deficit (*VPD*) and the stomatal conductance for CO2 (g_{co2}) (Jarvis & McNaughton, 1986):

$$E_{psun} = g_{co2sun} 1.6 \frac{VPD}{P} LAI_{sun}$$

(A23)

Where P is atmospheric pressure and LAI_{sun} and g_{co2sun} are leaf area index and stomatal conductance for CO2 of the sunlit leaves. The fraction of area shaded or illuminated are computed as a function of the zenith angle, the G projection function and the solar radiation reaching the canopy on an hourly basis, assuming an spheroidal canopy shape. A detailed description of the equations needed to compute the radiation parameters are described in section 5 . Equation A23 (and the following equations A24 and A25) refers only to sunlit leaves for the sake of concision; those for shaded leaves are analogous.

Equation A23 can be further developed using the adaptation of Leuning's equation proposed by Tuzet (2003), in which, g_{co2} is related to leaf assimilation, the concentration of CO2 at the substomatal cavities (C_i), the light compensation point (Γ), and reduced by leaf water potential through an empirical function (see Tuzet et al. (2003) for a detailed description). For a sunlit leaf, Tuzet's equation would read:

$$g_{co2sun} = g_0 + \frac{mA'_{sun}}{C_{isun} - \Gamma} f(\Psi_{lsun})$$

(A24)

$$f(\Psi_{lsun}) = \frac{1 + \exp[s_f \Psi_f]}{1 + \exp[s_f(\Psi_f - \Psi_{lsun})]}$$

(A25)

In eq. A24, the symbol g_0 is the night time conductance (i.e. for zero gross assimilation), m is a proportionality factor between

photosynthesis and stomatal conductance and *A'* is the gross assimilation, while in eq. 10 Ψ_f is a reference water potential which marks the initial value of Ψ_{lsun} at which g_{co2sun} is affected and s_f modulates the rate of the reduction.

The assimilation of CO2 is computed using Farquhar *et al.* (1980). On its general form, Farquar's equation for gross assimilation looks like:

$$A' = \frac{B(C_i - \Gamma)}{EC_i + D}$$

(A26)

The coefficients A, E, B would depend on the calculations of *A'* when the rate of carboxilation is limited by the saturation of the ribulose biphosphate (RuBP) carboxylase/oxigenase (A'_v) or by the regeneration of the RuBP according to the rate of electron transport A'_q (Farquhar *et al.*, 1980).

Photosynthesis limited by RuBP carboxylase/oxigenase is calculated as:

$$A'_v = \frac{V_{c,max}(C_i - \Gamma)}{C_i + k_c\left(1 + {}^{o_i}/_{k_o}\right)}$$

(A27)

Where $V_{c,max}$ is the maximum activity of RuBP carboxylase/oxigenase, o_i is the intercellular oxygen concentration, assumed constant and equal to 2.05×10^5 µmol mol air^{-1} and k_c and k_o are the Michaelis-Menten coefficients of RuBP carboxylase/oxigenase activity for CO2 and O2. No mesophyll conductance has been taken into account, thus,

the model assumes the same concentration for the intercellular spaces and the carboxylation sites of RuBP carboxylase/oxigenase.

Then again, photosynthesis limited by regeneration of RuBP is computed like:

$$A'_q = \frac{J(C_i - \Gamma)}{4C_i + 2\Gamma}$$

(A28)

Where J is the rate of electron transport, which increases with the photosynthetic photon flux Q according to the following expression:

$$\theta J^2 - (\alpha Q + J_{max})J + Q\alpha J_{max} = 0$$

(A29)

In eq. A29, α and θ are parameters describing the quantum efficiency and the degree of curvature of the parabola, respectively. On the other hand J_{max} is defined as the maximum electron transport rate.

The parameters $V_{c,max}$, J_{max} k_c and k_o are assumed to increase with temperature following the expression developed by Bernacchi *et al.* (2001):

$$Parameter = e^{\left(\frac{c-\Delta H_a}{R(T_l+273)}\right)}$$

(A30)

Where c and ΔH_a are a scaling constant and an activation energy, R is the molar gas constant and T_l is the leaf temperature. T_l depends on

the temperature of the air within the canopy, the leaf boundary layer resistance and leaf energy balance described by Leuning *et al.* (1995). As it was described above, a tree stand is coupled to the atmosphere (Jarvis & McNaughton, 1986); by definition, if the canopy is coupled, the boundary layer is negligible and the CO2 concentration and the vapour pressure deficit at leaf surface will equal the atmospheric CO2 and the VPD (Jarvis & McNaughton, 1986). The same is true for the temperature at leaf surface, meaning that T_l will be equal to the air temperature. Villalobos *et al.* (2000) observed that olive trees were coupled to the atmosphere.

Farquhar *et al.* (1980) computes assimilation for A'_v and A'_q and uses the minimum value.

$$A' = min\{A'_v, A'_q\}$$

(A31)

4.3. Coupling supply and demand

Tree *Ep* can be computed assuming no capacitance like (Campbell, 1985b):

$$Ep = \frac{\Psi_c - \Psi_l}{R_x} = \frac{\Psi_s - \Psi_c}{R_s + R_r}$$

(A32)

In eq. A32 Ψ_c appears in both sides of the expression. If Ψ_c from eq. A16 is substituted in the above expression and rearranged as a function of Ψ_l , eq. A32 would turn into:

$$\Psi_l = \frac{\sum \frac{\Psi_{si,j}}{R_{si,j} + R_{ri,j}} - Ep}{\sum \frac{1}{R_{si,j} + R_{ri,j}}} - EpR_x$$

(A33)

Equation A33 can be further simplified:

$$\Psi_l = \frac{\sum \frac{\Psi_{si,j}}{R_{si,j} + R_{ri,j}}}{\sum \frac{1}{R_{si,j} + R_{ri,j}}} - Ep\left(\frac{1}{\sum \frac{\Psi_{si,j}}{R_{si,j} + R_{ri,j}}} + R_x\right)$$

(A34)

For a canopy discretized into sunlit and shade leaves *Ep* can be substituted using eq A23:

$$\Psi_{lsun} = \frac{\sum \frac{\Psi_{si,j}}{R_{si,j} + R_{ri,j}}}{\sum \frac{1}{R_{si,j} + R_{ri,j}}} - g_{co2sun} 1.6 \frac{VPD}{P} 0.018 \left(\frac{\sum \frac{1}{R_{si,j} + R_{ri,j}} + R_x}{f_{sun}}\right) LAI_{sun}$$

(A35)

Where f_{sun} is the ratio LAI_{sun}/LAI and f_{shade} would be $1-f_{sun}$. As in eq. A23, A24 and A25, eq. A35 is formally the same for Ψ_{lshade}, simply changing the values of the corresponding parameters with those of the shaded leaves.

Equation A34 assumes that the tree is split in two parts according to the fractional area of sun and shade leaves. In other words, the model assumes that each leaf class will be sustained by a proportion of roots

and trunk equal to f_{sun} and f_{shade}, respectively. The factor 0.018 converts moles of H2O into kg of H2O.

To find the values for Ψ_l and g_{co2} for each leaf class an iterative procedure is followed using C_i as a convergence criterion. Before describing the iterative procedure to obtain g_{co2} and Ψ_l, we need to derive the equation of maximum stomatal conductance for *CO2* at no limiting leaf water potential (g_{co2max}). To compute gross photosynthesis one can use the general diffusion function which multiplies g_{co2} to the *CO2* concentration gradient between the substomatal cavities (C_i) and the atmosphere (C_a) set at 400 micromol mol^{-1} (NOAA, 2016) plus the leaf mitochondrial respiration (*Rd*):

$$A' = g_{co2}(C_a - C_i) + R_d$$

(A36)

Combining the general expression to compute assimilation derived by Farquhar *et al.* (1980) (eq A26) and the eq. A36 the value of g_{co2max} can be derived as:

$$g_{co2max} = \frac{B(C_i - \Gamma) - R_d(EC_i + D)}{(EC_i + D)(C_i - C_a)}$$

(A37)

The iteration starts with an initial value for *Ci* set as $0.7C_a$, the initial value is introduced in eq. A37 to compute g_{co2max}, then, *A'* from eq. A36 is computed using g_{co2max}. In the next step Ψ_l is calculated from eq. A35. Then, the Ψ_l obtained is used to compute actual g_{co2} from eq. A24. Finally a new C_i is calculated like:

$$C_{inew} = C_a - \frac{A' - R_d}{g_{co2}}$$

(A38)

If the convergence criterion is not satisfied, C_{inew} becomes C_i and the loop starts again. The process is repeated until the difference between *Ci* and C_{inew} is less than 1 micromol mol^{-1}. Figure A.1 represents a schematic diagram of the iterative process.

For each leaf class, two iterative processes are performed using the coefficients *B, E* and *D* for the limitation by the saturation of the ribulose biphosphate carboxylase/oxigenase on the one hand or by the regeneration of the ribulose biphosphate on the other hand. Final value for g_{co2} and Ψ_l would be chosen from the alternative giving lower *A'*.

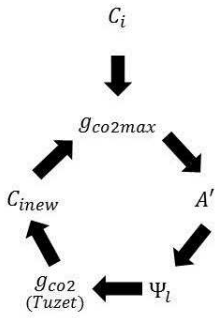

Fig A.1. Iteration procedure followed to find g_{co2} and Ψ_l

Once an equilibrium point for C_i is attained, values for *Ep* and Ψ_c are then obtained from eq. A23, A22 and A16.

5. Radiation interception

First solar position and the diffuse and direct components of radiation are computed. Then radiation interception is calculated in two steps:

1. The interception of an isolated tree crown with spheroidal shape is calculated depending on the geometric features of the crown and the daily solar trajectory applying the direct and diffuse radiation following the approach of Spitters *et al.* (1986).

2. Radiation interception is distributed between two leaf populations (i.e. sunlit and shaded leaves)

5.1. Solar radiation

The diurnal distribution of solar radiation is computed from solar elevation angle as:

$$sin\beta_s = sin\lambda_s\, sin\delta_s + cos\lambda_s\, cos\delta_s\, cos\left(\frac{2\pi(t-12)}{24}\right)$$

(S39)

In equation S39, β_s, λ_s and δ_s are the elevation angle of the sun, the latitude (>0 for the northern hemisphere) and the declination angle. The declination angle changes throughout the year due to the orbiting movement of the Earth and the inclination of its rotation axis respect to the plane of orbit. The declination angle can be computed like:

$$sin\delta_s = -\sin\left(\frac{23.45\pi}{180}\right) cos\left(\frac{2\pi(DOY+10)}{365}\right)$$

(S40)

The time between sunset (t_{ss}) and sunrise (t_{sr}) can be computed as:

$$DL = t_{ss} - t_{sr} = 12\left(1 + \frac{2}{\pi} arcsin\left(\frac{sin\lambda_s\ sin\delta_s}{cos\lambda_s\ cos\delta_s}\right)\right)$$

(S41)

On the other hand, the extra-terrestrial solar radiation (S_0) can be obtained as:

$$S_0 = S_k sin\beta_s\left(1 + 0.033cos\left(\frac{2\pi}{365}\right)\right)$$

(S42)

Where S_k is the solar constant. On a given day, the total solar extra-terrestrial radiation received ($S_{0,D}$) is computed as:

$$S_{0,D} = \int_0^{24} S_0 sin\beta_s dt =$$

$$= S_k\left(1 + 0.033cos\left[\frac{2\pi(DOY-1)}{365}\right]\right)3600\left(sin\lambda_s\ sin\delta_s DL + \frac{24}{\pi} cos\lambda_s\ cos\delta_s\sqrt{1 - \frac{sin\lambda_s\ sin{\delta_s}^2}{cos\lambda\ cos{\delta_s}^2}}\right)$$

(S43)

Before computing the amount of radiation absorbed by a canopy, the fractions of diffuse and direct radiation need to be known. The quantity of diffuse radiation depends mainly on the degree of

cloudiness, which can be related to the transmission coefficient of the atmosphere (τ_D). The value of τ_D can be calculated as the ratio of extra-terrestrial radiation and the solar radiation reaching the soil surface on a daily basis ($S_{G,D}$)

$$\tau_D = \frac{S_{G,D}}{S_{O,D}}$$

(S44)

Spitters *et al.* (1986) proposed a method to obtain the fraction of diffuse radiation (f_D) according to τ_D.

$$f_D = \frac{S_{df,D}}{S_{G,D}} = \begin{Bmatrix} 1 & if\ \tau_D < 0.07 \\ 1 - 2.3(\tau_D - 0.07)^2 & if\ 0.07 \leq \tau_D < 0.35 \\ 1.33 - 1.46\tau_D & if\ 0.35 \leq \tau_D < 0.75 \\ 0.23 & if\ 0.75 \leq \tau_D \end{Bmatrix}$$

(S45)

Where $S_{df,D}$ is the daily diffuse solar radiation. However, the diffusive fraction might vary due to scattering which depends: on the sizes of the particles in the atmosphere and the radiation wave length. Two types of scattering can be distinguished:

a) Mie scattering: produced by particles of a size in the other of magnitude of the wave length being scattered. Dust and aerosols are examples of this type of particles. This scattering is not perfectly isotropic because the intensity of the scattered radiation is higher in the direction of the propagation. To account for this scattering effect, the additional radiation due to Mie scattering is subtracted from the diffuse solar radiation and added to the direct component. This correction keeps the

assumption of an isotropic distribution of diffuse radiation, which in turn simplifies the equations but considering the Mie scattering effect. The corrected daily diffuse radiation ($S'_{df,D}$) would be:

$$S'_{df,D} = \frac{S_{df,D}}{1 + \left(1 - \left(\frac{S_{df,D}}{S_{G,D}}\right)^2\right) cos^2\left(\frac{\pi}{2} - \bar{\beta}\right) cos^3(\bar{\beta})}$$

(S46)

The symbol $\bar{\beta}$ correspond to the average solar elevation angle.

b) Rayleigh scattering: produced by particles with a much smaller sizes than the scattered photons. Gas molecules are responsible of the Rayleigh scattering in the atmosphere. Unlike Mie scattering, Rayleigh scattering is perfectly isoptropic but the intensity of the scattered radiation decreases with the wavelength. The Rayleigh effect is higher for PAR than for solar radiation, to account for this, Spitters *et al.* (1986) porposed the following expression:

$$\frac{PAR_{df,D}}{PAR_{G,D}} = \left(1 + 0.3\left(1 - \left(\frac{S_{df,D}}{S_{G,D}}\right)^2\right)\right)\frac{S'_{df,D}}{S_{G,D}}$$

(S47)

The subscript used for PAR means the same as for solar radiation.

5.2 Interception by isolated tree crowns with two leaf classes

The tree crown can be approximated by a spheroid with horizontal radius *r*, vertical radius *r'*, and a constant leaf area density (μ). Given an isolated tree crown and a zenith angle (θ_z), radiation interception is the product of the Projected Envelope Area in the θ_z direction ($PEA(\theta_z)$) and the mean interception over *PEA*. The latter may be calculated as:

$$1 - t(\theta_z) = 1 - \int_0^{l_x} f(l)\exp[-G(\theta_z)\,\mu\, l\, dl]$$

(A48)

Where $t(\theta_z)$ is the average transmissivity, $G(\theta_z)$ is the projection function in the θ_z direction, l is the path length and $f(l)$ is the frequency function of path length, which in this case can be expressed as:

$$f(l) = \frac{2l}{l_x^2}$$

(A49)

where l_x is the maximum path length.

The other factor in radiation interception, the PEA, is calculated following the approach proposed by Monteith and Unsworth (1990) for spheroids:

$$PEA(\theta_z) = \pi r^2 \sqrt{cos^2(\theta_z) + c'^2 sin^2(\theta_z)}$$

(A50)

where c' is r'/r. Note that PEA could be related to the area of the shadow envelope (S_s) projected by the tree on the horizontal plane as:

$$PEA(\theta_z) = S_s \cos(\theta_z)$$

(A51)

The average transmissivity of the canopy $t(\theta_z)$ is calculated assuming exponential extinction as described by Beer's law. For a spheroid, this transmissivity becomes:

$$t(\theta_z) = 2\frac{1-(1+A)\exp[-A]}{A^2}$$

(A52)

where:

$$A = G(\theta_z)\mu\, l_x(\theta_z)$$

(A53)

For spheroids, the maximum path length is theoretically 1.5 times the average path length, which in turn, is to be the ratio of canopy volume (V) and PEA. Therefore:

$$A = G(\theta_z)\mu\frac{3}{2}\frac{V}{PEA(\theta_z)}$$

(A54)

The product of volume and Leaf Area Density is the Plant Leaf Area (PLA) which leads to:

$$A = \mathrm{G}(\theta_z)\frac{3}{2}\frac{PLA}{PEA(\theta_z)}$$

(A55)

As a result, beam interception by the tree is computed as:

$$I_{dir} = I_n PEA(\theta_z)[1 - t(\theta_z)]$$
$$= I_n \pi r^2 \sqrt{cos^2(\theta_z) + c^2 sin^2(\theta_z)} \left[1 - 2\frac{1 - (1 + A)\exp[-A]}{A^2}\right]$$

(A56)

where I_n is the irradiance in the direction normal to θ_z.

Equation 9 may be applied to the calculation of the intercepted diffuse radiation as:

$$I_{dif} = I_n \pi r^2 \int_0^{\pi/2} \sqrt{cos^2(\theta_z) + c^2 sin^2(\theta_z)} \left[1 - 2\frac{1 - (1 + A)\exp[-A]}{A^2}\right] \sin(\theta_z) d\theta_z$$

(A57)

Once diffuse and direct intercepted radiations are computed, the area of sunlit and shaded leaves can be obtained as:

$$LAI_{sun} = I_{dir}\frac{\cos(\theta_z)}{G(\theta_z)}$$

(A57)

$$LAI_{shade} = LAI - LAI_{sun}$$

(A58)

List of Symbols

SYMBOL	DESCRIPTION	UNITS
r_r	Root specific hydraulic resistance	s m kPa kg^{-1}
α'	r_r value at which $\theta_{soil}/\ \theta_{sat} = \delta$'	Dimensionless
β'	Rate at which r_r approaches to infinity	Dimensionless
δ'	Critical value of $\theta_{soil}/\ \theta_{sat}$ at which r_r becomes limiting	Dimensionless
Rr	Total root system resistance	s m^2 kPa kg^{-1}
Rs	Total root-soil resistance	s m^2 kPa kg^{-1}
Lv	Root length density	m (root) m^{-3}(soil)
a_{root}	Root radius	m
SRL	Specific root length	m g-1
k	Unsaturated conductivity	kg s m^{-3}
k_s	Saturated conductivity	kg s m^{-3}
rt	Xylem specific hydraulic resistance	s m kPa kg^{-1}
Rx	Total xylem resistance	s m^2 kPa kg^{-1}
Z_{root}	Mean root depth	m
Z_{shoot}	Shoot height	m
SWA	Area of sapwood per unit ground area	m^2 m^{-2}
Ψ_l	Leaf water potential	kPa
Ψ_c	Collar water potential	kPa
Ψ_s	Soil water potential	kPa
Ψ_e	Air entry water potential	kPa
b	Shape factor	Dimensionless
d	Soil layer depth	m
θ_{soil}	Soil water content	m^3 m^{-3}
θ_{ll}	Soil water content at lower limit	m^3 m^{-3}
θ_{ul}	Soil water content at upper limit	m^3 m^{-3}
θ_{sat}	Soil water content at saturation	m^3 m^{-3}
Ep	Transpiration	kg s^{-1} m^{-2}
VPD	Vapour Pressure Deficit	kPa
P	Atmospheric pressure	kPa
g_{co2}	Stomatal conductance for CO2	molCO2 m^{-2} s^{-1}
g_{co2max}	Maximum stomatal conductance for CO2 for no limiting leaf water potential	molCO2 m^{-2} s^{-1}
A'	Gross photosynthesis	micromol m^{-2} s^{-1}
C_i	Internal concentration of CO2	micromol mol^{-1}
C_a	External concentration of CO2	micromol mol^{-1}

g_o	Night time stomatal conductance for CO2 at null gross photosynthesis	molCO2 m^{-2} s^{-1}
m	Proportionality factor between photosynthesis and stomatal conductance	Dimensionless
$f(\Psi_l)$	Empirical function relating stomatal conductance with leaf water potential	Dimensionless
Ψ_f^*	Reference water potential	kPa
sf	Shape factor	kPa^{-1}
LAI	Leaf Area Index	m^2(leaf) m^{-2}(soil)
LA	Leaf area	m^2
$LAI_{sun\ or\ shade}$	Leaf area of sunlit or shaded leaves	m^2(leaf) m^{-2}(soil)
$f_{(sun\ or\ shade)}$	Fraction of Leaf area index shaded or illuminated	Dimensionless
θ	Degree of curvature of the response to PAR of the electron transport rate	Dimensionless
α	Quantum efficiency	mol e mol^{-1} quanta
K_c	Michaelis constant for CO_2	mol mol^{-1}
K_o	Michaelis constant for O_2	mol mol^{-1}
Γ	CO2 compensation point	µmol CO2 mol^{-1}
V_{cmax}	Maximum catalytic activity of Rubisco in the presence of saturating amounts ribulose biphosphate and CO2	µmol m^{-2} (leaf) s^{-1}
J_{cmax}	Maximum ratio of electron transport	µmol m^{-2} (leaf) s^{-1}
R_d	Rate of CO2 evolution in the light resulting from process other than photorespiration	µmol m^{-2} (leaf) s^{-1}
ΔH_a	Activation energy	J mol^{-1}
c	Dimensionless constant for the response to temperature	Dimensionless
β_s	Elevation angle of the sun	Radians
λ_s	Latitude	Radians
δ_s	Declination angle	Radians
DOY	Day of Year	Dimensionless
t_{ss}	Time of sun set	Hour
t_{sr}	Time of sun rise	Hour
DL	Day length	Hour

S_k	Solar constant	W m^{-2}
S_0	Extra-terrestrial solar radiation	W m^{-2}
$S_{0,D}$	Daily extra-terrestrial solar radiation	W m^{-2}
$S_{G,D}$	Daily solar radiation reaching the ground	W m^{-2}
$S_{df,D}$	Daily diffuse solar radiation	W m^{-2}
$S'_{df,D}$	Corrected daily diffuse solar radiation for Mie scattering	W m^{-2}
τ_D	Transmission coefficient of the atmosphere	Dimensionless
f_D	Fraction of diffuse radiation	Dimensionless
$\bar{\beta}$	Average solar elevation angle	Radians
$PAR_{df,D}$	Daily diffuse Photosynthetically active radiation	W m^{-2}
$PAR_{G,D}$	Daily Photosynthetically active radiation reaching the ground	W m^{-2}
θ_z	Solar Zenith angle	rad
$t(\theta_z)$	Canopy transmissivity	Dimensionless
$G(\theta_z)$	Projection function in the θ_z direction	Dimensionless
l	Path length	m
l_x	the maximum path length	m
$f(l)$	Frequency distribution of the path length	m^{-1}
μ	Leaf area density	m^2 m^{-3}
$PEA(\theta_z)$	Projected envelope area in the θ_z direction	m^2
V	Canopy volume	m^3
r'	Vertical canopy radious	m
r	Horizontal canopy radious	m
I_n	Irradiance in the direction normal to θ_z	W m^{-2}
I_{dir}	Intercepted direct radiation	W m^{-2}
I_{diff}	Intercepted diffuse radiation	W m^{-2}

'-' Variables derived from the calculations.

References

Bernacchi C.J., Singsaas E.L., Pimentel C., Portis Jr A.R. & Long S.P. (2001) Improved temperature response functions for models of Rubisco-limited photosynthesis. *Plant, Cell & Environment*, **24**, 253-259.

Bonachela S., Orgaz F., Villalobos F.J. & Fereres E. (2001) Soil evaporation from drip-irrigated olive orchards. *Irrigation Science*, **20**, 65-71.

Bristow K.L., Campbell G.S. & Calissendorff C. (1984) The effects of texture on the resistance to water-movement within the rhizosphere. *Soil Science Society of America Journal*, **48**, 266-270.

Campbell G.S. (1985a) *Soil physics with BASIC : transport models for soil-plant systems*. Elsevier, Amsterdam ; New York.

Campbell G.S. (1985b) Transpiration and plant water relations. In: *Soil physics with BASIC : transport models for soil-plant systems*, pp. xvi, 150 pages. Elsevier, Amsterdam ; New York.

Cowan I.R. (1965) Transport of Water in the Soil-Plant-Atmosphere System. *Journal of Applied Ecology*, **2**, 221-239.

dePury D.G.G. & Farquhar G.D. (1997) Simple scaling of photosynthesis from leaves to canopies without the errors of big-leaf models. *Plant Cell and Environment*, **20**, 537-557.

Farquhar G.D., von Caemmerer S. & Berry J.A. (1980) A biochemical model of photosynthetic CO2 assimilation in leaves of C3 species. *Planta*, **149**, 78-90.

García-Tejera O., López-Bernal Á., Villalobos F.J., Orgaz F. & Testi L. (2016) Effect of soil temperature on root resistance: implications for different trees under Mediterranean conditions. *Tree Physiology*.

Gardner W.R. (1960) Dynamic aspects of water availability to plants. *Soil Science*, **89**, 63-73.

Hacke U.G., Sperry J.S., Wheeler J.K. & Castro L. (2006) Scaling of angiosperm xylem structure with safety and efficiency. *Tree Physiology*, **26**, 689-701.

Herkelrath W.N., Miller E.E. & Gardner W.R. (1977) Water Uptake By Plants: II. The Root Contact Model. *Soil Science Society of America Journal*, **41**, 1039-1043.

Jarvis P.G. & McNaughton K.G. (1986) Stomatal control of transpiration - scaling up from leaf to region. *Advances in Ecological Research*, **15**, 1-49.

Leuning R., Kelliher F.M., De Pury D.G.G. & Schulze E.D. (1995) Leaf nitrogen, photosynthesis, conductance and transpiration: scaling from leaves to canopies. *Plant, Cell & Environment*, **18**, 1183-1200.

Newman E.I. (1969) Resistance to Water Flow in Soil and Plant. I. Soil Resistance in Relation to Amounts of Root: Theoretical Estimates. *Journal of Applied Ecology*, **6**, 1-12.

NOAA (2016) Trends in atmospheric Carbon Dioxide.

North G.B. & Nobel P.S. (1992) Drought-induced changes in hydraulic conductivity and structure in roots of ferocactus-acanthodes and opuntia-ficus-indica. *New Phytologist*, **120**, 9-19.

North G.B. & Nobel P.S. (1997) Root-soil contact for the desert succulent Agave deserti in wet and drying soil. *New Phytologist*, **135**, 21-29.

Orgaz F., Villalobos F.J., Testi L. & Fereres E. (2007) A model of daily mean canopy conductance for calculating transpiration of olive canopies. *Functional Plant Biology*, **34**, 178-188.

Ritchie J.T. (1998) Soil water balance and plant water stress. In: *Understanding Options for Agricultural Production* (eds G.Y. Tsuji, G. Hoogenboom, & P.K. Thornton), pp. 41-54. Springer Netherlands, Dordrecht.

Sperry J.S., Adler F.R., Campbell G.S. & Comstock J.P. (1998) Limitation of plant water use by rhizosphere and xylem conductance: results from a model. *Plant Cell and Environment*, **21**, 347-359.

Spitters C.J.T., Toussaint H.A.J.M. & Goudriaan J. (1986) Separating the diffuse and direct component of global radiation and its implications for modeling canopy photosynthesis Part I. Components of incoming radiation. *Agricultural and Forest Meteorology*, **38**, 217-229.

Steudle E. (2000) Water uptake by roots: effects of water deficit. *Journal of Experimental Botany*, **51**, 1531-1542.

Steudle E. & Peterson C.A. (1998) How does water get through roots? *Journal of Experimental Botany*, **49**, 775-788.

Tuzet A., Perrier A. & Leuning R. (2003) A coupled model of stomatal conductance, photosynthesis and transpiration. *Plant Cell and Environment*, **26**, 1097-1116.

Tyree M.T. & Ewers F.W. (1991) The hydraulic architecture of trees and other woody plants. *New Phytologist*, **119**, 345-360.

Tyree M.T. & Zimmermann M.H. (2002) Hydraulic architecture of whole plants and plant performance. In: *Xylem Structure and the Ascent of Sap*, pp. 175-205. Springer-Verlag Berlin Heidelberg.

Villalobos F.J., Orgaz F., Testi L. & Fereres E. (2000) Measurement and modeling of evapotranspiration of olive (Olea europaea L.) orchards. *European Journal of Agronomy*, **13**, 155-163.

Wheeler J.K., Sperry J.S., Hacke U.G. & Hoang N. (2005) Inter-vessel pitting and cavitation in woody Rosaceae and other vesselled plants: a basis for a safety versus efficiency trade-off in xylem transport. *Plant, Cell & Environment*, **28**, 800-812.

Appendix II: Transpiration and fluxes on split root olive and almond trees

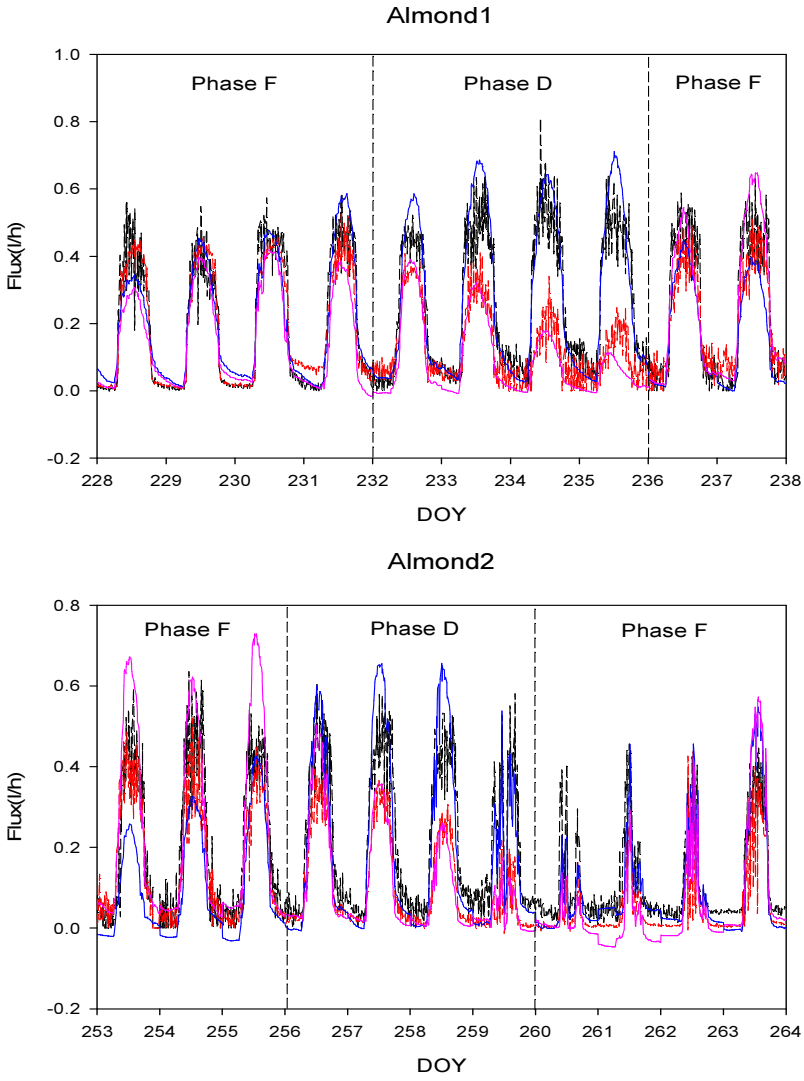

Fig A1. Variation of measured and modelled fluxes for almond one and two at different irrigation phases. Black and red line are the measured fluxes from sides one and two while blue and purple lines correspond to modelled fluxes from sides one and two.

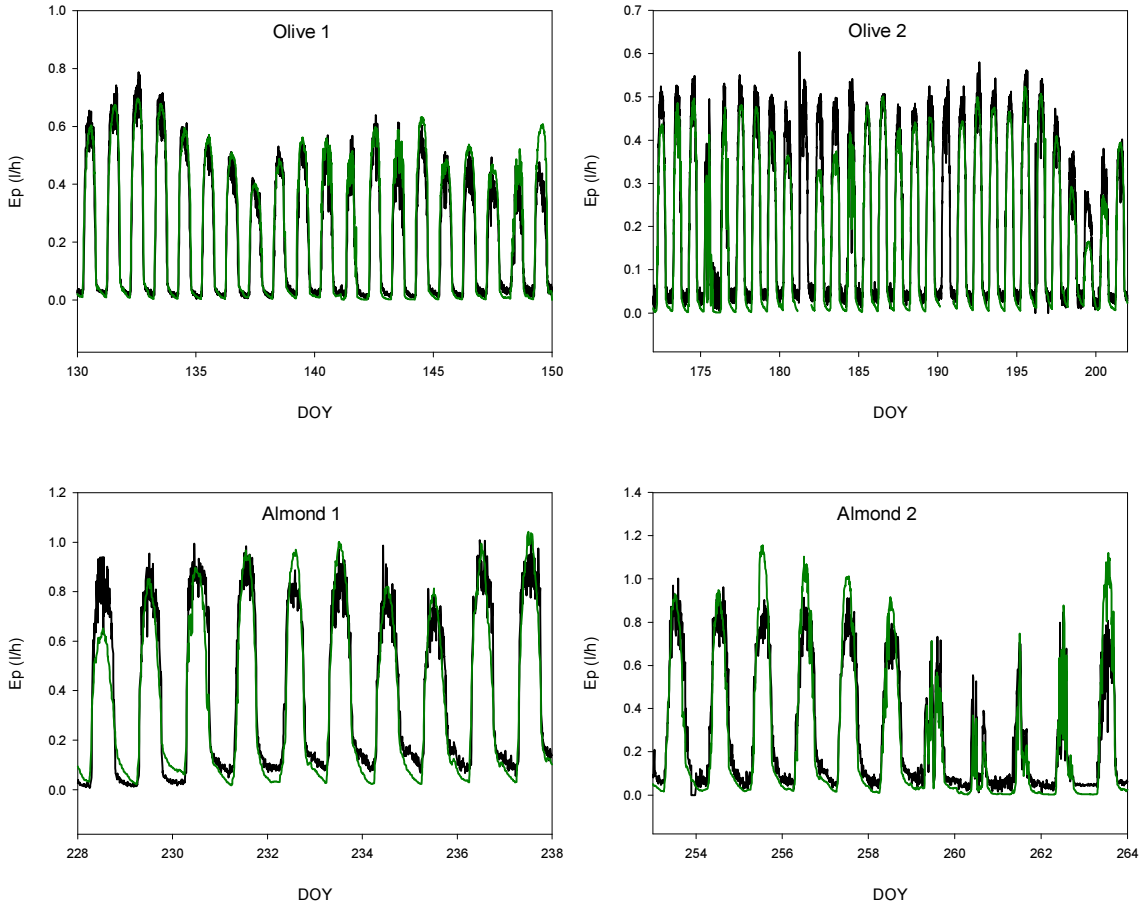

Fig A2. Measured (black) and modelled (green) E_p for the four trees used in the experiment

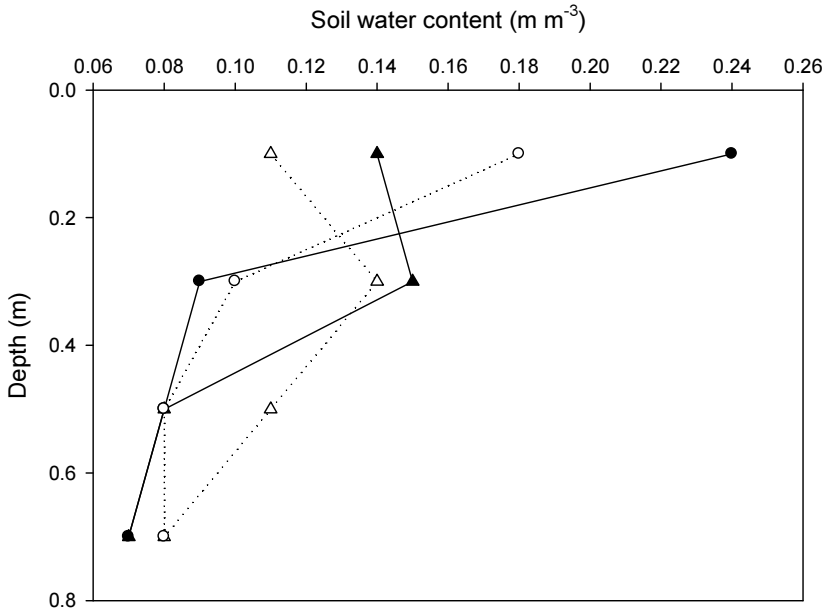

Fig A3. Modelled (circles) and measured (triangles) soil water content at 1 hour (straight lines) and 8 hours (dotted lines) after irrigation.

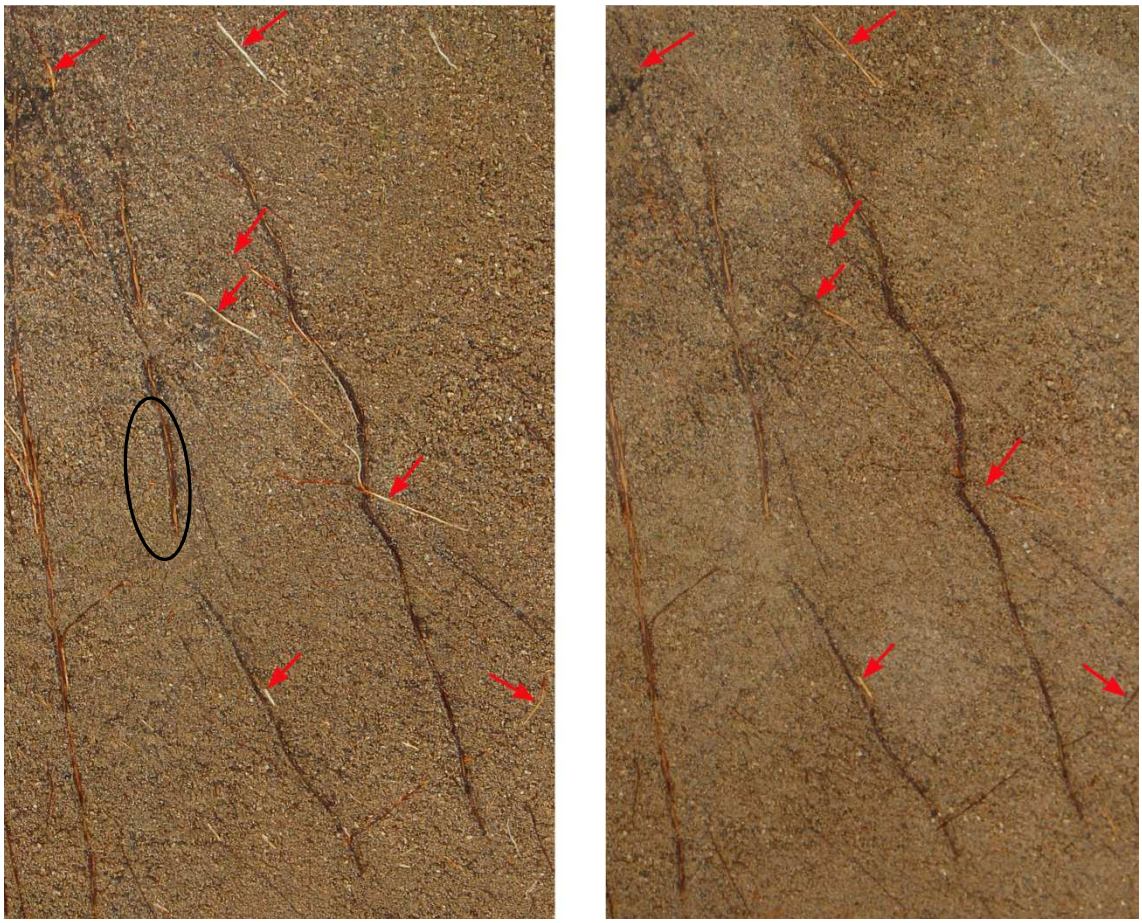

Fig A4. Almond roots impacting the transparent sheet of the lysimeter before (left image) and after (right image) a drying cycle. Roots with a noticeable change in color after the dried phase have been highlighted with the red arrows. The black circle indicate a group of clumped roots.